UNIVERSITY OF BIRMINGHAM

Microwave Sensing Techniques for Materials Characterisation

By
ALI MUSA MOHAMMED

A thesis submitted to
The University of Birmingham
for the degree of
DOCTOR OF PHILOSOPHY

School of Engineering
College of Engineering and Physical Science
University of Birmingham
March 2022

Abstract

Microwave cavity resonators are of major interest for characterisation of dielectric materials in many applications such as petroleum and chemical, biomedical and pharmaceutical, food and agriculture industries. In this thesis new and improved techniques for implementing microwave measurement techniques for dielectric characterisation of both liquid and solid materials have been developed. This has been actualised through several original contributions: a new high-Q and sensitive re-entrant cavity resonator structure; novel techniques of materials measurements for liquids enabled by a coaxial cavity resonator using a simplified analytical formula; a new concept of sample placement and measurements of substrate materials of varying thickness using resonant method; higher order mode re-entrant cavity resonator for dielectric property measurements at millimetre-wave frequencies; insight into capabilities of 3D printing in making effective and low-cost sensing device at both microwave and millimetre-wave frequencies; simplified evaluation method of materials effective conductivity by resonant technique; and the development of new unified analytical model for the extraction of dielectric properties of materials under test. The performance of these improved and new sensors, novel measurement techniques and the new derived analytical models of extracting the materials properties were verified through a large number of measurements on various materials. Dielectric characterisation of crude oils and their derivatives at 2 GHz using re-entrant cavity and concentration measurements of both binary and ternary mixtures at discrete resonance frequencies of 2 GHz and 6 GHz were reported. Measurements of low and medium dielectric loss liquids over a broadband using the coaxial cavity resonator at four different resonant modes from 2 GHz to 8 GHz were presented. Furthermore, measurement of liquid materials using a 60 GHz cavity resonator,

dielectric constant measurement of substrates materials using modified re-entrant cavity at 2 GHz and estimation of the effective conductivity of the metals, metal coated polymers and alloys made using different fabrication technology were carried out to validate the devices and measurement techniques. Experimental results are in good agreement with both simulation and reported data in the literature.

Dedication

This thesis is proudly dedicated to my beloved parents, family (wife and kids) and siblings who offered unconditional support and love throughout my life.

Acknowledgement

I would begin by expressing gratitude to Almighty ALLAH for the successful completion of this work. I would also like to say a special thanks to my sponsor the Petroleum Technology Development Fund (PTDF), Nigeria for the financial support throughout my Ph.D.

To my supervisor Prof Yi Wang, it is absolutely a great honour to have work with him over the last 5 years since my MSc time. Thank you for your continuous support, immense knowledge and guidance, motivation and encouragement, patience and ideas during my Ph.D. study with Emerging Device Technology (EDT) Research Group here at the University. I would like to express thanks to my co-supervisor Prof Michael J Lancaster (now retired) for his useful comments, suggestions, encouragement and corrections in my writing during the first 2 ½ years of my Ph.D. study. I am honoured having him as co-supervisor. To Dr Timothy Jackson who later became the co-supervisor. I appreciate your consideration and support in this regard.

My appreciation to my colleagues in the EDT research group and in particular Milan Salek and Talal Skaik who have helped technically in achieving this Ph.D. I would like to also extend my appreciation to Dr Abarasi Hart of Chemical Engineering for the collaboration and help in crude oils analysis.

My sincere appreciation to my family members (parents, siblings, wife and kids). Thank you all for being there at all times with your prayers and encouragement. To all my friends and extended families, I also value your support and prayers during this time.

Table of Content

List of symbols

a	Inner conductor radius
b	Outer cavity radius
c	Speed of light
C_e	Equivalent capacitance
C_p	Parallel capacitance
C_s	Series capacitance
C_o	Gap capacitance
C_1	Capacitance of the cavity
d	Diameter of the guarded electrode
f_r	Resonant frequency
f_o	Frequency without sample
f_1	Frequency with sample
g	Gap
h	Height of the cavity
L	Inductance
l	Length
K	Correct root
n	Mode number
p	Coefficient of curve fitting
Q	Quality-
Q_o	Q-factor after sample insertion
Q_1	Q-factor before sample insertion
Q_u	Unloaded Q-factor

Q_l	Loaded Q-factor
Q_c	Q-factor due to conductor loss
Q_r	Q-factor due to radiation loss
Q_t	Q-factor due to tube loss
Q_s	Q-factor due to sample
Q_{sim}	Simulated Q-factor
Q_{mea}	Measured Q-factor
Q_{tq}	Q-factor due to quartz tube
Q_{ac}	Q-factor due to acetone
Q_{eth}	Q-factor due to ethanol
Q_{mth}	Q-factor due to methanol
r	Cavity radius
r_0	Post radius
r_1	Cavity radius
r_r	Radius of the ring
r_s	Radius of the sample
r_c	Radius of the curvature
R_s	Surface resistance
R_{sh}	Shunt resistance
S_a	Selected area
S_{11}, S_{22}	Reflection scattering parameters
S_{12}, S_{21}	Transmission scattering parameters
T	Transmission coefficients
t_a	Average thickness of test material

t_g	Gap between guarded electrode and unguarded electrode.
V_c	Volume of the cavity
V_s	Volume of the sample
Z_0	Waveguide impedances of the empty cell
Z	Waveguide impedances filled cell
Δ	Change
ω	Angular frequency
Γ	Reflection coefficients,
Λ	Guided wavelengths loaded waveguide
ε	Complex permittivity
ε'	Dielectric constant
ε''	Loss factor
ε_r	Relative permittivity
ε_s	Static permittivity
ε_∞	Infinite permittivity
μ	Complex permeability
μ_r	Relative permeability
μ_o	Permeability of free space
λ_0	Free space wavelength
λ_c	Cut off wavelength
λ_{0g}	Guided wavelengths of the empty waveguide
δ	Skin depth
τ	Time constant

List of Figures

List of Tables

CHAPTER ONE: INTRODUCTION

1.1 Background and Motivation

Microwave and millimetre wave frequencies have been used extensively in making various passive devices for utilisation in many areas of applications. These include sensors for medical application [1], power dividers and filters for communications [2] and antennas for radio detection and radar [3]. Others include measurement and instrumentations, security instruments and microwave heating and process of materials [4], etc. One important application area of microwave-based devices is their utilisation in dielectric measurements, which have been useful in various fields such as chemical and petroleum industry [5], biomedical [6], food and agriculture [7] industries. More details on the areas of applications that use microwave techniques for measuring dielectric properties will be provided in Chapter 3. These areas of applications have tremendous impact on the economy and livelihood of the people. Similarly, these fields are growing and the demand for new technology is also increasing for an effective optimisation of the production and quality control processes. Maintaining the economic progress of these fields is highly dependent on the adequate utilisation of the resource through the cutting-edge technology for an improved production rate, quality control and analysis at a lower cost. One of the important aspects of material measurements is the ability to precisely interrogate the composition of the materials: for example, the concentration in liquids mixture and the properties of solid materials in the mentioned application scenarios. In response to this needs much effort has been directed to finding new technological tool to ensure accurate, reliable, efficient, safe and cost-effective measuring and monitoring techniques. Microwave-based techniques are one of the measurement technologies developed and used

in the characterisation and detection of materials properties through permittivity measurement. This technology has the benefit of flexibility because of its wide frequency range, its non-invasive nature, and the functionality rendered by its sensitivity and selectivity [8].

Microwave dielectric metrology relies on the fact that many materials have distinct set of dielectric properties at microwave frequencies. Many microwave-based sensors use the resonant characteristics to determine the dielectric properties of the material under test. The main property monitored by microwave signals is the complex permittivity. Thus, the precise determination of the permittivity is key to the design of microwave sensors and measurement systems. An important measurement technique is the microwave resonator-based sensor for real time detection and characterisation of liquids, solids and gaseous materials [9] [10]. Following the development and advancement of some novel microwave sensing devices, such as high quality-factor resonators [11] and metamaterials [12], there have been enormous interests in this area. Similarly, the advent of new fabrication method such as 3D printing and micromachining that allows the realisation of complex shapes and geometries is a new driver in passive device development [13]. Other promising techniques include dielectric measurements methods supported by microfluidic channels [14] reactive thin films for gas sensing [15] and the use of cost-effective materials (such as PCBs or paper-based substrates) [16]. Remarkable achievements have been recorded in dielectric metrology. However, owing to the increasing demand in measurement of dielectric materials and in response to the new opportunities and challenges, a new approach to dielectric measurements at both microwave and millimetre wave frequencies is presented in this thesis.

In this work, cavity resonators have been developed and utilised for characterisation, and compositional analysis of complex fluids (crude oils and their derivative) and mixtures of binary and ternary samples. The cavity sensors have also been modified and utilised in determining the permittivity of substrate materials using a novel approach as well as the extraction of effective conductivity of 3D printed metals and alloys manufactured using different fabrication technology.

1.2 Aim and Objectives

The general aim of the proposed research project is to demonstrate microwave resonator-based sensors capable of characterisation and identification of liquid and solid materials for industrial applications. The cavity sensors will be based on high quality factor (Q-factor) resonators. High accuracy, sensitivity and simplicity of the analysis are highly desired. This is especially so for materials with low dielectric loss such as many oils. The research also aims to identify and investigate other useful liquid and solid materials that are of potential interest to industry applications.

The following objectives are set out in the attainment of the research goals:

1) To identify the materials to be characterised and the appropriate frequency band in the areas of petroleum (crude oils), wireless communication (substrates) and quality control (concentration of solution).
2) To establish the design requirements (e.g. in terms of required Q-factor for different sensing scenarios) by theoretical analysis and simulations.
3) To design new structures, fabricate and dry-test (without loading materials) resonators.

4) To test and characterise the materials using the designed sensors and make comparisons with other techniques.
5) To develop new ways of extracting the dielectric properties of materials based on electromagnetic analysis by simulation in CST rather than the use of conventional perturbation theory.
6) To demonstrate the application of 3D printing technology in the area of microwave-based sensors.

1.3 Statement of Contributions

This research has demonstrated the use of cavity-based resonator sensors for the effective measurement of complex permittivity of low and medium dielectric loss fluids and solids materials at microwave and millimetre-wave frequencies. This is by establishing new ways of characterising the materials through:

1) The development of new cavity-based microwave resonant sensors for dielectric property characterisation and identification of materials by non-invasive and invasive techniques.
2) The application of 3D printing technology in the manufacture of microwave cavity sensors.
3) The development and use of effective simulation-based extraction model for the evaluation of materials properties.
4) Error analysis in dielectric characterisation of materials in the cavity-based measurements.
5) Analysis of binary and ternary solution based on concentration measurements

Specifically, the main novelties and contributions are:

1) The design of a modified high-Q cavity resonator with a new unified analytical formula for the extraction of the dielectric properties of liquid materials has been realised. The device has also been used in the analysis of complex fluids based on dielectric measurements by establishing correlation between dielectric permittivity and crude oil categories, as an alternative to the traditional use of sophisticated equipment and chemicals.
2) A novel technique for dielectric characterisation of liquid materials over a wide frequency range has been realised. This has provided simple and accurate method of extracting dielectric properties of materials without analytical approximation.
3) The design and fabrication of low cost and effective higher –order mode modified re-entrant cavity structure for liquids characterisation at millimetre wave frequency, enabled by 3D additive manufacturing, has been achieved.
4) A novel use of cavity resonator as a substrate measurement technique has also been realised. It has the advantage of measuring samples irrespective of their thickness in relation to their dielectric constant values as compared to conventional coaxial probes.
5) A method of resonant cavity characterisation of effective conductivity has been demonstrated. The approach offers a simplified analytical method and supports the measurements of samples with arbitrary thickness.

1.4 Thesis Outline

This thesis has been structured into eight chapters.

- **Chapter One: Introduction**

This chapter has provided the background and motivation of the research study, the aim and objectives, contribution to knowledge from this study and organisation of the thesis.

- **Chapter Two: Microwave Dielectric Measurement Method and Theory of Cavity Resonators**

  This chapter presents the fundamental techniques of microwave measurement and further describes the theory and principle of microwave cavity resonators. The importance of quality factor in relation to dielectric characterisation has been highlighted. The interaction of electromagnetic energy and materials at microwave frequency and principle of Debye model are also discussed. The concept of cavity perturbation theory for the extraction of dielectric properties and its derivation of formula are fully captured in this chapter.

- **Chapter Three: Literature Survey**

  This chapter covers the literature survey on cavity-based resonators for materials characterisation and identification covering frequencies from S-band up to J-band. Various cavity structures of cylindrical, rectangular, spherical, and re-entrant cavities used in dielectric property measurements have been discussed in detail. Furthermore, a comparison in terms of frequency, unloaded Q-factor, method of fabrication, applications, and method of extraction of the dielectric properties has also been presented in tabular form. The review and comparison reveal the state of the art in dielectric metrology and also informs the choice of the cavity structure, type of fabrication and method of extraction adopted and used in this work.

- **Chapter Four: Re-entrant Cavity Resonator Sensor for Liquids Measurement**

  This chapter provides the detailed design, fabrication and measurements of liquids samples at 2 GHz using a re-entrant cavity resonator. Common solvents have been measured to validate the resonator sensor. The sensor was then used for the measurements of dielectric properties of crude oils and their derivatives. Chemical Saturate Aromatic Resin and Asphaltene (SARA) separation of crude oils has been carried out. Analytical model for the extraction of the permittivity derived from simulation data, is also presented. Furthermore, concentration measurements of binary and ternary solutions and the use of harmonics for measurements at higher frequency around 6 GHz using the 2 GHz cavity resonator has also been demonstrated in this chapter.

- **Chapter Five: Coaxial Microwave Resonator Sensor for Dielectric Measurements of Liquid**

  This chapter presents the design and fabrication of coaxial microwave cavity resonator for the measurements of low loss liquids at multiple resonant frequencies up to 8 GHz. The new approach (filling the entire cavity with material under test) for low and medium crude oils samples at four resonances of 2 GHz, 4 GHz, 6 GHz and 8 GHz have been presented. The main advantage of the measurement approach using the coaxial cavity over the re-entrant cavity resonator is the simple and straightforward parameter extraction of the dielectric properties of materials. The results obtained have demonstrated good dielectric measurement capability over the frequency range. The challenge of the approach is also discussed.

- **Chapter Six: 60 GHz Higher Order Mode Re-Entrant Cavity Resonator for Liquids Characterisation**

  This chapter reports the design, mode analysis and fabrication of higher order re-entrant cavity at 60 GHz. Parametric study of the designed cavity for dielectric measurement based on simulation have been presented in detail. The fabrication of the device and calibration using hexane sample have also been captured to validate the measurement device. The device demonstrated the effectiveness of dielectric metrology at millimetre wave as well as the usability of 3D printing in manufacturing.

- **Chapter Seven: Dielectric Constant and Conductivity Measurements of Materials**

  This chapter is further divided into two parts: Part A covers the dielectric constant measurement of substrates materials using a further modified re-entrant cavity resonator. Several samples of substrate of 20 mm in diameter and varying thickness have been measured using the designed cavity resonator and results are compared with measurement using an industrial dielectric kit. Part B provides the measurements of the effective conductivity of different metal and alloy materials using re-entrant cavity resonator. Analytical formula derived for the extraction of the effective conductivity based on the knowledge of energy stored in the volume of the cavity is also given. Aluminium, copper and stainless-steel flat samples manufactured by CNC and additive manufacturing (based on metals and polymers) are measured to validate the device.

- **Chapter Eight: Conclusion and Future work**

  This chapter presents the conclusion of this work and some recommendations for future work.

1.5 List of Publications

Journal Article

- A. M. Mohammed, Y. Wang and M. J. Lancaster, "3D Printed Coaxial Microwave Resonator Sensor For Dielectric Measurements of Liquid," *Microw. Opt. Techn. Lett,* vol. 16, no. 3, pp. 805-810, 2021
  https://doi.org/10.1002/mop.32679
- A. M. Mohammed, A. Hart, J. Wood, Y. Wang and M. J. Lancaster, "3D Printed Re-Entrant Cavity Resonator for Complex Permittivity measurement of Crude Oils," *Sens. Actuators A: Physical,* vol. 317, no. 112477, pp. 1-10, 2021.
  https://doi.org/10.1016/j.sna.2020.112477
- A. M. Mohammed, Y. Wang, T. Skaik, S. Li and M. Attallah, "Conductivity Measurement Using 3D Printed Re-entrant Cavity Resonator," *Measurement Science and Technology, Volume 33, Number 5,* vol. 33, no. 5, pp. 1-7, 2022
  https://doi.org/10.1088/1361-6501/ac5134

Conference Paper

- A. M. Mohammed, Y. Wang and M. Salek, "Dielectric Measurement of Substrate Materials Using 3D Printed Re-Entrant Cavity Resonator," Presented at *2021 Euro. Microw. Conf*, London, in April 2022.

CHAPTER TWO: MICROWAVE MEASUREMENT METHOD AND THEORY OF CAVITY RESONATORS

This chapter covers the fundamental techniques of microwave dielectric measurement and the theories of cavity resonators. Different types of cavity structures such as cylindrical cavity and re-entrant cavity are discussed. The theory of microwave cavity, with quality factors as an important parameter in cavity base resonators for characterisation of materials, has been covered in detail. The interaction of dielectric materials with electromagnetic fields at microwave frequencies and the concept of Debye theory are also highlighted. The conventional method of extracting dielectric properties of material is based on the principle of cavity perturbation theory, which is also discussed to help understand the concept on which the measurement is based.

2.1 Introduction

Electromagnetic (EM) radiation is a form of energy propagating through a medium at the speed of light, consisting of both electric and magnetic fields oscillating orthogonal to each other and to the direction of propagation. Electromagnetic radiation in a free space is classified by wavelength as shown by the electromagnetic spectrum in Figure 2.1. Microwaves and millimetre waves form part of the spectrum with frequency ranging from 300 MHz to 30 GHz (wavelength of 1 m – 1 cm) and 30 GHz to 300 GHz (wavelengths of 1 cm – 1 mm), respectively [17], [18]. This frequency range has been considered useful for number of applications as earlier outlined in Section 1.1 of Chapter 1.

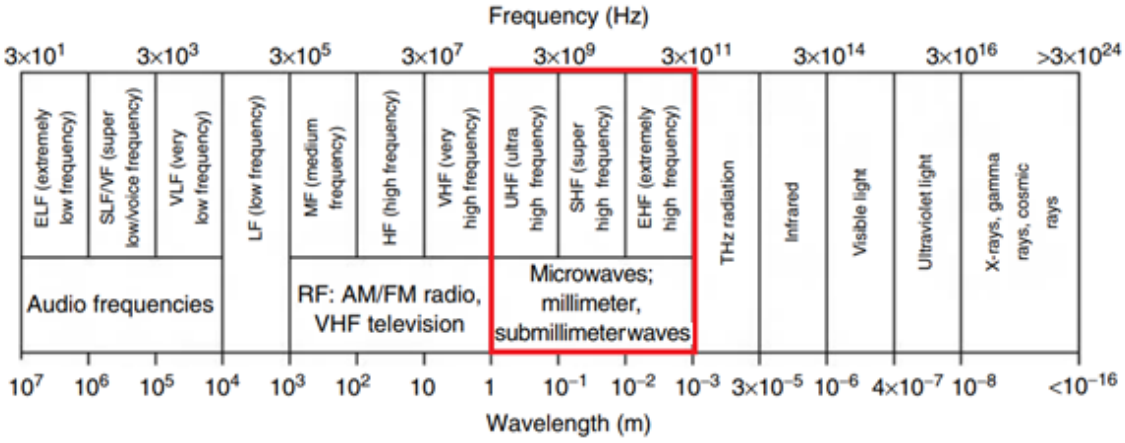

Figure 2.1 Electromagnetic spectrum [17]

2.2 Methodology of Microwave Materials Characterisation

Many methods have been proposed and used within the microwave frequency range for material characterisation. These techniques can be classified into two main methods: non-resonant and resonant methods. Non-resonant methods include transmission line method, free space method and near-field method which are used in getting the general knowledge of EM properties over a frequency range. In resonance methods, single or several discrete frequencies are utilised to get the information of EM properties [19]. The basic principle of these methods, their pros and cons when it comes to dielectric measurement of materials are discussed below.

2.2.1 The Transmission Line Method

Transmission line measurement method involves placing a sample in a section of an enclosed transmission line. This can be a coaxial line or rectangular waveguide. The scattering parameter S_{11} and S_{21} (i.e reflection and transmission) are acquired by connecting the transmission line to a two-port Vector Network Analyser (VNA), which is then utilised to determine the complex permittivity of the material under test (MUT).

Transmission line methods cover a broad frequency range and can be used for the measurement of materials that possess medium and high loss dielectric properties. Small samples are more suitable for coaxial line, while larger samples can be measured using waveguides as shown in Figure 2.2. This method is considered cost-effective. However, it lacks accuracy, and the sample preparation remains a challenge [20].

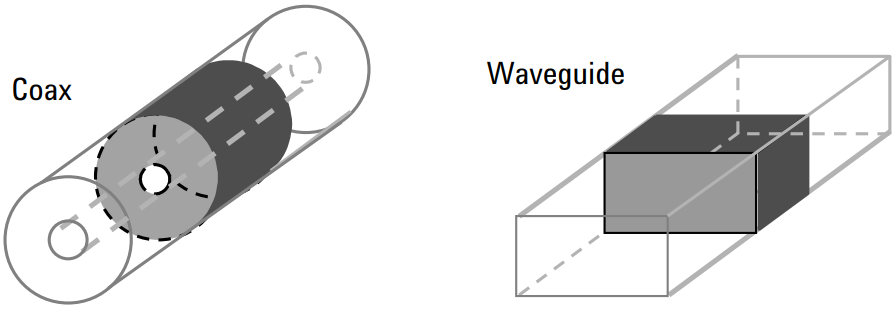

Figure 2.2 Transmission line method: coaxial (left) and waveguide (right) [19]

The two most common approaches for the extraction of complex permittivity using this method are: the calculation procedure introduced by Nicolson-Ross-Weir (NRW) and the NIST iterative conversion method [21]. Both methods use all or a pair of the S-parameters (S_{11}, S_{21}, S_{12}, S_{22}) to compute for the transmission and reflection coefficient of the MUT. The two methods are compared in terms of measurement capabilities, advantages and disadvantages in Table 2.1. A detailed derivation of the procedure introduced by NRW line is further presented. The derived equations can be applied to both coaxial line cell and rectangular waveguide cell [22] [23].

Table 2.1: Comparison between NRW and NIST iterative calculation methods

	Nicolson-Ross-Weir (NRW)	**NIST iterative**
1	Direct calculation of the dielectric properties	Calculation is based on Newton-Raphson's root finding
2	Use for both permittivity and permeability	Only used for permittivity
3	Affected by divergence at certain frequencies	There is no effect of divergence
4	Not suitable for low dielectric loss materials	Suitable for low and high dielectric loss materials
5	Fast, non-iterative with medium accuracy	Slow, iterative with good accuracy
6	Requires small sample for measurement	Measure arbitrary sample size

The permittivity and permeability equation of the NRW line is deduced from the S-parameter equations which can be obtained from the network analyser given by

$$S_{11} = \frac{\Gamma(1 - T^2)}{1 - \Gamma^2 T^2} \tag{2.1}$$

$$S_{21} = \frac{\mathrm{T}(1 - \Gamma^2)}{1 - \Gamma^2 T^2} \tag{2.2}$$

where S_{11} and S_{21} are the reflection and transmission scattering parameters, while Γ and T are the first reflection and the transmission coefficients, respectively.

The reflection coefficient is further defined by

$$\Gamma = \frac{\mathrm{Z} - Z_0}{\mathrm{Z} + Z_0} \tag{2.3}$$

$$\Gamma = \mathrm{K} \pm \sqrt{(K^2} - 1) \tag{2.4}$$

where Z_0 and Z represent the waveguide impedances of the empty and filled cells, K is the correct root and is given in terms of S-parameters as:

$$K = \frac{S_{11}^2 - S_{21}^2 + 1}{2S_{11}} \tag{2.5}$$

The transmission coefficient can be written as:

$$T = \frac{S_{11} - S_{21} + \Gamma}{1 - (S_{11} + S_{21})\Gamma} \tag{2.6}$$

The complex permeability μ is given by

$$\mu = \frac{\lambda_{0g}}{\Lambda}\left(\frac{1+\Gamma}{1+\Gamma}\right) \tag{2.7}$$

where λ_{0g} and Λ are the guided wavelengths of the empty and loaded waveguides respectively and they are defined by

$$\lambda_{0g} = \frac{\lambda_0}{\sqrt{1 - (\frac{\lambda_0}{\lambda_c})^2}} \tag{2.8}$$

$$\Lambda = \frac{\lambda_0}{\sqrt{\varepsilon\mu - (\frac{\lambda_0}{\lambda_c})^2}} \tag{2.9}$$

and λ_0 and λ_c are the free space and the cut off wavelength. The complex permittivity ε can therefore be found by substituting (2.8) and (2.9) into (2.7) which gives

$$\varepsilon = \frac{\lambda_0^2\left(\frac{1}{\Lambda^2} - \frac{1}{\lambda_c^2}\right)}{\mu} \tag{2.10}$$

where the complex guided wavelength is further defined as a function of T given as:

$$\frac{1}{\Lambda} = \frac{j}{2\pi l_s}\ln(T) \tag{2.11}$$

l_s is the sample length.

2.2.2 The Free Space Method

In this measurement method, two antennas (transmitting and receiving) are placed facing each other and the MUT (a large flat sample) is placed between the two antennas as shown in Figure 2.3. Unlike the transmission line method, the technique is non-contacting and allows for measurement over a wide range of frequency, even under high temperatures or

in hostile environments. To extract the dielectric properties of the material, the attenuation and phase shift of the signal are measured and can be evaluated using the NRW calculation method [21] [24]. This method is considered accurate, however it is often expensive as it requires highly directional antennas for excitation. The technique also requires larger sample in some cases to get an accurate measurement due to diffraction effects at the edge of the sample [25]. However, the use of optical and beam focusing can be deployed for measurement of small samples, this can of course increase the cost further.

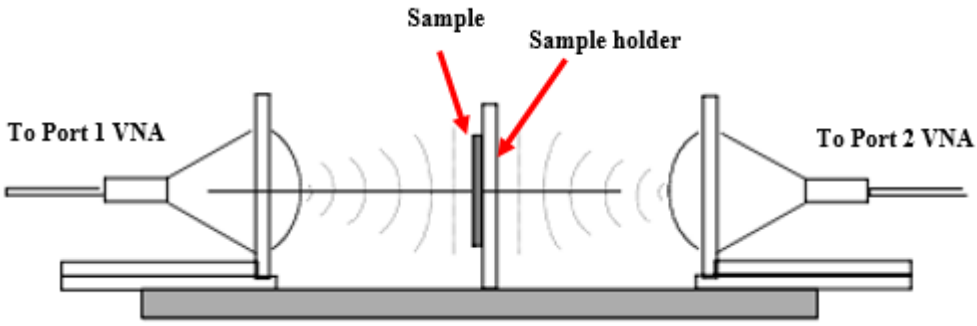

Figure 2.3 Free space measurement setup [19]

2.2.3 The Near-Field Method

The near field method, such as an open-ended coaxial probe, has been the most commonly used method for material's dielectric measurement. The open-ended coaxial sensor consists of a cut-off section of a transmission line. The measurement is achieved by inserting the probe end into a liquid or placing it in a proper contact with flat solid or powder samples as demonstrated in Figure 2.4 [24]. The reflection coefficient is measured as the electromagnetic field at the probe end infringes into the sample. This signal is related to the dielectric constant of the material. The method is quite simple, non-destructive and requires minimal sample handling with measurement over a wide frequency range. It has

been widely used due to its low cost and flexibility in a number of applications [20, 26]. However, the method suffers from accuracy, calibration and computation problem resulting from air gaps, air bubbles, and un-even surfaces with limit to the magnitude of the measurable dielectric value especially for solid sample [27].

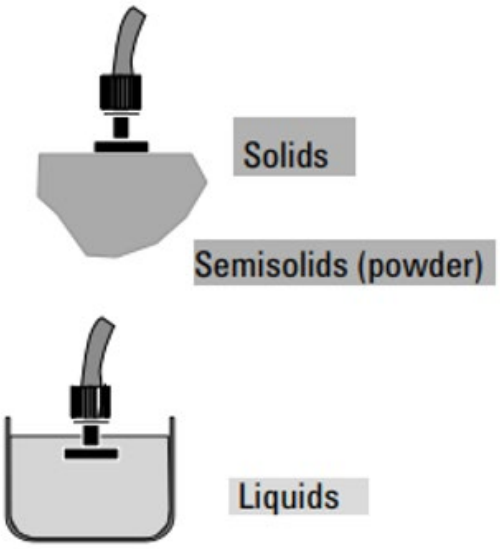

Figure 2.4 Coaxial probe measurement setup [21]

2.2.4 The Resonant Method

This technique is considered more accurate and sensitive to changes due presence of materials. Therefore, they are considered a good candidate for the realisation of simple and sensitive microwave dielectric properties measurement than the non-resonant methods [26, 28]. The resonant methods are classified as resonator methods and resonant-perturbation methods. In this work, the resonant perturbation methods would we use. The most common types of the resonant-perturbation techniques are the cavity resonators and planar resonators. An example of cavity resonant method is a typical cylindrical cavity with resonant frequency at TM_{010} mode for liquids measurement enabled by a sample holder, as shown in Figure 2.5. The measurement is achieved by inserting a sample (a

small fraction of the cavity volume) into the cavity and thus the resonant properties of the cavity is altered/perturbed due to the presence of the material. In this type of measurement, the samples are usually placed in high electric field density region for dielectric permittivity measurements [29].

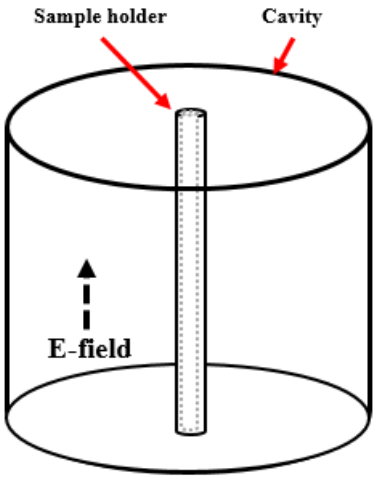

Figure 2.5 TM_{010} mode cylindrical cavity resonator with central tube for liquid measurement

The dielectric constant can be accurately determined from the measured change in frequency of the cavity with and without the samples. However, there are a number of uncertainty factors such as the accuracy of the fabricated device, change in environmental temperature during measurements, measurement repeatability of the set-up and air gaps (solid samples) or air bubbles (liquid sample), etc. All of these can influence the results of the measurement; however, they can be quantified. Further explanation is given in detail in Chapter 4 and 5 for liquid measurements and in Chapter 7 for solid sample measurement. The dielectric loss of the materials can be extracted from the measured *Q*-factor. Perturbation theories have been generally used in extracting the properties of the material

from the measured resonance properties [20]. There are various types of resonators such as dielectric resonators, open resonators, coaxial resonators, fabry-perot resonators, cavity resonators and planar resonators. The latter two are the most commonly used types of resonators for materials permittivity measurement using resonant-perturbation methods. These are briefly reviewed and presented as follows.

1) Planar Resonator Technique

Planar resonators have been utilised in sensing domain due to their non-invasive nature, simple fabrication process and cost effectiveness [28]. They have been the most widely used method compared to cavity resonators for their compatibility with integrated circuits and ability for in-situ measurement among others [30]. However, they generally suffer from low *Q*-factor (poor resolution and relatively low sensitivity) [31]. The split ring resonator (SSR) and their modified structures such as complementary split ring resonator (CSRR) and double split ring resonator (DSRR) have been reported for various applications. For example, DSSR incorporated with conducting polymers has been used for gas sensing [32]; extended gap SRR for concentration detections of both low and high glucose level using amplitude and frequency response, respectively [33]; and thin-film detection and characterisation of low dielectric loss liquids with submersible ability at lower gigahertz using SRR based sensor [34] were reported. Another example is the triple complementary split-ring resonator (TCSRR) aimed at reducing the measurements error associated with planar SRR resonator in the measurement of dielectric constant of materials [35]. The planar SRR is an electrically small resonator and made up of a loop with a gap separation. They are often implemented using microstrip line. When excited, the circulating current induces an inductance in the loop while a capacitance is developed across the gap and the circuit resonates. The change in capacitance as a result of the

material insertion determines the permittivity of the MUT. The material measurement is such that the sample is placed within the gap region of the resonator where the electric field is intense for permittivity measurement.

As a way of improving the Q-factor of planar based sensors, recently, a circuitry technique that combines planar with active components and a feedback loop has been reported. This is to compensate for the loss factor and enable high resolution and better sensitivity [36]. The use of microfluidic channels in a planar resonator has also been a milestone in sensing flowing fluids, especially in the pharmaceutical and bio-chemical industry [37]. The use of a fluidic channel offers a convenient way of instantaneous measurement of liquids at the microscale, resulting in size miniaturization and low-cost system [38]. However, in general owing to the low frequency application and low Q-factor associated with this method, a cavity-based resonator will be considered for this work as described below.

2) Cavity Resonator Techniques

Cavity resonator is also one of the most widely used permittivity measurement techniques for various applications [39, 40]. The technique offers a higher Q-factor than the planar resonators due to the more distributed current density over the surrounding conductors [31], making them more desirable for characterising low dielectric loss materials [40]. The permittivity measurement can be performed by simple insertion or immersion of an appropriate shaped sample into the cavity. The resultant changes in the resonant frequency (shift in frequency Δf) and Q-factor determine the properties of the sample introduced into the cavity [41]. This principle of measurement is often referred to as the cavity perturbation method. The perturbation theory simply refers to as the small boundary surface deformation of the cavity or change in cavity resonance properties due presence of

materials developed by Bethe and Schwinger [42]. The two most common types of cavity resonators are: the rectangular cavity and cylindrical cavity with the latter considered to have higher *Q*-factor. Both types of cavities have been utilised in materials characterisation. For example: cylindrical cavity for complex permittivity measurements using different modes at various frequencies in lower frequency of the L-band and higher frequency of V-band have been reported [43] [44]. The TE_{011} and TM_{010} modes have been the most widely used modes for permittivity measurements based on reported literature. The TM_{010} has most of its electric field intensity confined at the centre of the cavity. For accurate measurement of the dielectric constant of the MUT, samples are placed in the region of higher electric field for permittivity measurements [43].

A rectangular cavity with two ports excitation at lower frequency using the fundamental TE_{101} mode was demonstrated in [45]. The authors investigated the concentration in binary solutions and the choice of capillary tube sizes for accurate measurements of the binary composition. The binary samples are passed through the capillary tube in continuous flow to avoid air within the tube. Capillary tubes with larger radii tend to introduce a more significant shift in frequency and therefore, it is desirable if one's aim is to improve sensitivity. However, the *Q*-factor tends to reduce [45]. To increase the bandwidth of the operational frequency, a doubled-ridged rectangular cavity was proposed. The novelty was to overcome the use of single-mode configuration and the device was validated by permittivity measurement of solid materials using the TE_{101}, TE_{102}, and TE_{103} modes. The complex permittivity was evaluated based on cavity perturbation methods. A comprehensive literature survey of cavity resonators for dielectric characterisation using various conventional and unconventional cavity structure will be presented in Chapter 3.

2.3 Theories of Resonant Cavities

A resonant cavity is a device that encloses the electromagnetic energy within a body of a certain geometry, also known as a resonator. The conventional and easy-to-construct cavity structures (resonators) with determined field distribution include: the rectangular, cylindrical and spherical cavity structure. There dimensions are related to the desired operational wavelength and mostly constructed from materials of high conductivity. This is to retain the oscillating electromagnetic field within the cavity, as it decays due to a number of loss mechanisms [46]. The losses associated with cavity resonators will be discussed further in a subsequent section. The relevant types of cavity structure for this work are discussed based on the transmission line configuration i.e two-port network connection.

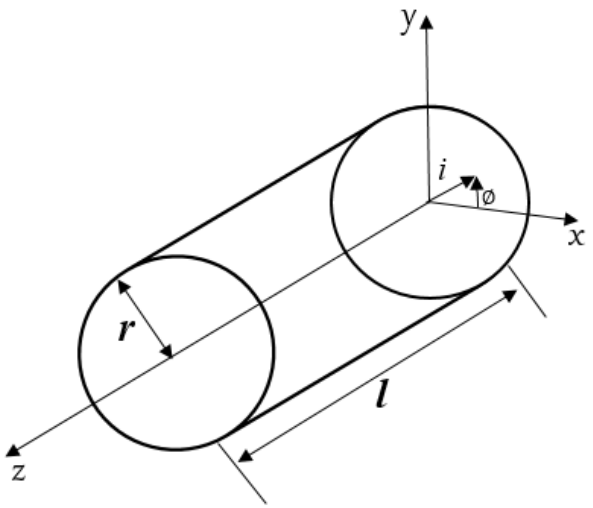

Figure 2.6 Cylindrical cavity geometry

2.3.1 Cylindrical Resonant Cavities

A cylindrical resonant cavity is a section of circular waveguide (a round metal pipe that propagates transverse electric (TE) and transverse magnetic (TM) modes) terminated by

short-circuit surface at both ends [46]. The configuration is shown in Figure 2.6, where $2r$ is the diameter of the cylindrical cavity and l is its length. The EM fields form standing waves in the longitudinal direction (z-axis).

The resonant frequencies f_r of a cylindrical cavity are given by (2.12) and (2.13), that are defined by the Bessel Function $J_n(X'_{mn}) = 0$ and $J_n(X_{mn}) = 0$ for TE and TM modes respectively [47].

$$f_{r(TM),} = \frac{c}{(2\pi\sqrt{\mu_r \varepsilon_r})} \sqrt{\left(\frac{X_{mn}}{r}\right)^2 + \left(\frac{p\pi}{l}\right)^2} \tag{2.12}$$

$$f_{r(TE),} = \frac{c}{(2\pi\sqrt{\mu_r \varepsilon_r})} \sqrt{\left(\frac{X'_{mn}}{r}\right)^2 + \left(\frac{p\pi}{l}\right)^2} \tag{2.13}$$

where, c is the speed of light, 3×10^8 m/s, μ_r and ε_r are the relative permeability and permittivity of the material filling the cylindrical cavity resonator, respectively. l and r are the length and radius of the cylindrical cavity resonator respectively. The values of the roots of Bessel functions for the TM and TE mode for $n = 1 \cdots 3$ and $m = 0 \cdots 2$ are given in Table 2.2.

For the TMmnp modes, $H_Z = 0$ and $E_Z \neq 0$ and in the TEmnp modes $E_Z = 0$ and $Hz \neq 0$. The coordinates are polar r, φ, and z. The index m is the number of full-cycles in the ∅-direction, n is the radial variation of the field and p is the number of half-wave field variation in the z-direction. The primary mode in the cylindrical cavity is either the TE_{111} for $l \geq 2r$ or TM_{010} for values of $2r > l$ for the geometry shown in Figure 2.6. For the design of a cylindrical cavity, understanding the mode excited at a given frequency is an important factor. This is guided by the relationship between the resonant frequency and diameter-to-length ratio ($2r/l$) known as the cavity mode chart. Figure 2.7 shows the lower order resonant modes of a cylindrical cavity [47]. Changing the length of the cavity

can cause changes in the resonance frequency, thus a tunable resonant circuit at microwave frequencies can be realised. However, this is an exception in case of TM mode with $p = 0$ where the resonant condition is independent of the length of the cavity. The simulation field pattern of the lower-order mode of the TM_{010} of the circular cylindrical cavity is given in Figure 2.8 [48].

Table 2.2: Values of the roots of Bessel function for TM and TE modes [47]

Mode No	TM mode			TE mode		
M	X_{m1}	X_{m2}	X_{m3}	X'_{m1}	X'_{m2}	X'_{m3}
0	2.405	5.520	8.654	3.832	7.016	10.174
1	3.832	7.016	10.174	1.841	5.331	8.536
2	5.135	8.417	11.620	3.054	6.706	9.970

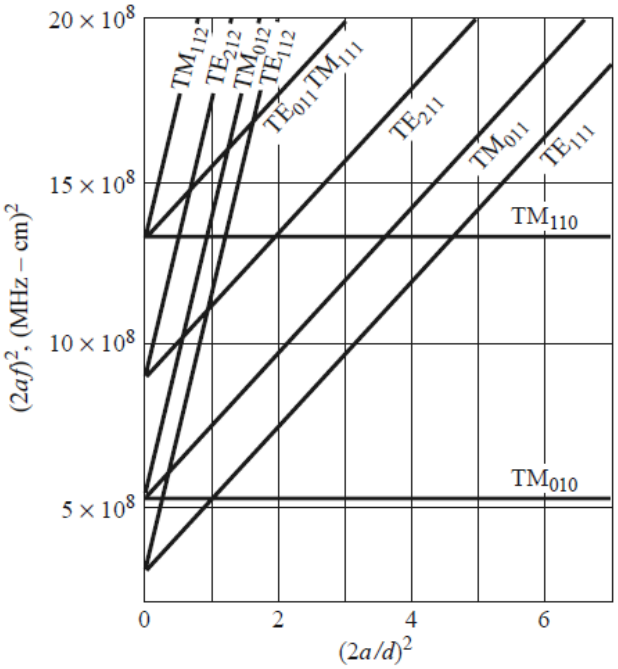

Figure 2.7 Cylindrical cavity lower order resonant mode chart [44]

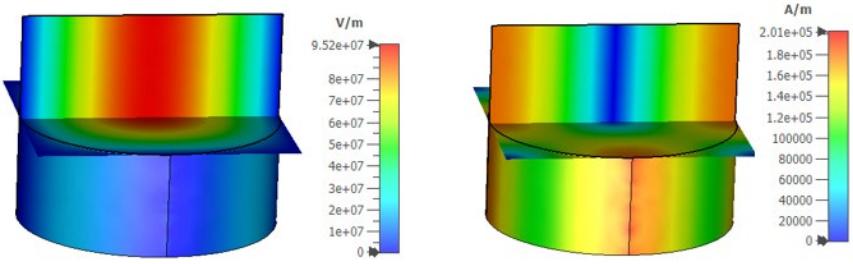

(a) **(b)**

Figure 2.8 Field pattern of the TM_{010} mode for cylindrical cavity (a) electric field and (b) magnetic field

2.3.2 Coaxial Cavity Resonator

A coaxial resonator is usually in the form of a cylindrical cavity with a centre conductor (referred to as a resonant line) as shown in Figure 2.9. The cavity has an inner conductor radius *a*, outer cavity radius of *b* and *l* as the length. The length of this resonator is usually close to half-wave (λ/2) or quarter-wave (λ/4) length of the frequency of interest. The resonator can then be classified as either half or quarter wavelength type. A quarter-wavelength resonator is shorted at one end and also referred to as open-end resonator, while the half-wavelength is effectively shorted at both end as shown in Figure 2.10(a) and Figure 2.10(b), respectively. The cross-sectional view of the transverse electromagnetic (TEM) mode as the fundamental propagating mode in a coaxial resonator is also shown in Figure 2.10 (c).

Beside the TEM mode, other resonances that are non-harmonic to the fundamental mode also exist. This can be TE or TM modes [46]. They are non-harmonically related because of the effect of cut-off. However, their resonant condition is determined by the length *l* as a multiple of wavelength. Therefore, the device has to work in a pure TEM

mode to ensure the sensitivity and accuracy of the device in characterisation of material properties [49].

The resonance occurs at frequencies where the conductor length is an even or odd multiple of the wavelength for half-wave or quarter-wavelength resonator, respectively. The *Q*-factor of the coaxial resonator derived considering standing waves resulting from the reflection at the end of the coaxial is given by the following equations [50].

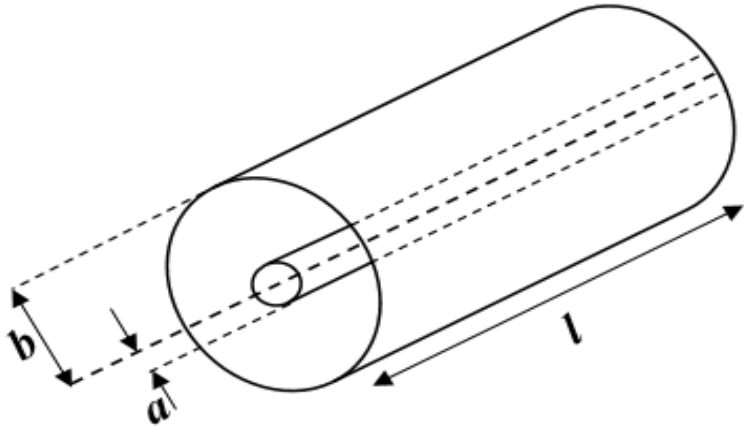

Figure 2.9 Coaxial cavity resonator

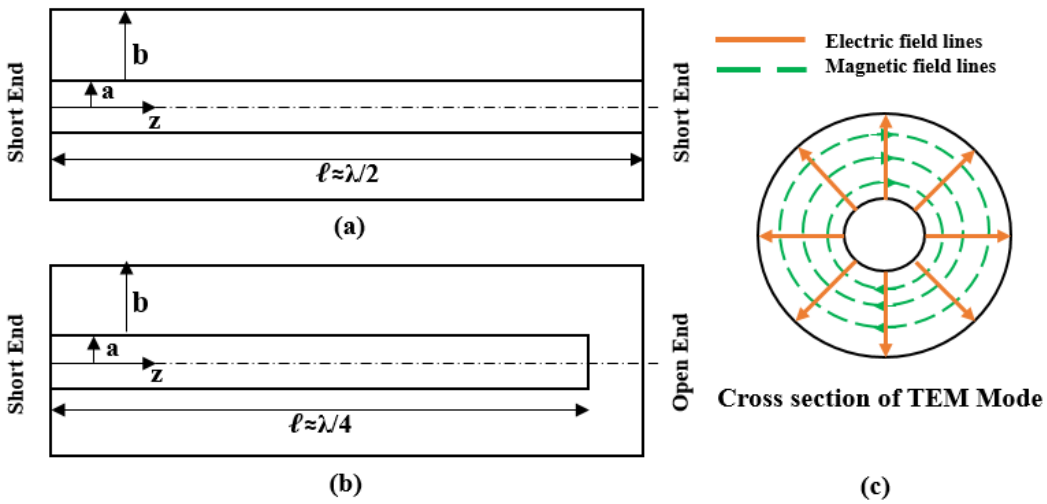

Figure 2.10 Coaxial cavity resonator: (a) half-wave (b) quarter-wave (c) cross-sectional view of TEM mode

$$Q_c(open-circuited) = \frac{\omega\mu_o \ln\left(\frac{b}{a}\right)}{R_s\left(\frac{1}{a}+\frac{1}{b}\right)} \tag{2.14}$$

$$Q_c(short-circuited) = \frac{\omega\mu_o \ln\left(\frac{b}{a}\right)}{R_s\left(\frac{1}{a}+\frac{1}{b}+\frac{4\ln\left(\frac{b}{a}\right)}{l}\right)} \tag{2.15}$$

$$R_s = \sqrt{\frac{\pi f_r \mu_o}{\delta}} \tag{2.16}$$

where Q_c is the Q-factor associated with conductor loss, μ_o is the permeability of free space, ω is the angular frequency, R_s is the surface resistance and l is the length of the resonator. The inner and outer radius of the coaxial resonator are a and b, while δ is the conductivity of the conductor and f_r is the resonant frequency. The Q-factor for open-circuited coaxial resonator is determined by (2.14) while (2.15) is used for evaluating the Q-factor of a short-circuited resonator. The cut off frequency for the TE and TM mode is approximately determined by

$$f_{cutoff(TE)} = \frac{nc_o}{\pi\sqrt{\varepsilon'}(b+a)} \tag{2.17}$$

$$f_{cutoff(TM)} = \frac{nc_o}{2\sqrt{\varepsilon'}(b-a)} \tag{2.18}$$

where ε' is the dielectric constant of the material between a and b, n is the mode number.

2.3.3 Re-entrant Cavity Resonator

A re-entrant cavity is a type of circular cylindrical cavity whose metallic boundaries extend into the interior of the cavity. They produce strong electric field enabled by a small gap in the interacting region at the central post of the cavity [51]. Figure 2.11 shows the cross-sectional view of a single and a double re-entrant cavity.

Considering re-entrant cavity shown in Figure 2.11, the boundary surface of z = constant is no longer uniform in the x direction. For this, the boundary condition becomes complicated and therefore cannot be satisfied by the fields with simple single harmonic (using sine or cosine function) in the z plane, but rather an infinite number of space harmonics. This is because the actual electric field (E-field) in the gap region is assumed to be uniform, while the magnetic field (H-field) is infinitesimally small near the axis as shown in Figure 2.12 for a single re-entrant cavity geometry. Thus, the gap between the top post and central cap is considered as a parallel-plate capacitance [52]. Detailed analytical solution of the field for both exact and approximate solution has been provided which requires a series of iteration and is complex [51]. The resonance properties of the microwave re-entrant cavity resonator can be easily estimated using the equivalent circuit [53] shown in Figure 2.13 based on the geometry shown in Figure 2.11 (a).

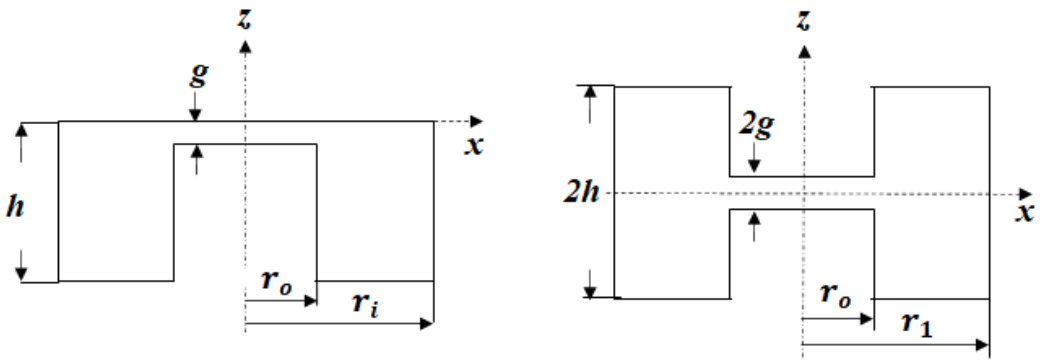

(a) (b)

Figure 2.11 Re-entrant cavities: (a) single re-entrant, (b) double re-entrant.

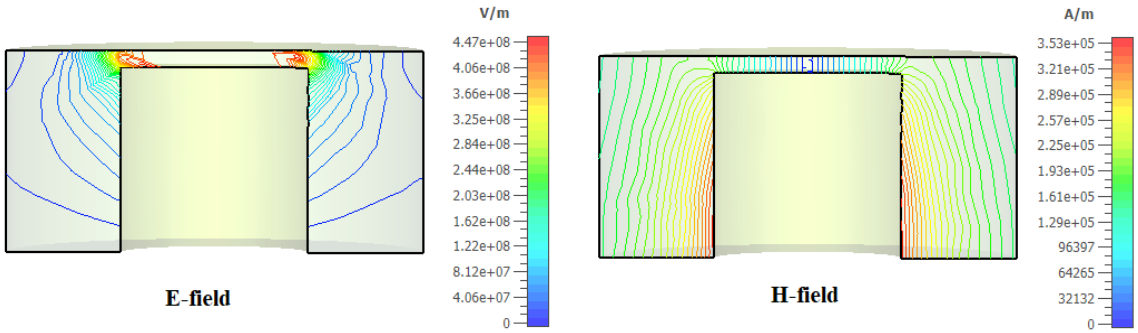

Figure 2.12 Simulation field patterns of a re-entrant cavity resonator.

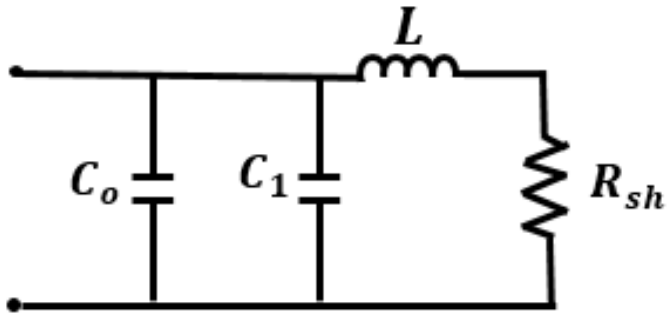

Figure 2.13 Equivalent lumped element circuit of re-entrant cavity

The mathematical expression for equivalent circuit is described by the following equations [53]:

The total equivalent capacitance C_e of the cavity is given by

$$C_e = C_o + C_1 \tag{2.19}$$

where C_o is the gap capacitance assumed to be a parallel plate defined by the relation

$$C_o \approx \frac{\varepsilon_o \pi {r_o}^2}{d} \tag{2.20}$$

and C_1 is the capacitance of the cavity in relation to the side wall of the post which can be determined by

$$C_1 \approx 4\varepsilon_o r_o \ln \frac{\sqrt{(r_i - r_o)^2 + h^2}}{2d} \tag{2.21}$$

where ε_o is permittivity of free space. The equivalent inductance L and the shunt resistance R_{sh} are defined by the following relationships.

$$L \approx \frac{\mu_o h}{2\pi} \ln \frac{r_i}{r_o} \tag{2.22}$$

$$R_{sh} \approx \frac{2\pi\delta\sigma\omega^2 L^2}{\frac{h-d}{r_o} + \frac{h}{r_i} + 2\ln\frac{i}{r_o}} \tag{2.23}$$

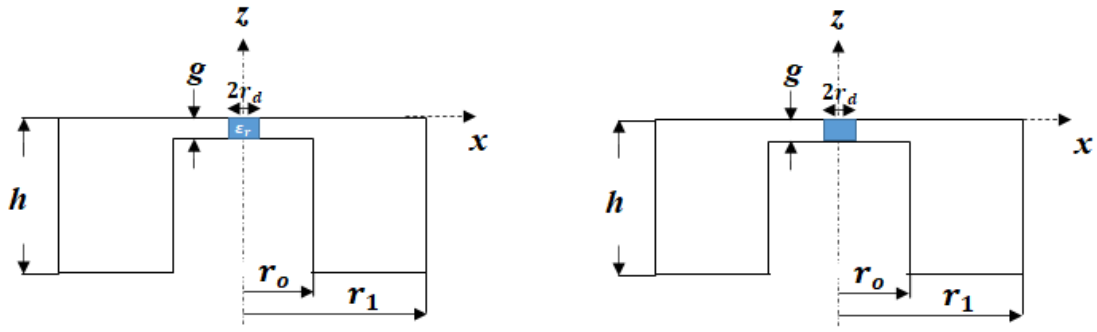

(a) (b)

Figure 2.14 Re-entrant cavity with a gap (a) empty (b) partially filled with a dielectric

where, μ_o is the permeability of free space, δ is the skin depth, and σ is the metal conductivity. The cavity resonant frequency f_r and the unloaded Q-factor Q_u can be calculated using

$$f_r = \frac{1}{2\pi\sqrt{LC_e}} \tag{2.24}$$

$$Q_u = \frac{\omega L}{R_{sh}} \tag{2.25}$$

From the equivalent lumped circuit and the expression given in (2.20) and (2.21) we can write the expression for the equivalent circuit of an empty gap region shown in Figure 2.14 (a) in the cavity as follows [54]:

$$C_e \approx \frac{\varepsilon_o \pi r_o}{d}(r_o + 2\ln\sqrt{(r_i - r_o)^2 + h^2}). \tag{2.26}$$

When a dielectric material of ε_r is placed into the active gap region of the re-entrant cavity where the field is strong as shown in Figure 2.14 (b) a new perturbed capacitance emerges. In this case the gap capacitance is made of two concentric regions of the inner and outer region containing the sample dielectric constant and air respectively. The new capacitance in this region is given by

$$C_0^* \approx \frac{\varepsilon_o \pi}{d}[({r_d}^2(\varepsilon_r - 1) + {r_o}^2) + 2r_o \ln\sqrt{(r_i - r_o)^2 + h^2}] \tag{2.27}$$

These equations represent the approximate formula for the equivalent gap capacitance of re-entrant cavity resonator with a narrow gap shown in Figure 2.14. Generalised treatment of various re-entrant cavity geometries can be found in [55]. This simple approximation formula can be adopted to derive an approximate perturbation formula for complex permittivity of a dielectric material.

2.4 Microwave Cavity Quality Factors

Quality factor is an important quantity in microwave measurement, and it is defined as the ratio of the energy stored in the cavity to the average energy lost [50]. Here the energy can be lost in a number of mechanisms, depending on the structure of the cavity. The most significant is the loss due to conductor currents in the cavity walls. Other losses may arise due to non-zero loss tangent of the dielectric material filling the cavity and losses due to radiation in the presence of an open aperture in the cavity. In permittivity measurement, irrespective of cavity structures, the evaluation of dissipation factor is based on measuring the loaded Q-factor Q_l. The unloaded Q-factor Q_u is associated with the total loss from the aforementioned loss mechanisms and can be calculated using

$$\frac{1}{Q_u} = \frac{1}{Q_c} + \frac{1}{Q_d} + \frac{1}{Q_r} \tag{2.28}$$

Alternatively, this can be calculated from the measured loaded Q-factor given by [50].

$$Q_u = \frac{Q_l}{1 - |S_{21}(f_r)|} \tag{2.29}$$

where Q_c is the conductor loss, Q_d is the dielectric loss and Q_r is the loss due to radiation in (2.28), while S_{21} is the transmission coefficient and f_r is the resonant frequency in (2.29). Typically, it is assumed that if $S_{21}(f_r) \ll 1$ then $Q_u \approx Q_l$. However, in this project this is not assumed and (2.29) is used to extract the unloaded Q-factor throughout the thesis.

Additional energy loss is introduced as a result of coupling to an external circuit, known as the coupling loss. Therefore, the loaded Q-factor of the cavity (which refers to a resonator coupled with an external circuit) whose relationship with the unloaded Q-factor depends on the coupling coefficient is given by [56]

$$\frac{1}{Q_l} = \frac{1}{Q_u} + \frac{1}{Q_e} \tag{2.30}$$

Alternatively,

$$S_{21}|_{dB} = 20\log(Q_l/Q_e) \tag{2.31}$$

where Q_e is the so-called external Q-factor. Theoretically, the unloaded Q-factor can be estimated based on the frequency wavelength (λ), skin depth of the cavity material (δ), the height (h) and the radius (r) of the cavity. For example, in conventional cylindrical cavity operating at the TM_{010} mode, the unloaded Q-factor is given by [47]

$$Q_u = \frac{\lambda}{\delta} \times \frac{2.405}{2\pi\left[1 + \frac{r}{h}\right]} \tag{2.32}$$

In practice the loaded Q-factor can be determined experimentally in a two-port measurement system by simply taking the ratio of resonant frequency and 3 dB bandwidth (half power point) of the transmission responses as demonstrated in Figure 2.15. The resonator bandwidth is related inversely proportional to the Q-factor and therefore high Q-

factor resonator would have a narrow bandwidth. To achieved high Q-factor or have loaded Q-factor approximately equal the unloaded Q the coupling is made weak (coupling coefficient << 1) [57].

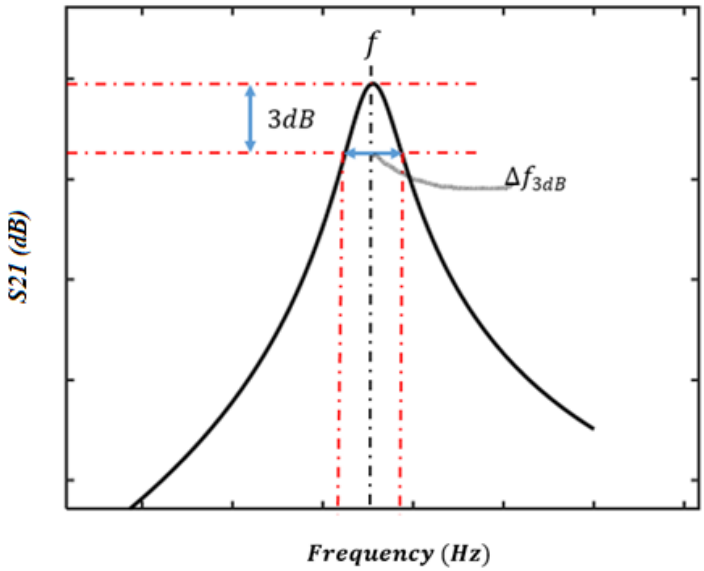

Figure 2.15 Typical resonant peak and associated parameters

The loaded Q-factor can be computed from the resonance response using the expression given by:

$$Q_l = \frac{f_r}{\Delta f_{3dB}} \tag{2.33}$$

2.5 Dielectric Materials and their Interaction with Electromagnetic Fields at Microwave Frequency

Understanding the interaction of material with EM field at microwave frequencies is an important phenomenon in the design of microwave-based resonator sensors and

applicators, especially for dielectric materials such as liquids. This is because the electrical properties of the interested material become part of the device's functionality [58]. Processing the dielectric properties of materials using a microwave resonator sensing device requires a better understanding of the materials and how they respond to the applied field. For this, the interaction mechanism should be fully discussed, first by understanding the types of liquids, the dielectric properties of the materials and the dielectric polarisation.

2.5.1 Polar and Non-polar Liquids

For material characterisation such as liquids, it is important to understand the liquids in terms of polarity. Generally, liquids are classified into polar and non-polar. Polar liquids are those made of molecules that have permanent electric dipole moment (i.e. positive charge on one side and negative charge on the other). Whereas non-polar liquids are those whose molecules share electron equally, there is no net electric charge across the molecule [59]. Polar liquids have a higher permittivity ε (typically ranging from 10 -100) than non-polar liquids which is between (2 and 3), with the permittivity value determining the extent of being polar. That is, the higher the dielectric constant, the more of the energy is stored in the presence of an electric field. The most common examples are highly purified water and ethanol as polar liquids, while silicon oil and hydrocarbon liquids as non-polar liquids. The dielectric loss value is also higher in polar than non-polar with magnitude in the order of 10^{-1} and 10^{-3}, respectively [20].

2.5.2 Dielectric Material and Complex Permittivity

Material interactions with electromagnetic field at microwave region are of many kinds. The general electrodynamic properties of matter, permittivity ε, permeability μ and

conductivity σ, determine their complete behaviour as the materials interact with EM energy at microwave region. Most specifically, the electric permittivity or dielectric constant provides information on the polarisation of the dielectric materials [60].

Dielectric material normally cannot participate in electric conduction as most of the charge carriers are bound. However, applying an electric field to the material may cause the bound charges to be displaced. This displacement causes the atom to become polarised. The interaction between wave and dielectric material results in two main polarisation phenomena: the storage of energy within the medium and thermal conversion. These main points are expressed as the complex permittivity of the material given by (with the storage of electromagnetic energy expressed by the real part whereas the thermal conversion to the imaginary part) [61].

$$\varepsilon = \varepsilon' - j\varepsilon'' = \varepsilon_o \varepsilon_r' - j\varepsilon_o \varepsilon_r'' \tag{2.34}$$

where ε_o is the dielectric permittivity of a vacuum,

ε' and ε'' are the real and imaginary parts of the complex dielectric permittivity.

ε_r and ε''_r are the real and imaginary parts of the relative complex dielectric permittivity.

2.5.3 Dielectric Polarisation

Polarisation plays a significant role in determining the conductivity and losses in materials dielectric characterisation. The complex permittivity is defined by (2.34), which relates to a material's ability to respond to the electric field by its polarisation. The real part of the complex permittivity is a measure of the amount of polarisation while the imaginary part gives the measure of the losses involved in the polarisation processes [62]. There are number of active polarisation mechanism relating to permittivity of a dielectric material as illustrated by the frequency dependent polarisation spectrum in Figure 2.16.

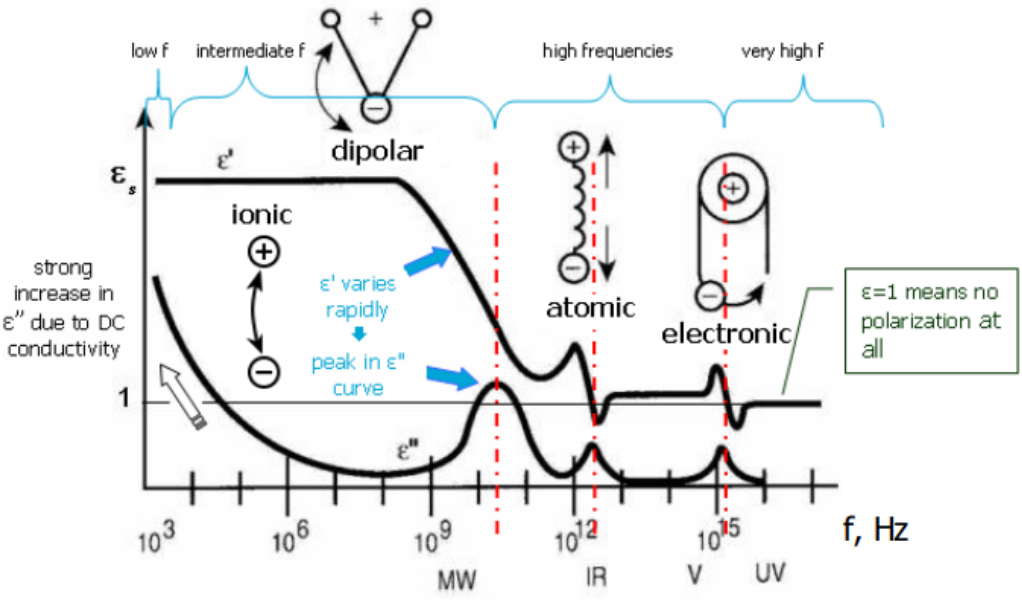

Figure 2.16 The polarization spectrum over a wide range of frequencies [60]

These mechanisms include ionic conduction which influences the permittivity at the lower and intermediate frequencies range; dipolar relaxation causing the variation of permittivity in the microwave frequencies range, while absorption peaks at high frequencies such as infrared and ultraviolet is mainly due to atomic and electronic polarization [62]. Beyond these, at very high frequencies (i.e optical) even the electrons cannot withstand the changing field, therefore no polarisation and result of the relative permittivity equal to 1. Polarisation mechanism can be generally classified into three or four main categories as described below [59] [63].

1) Displacement Polarisation

This type of polarisation is further classified into electronic polarization and ionic or atomic polarisation. The displacement of the electron charges surrounding the nuclei as a result of the influence of external electric field, resulting in an induced dipole moment is referred to as the electronic polarisation. In electronic polarisation, there is no dipole

moment in the absence of an applied electric field and the net charge around a neutral atom is zero as shown in Figure 2.17. When electric field is applied the displacement of the charge occurs, resulting in an induced dipole moment. This type of polarisation only takes place in hydrocarbon, a common example is hexane. The ionic polarisation occurs when positive and negative ions or atoms are displaced within molecules and crystal structures as a result of the applied electric field from their equilibrium position. In this case, the net dipole moment is no longer zero as illustrated in Figure 2.18 [63]. An example of such crystal is sodium chloride NaCl.

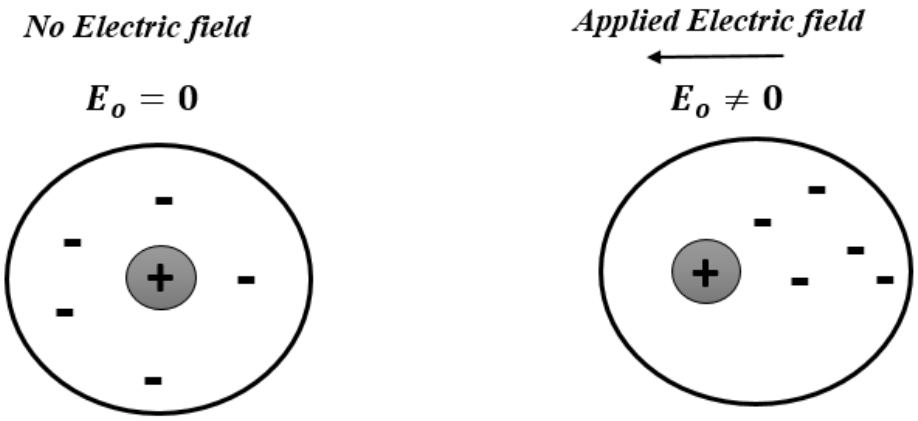

Figure 2.17 Electronic polarisation in a dielectric material

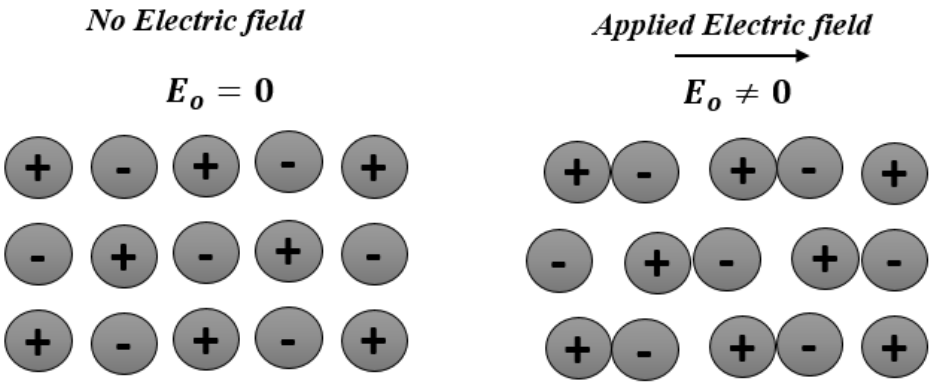

Figure 2.18 Ionic polarisation in a dielectric material

2) Orientation Polarisation

This type of polarisation takes place in liquids and gases materials such as water and hydrogen chloride whose molecule contain permanent dipole moments. The molecules are randomly oriented when no electric field is applied. This is due to thermal activation and the net dipole moment is zero. When electric field is applied, the asymmetric (polar) molecules will be aligned in parallel to the direction of the applied field. During the rotation of the dipole due to applied electric field in order to align with the field under microwave frequencies, a phase difference exist between the orientation of the field and that of the dipole. This is due to time lag between field and dipole orientation. Figure 2.19 shows the orientation polarisation of a polar dielectric [59] [63].

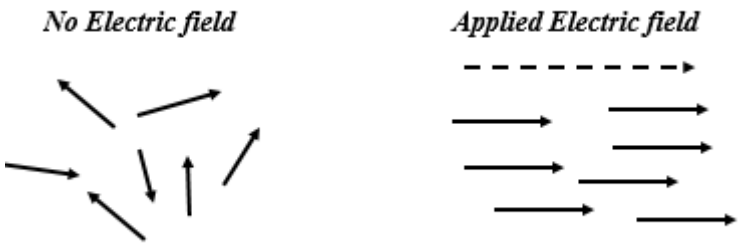

Figure 2.19 Orientation polarisation in a dielectric material

3) Space Charge Polarisation

This is also known as interfacial polarisation and occurs in heterogeneous dielectric material (solid material such as crystalline). The positive and negative ions are equal in such material, and therefore the charges do not separate in the absence electric field. When an external electric field is applied, the more mobile charge carriers in the dielectric are displaced. This causes them to move towards the opposite polarity electrode surfaces resulting into interfacial polarisation [59] [63].

2.6 Debye Model

The Debye model is one of the means used in determining the complex permittivity of fluids. It can be used to generate simulation results for liquids under measurement by coding the equation into the simulation software [64]. The behaviour of a polar dielectric is described by the Debye equation at various resonant frequencies. To compute the dielectric constant and loss factor, the Debye parameter $(\varepsilon_\infty, \varepsilon_s, \tau)$ for known liquids at room temperature are used. These parameters are temperature dependent due to the presence of relaxation time. [65]. The Debye model is given by

$$\varepsilon(\omega) = \varepsilon_\infty + \frac{\varepsilon_s - \varepsilon_\infty}{1 + j\omega\tau} \tag{2.35}$$

where ε_∞ is permittivity at infinite frequency and ε_s is the static permittivity and τ is the relaxation time. For $\varepsilon(\omega) = \varepsilon' - j\varepsilon''$

Equation (2.35) can further be simplified to real and imaginary part of the complex permittivity as

$$\varepsilon' = \varepsilon_\infty + \frac{\varepsilon_s - \varepsilon_\infty}{1 + \omega^2\tau^2} \tag{2.36}$$

$$\varepsilon'' = \varepsilon_\infty + \frac{(\varepsilon_s - \varepsilon_\infty)\omega\tau}{1 + \omega^2\tau^2} \tag{2.37}$$

The detailed derivation is given in [66] and this approach has been utilised by many authors for validation of measured polar solvent extracted using design dielectric measurement sensors [65].

2.7 Relaxation Time

When an electric field interacts with materials, it takes time for the dipoles to orient themselves. The measure of the mobility of dipoles that exist in the material is referred to

as relaxation time [64]. Materials such as liquid and solid have molecules that have limited ability to move when electric field is applied due to their condense state. As a result of constant collisions and internal friction is caused. The molecules then begin to turn slowly and exponentially approaching a final state of orientation polarisation with relaxation time constant τ. When the electric field is turn off, the process is reversed, and random distribution is restored for the same relaxation time constant. The time constant is inversely related to the relaxation frequency as given by the relationship below [24]:

$$\tau = \frac{1}{\omega_c} = \frac{1}{2\pi f_c} \tag{2.38}$$

The characteristic response in permittivity as a function of frequency for methanol at temperature of 25 °C is shown in Figure 2.20. The Debye relation given in (2.35) can be used to model materials that exhibit single relaxation time constant as given by the characteristic curve. The electric field interaction with material is slow enough to keep the dipoles at pace with field variations at frequencies below relaxation. This is because of the ability of the polarisation to develop fully; the loss factor relates directly proportional to the frequency as shown in Figure 2.19. With increase in the frequency the loss factor ε'' continue to increase but the dielectric constant ε' begins to decline due to the phase lag between the electric field and dipole alignment. Both ε' and ε'' decline at frequencies above relaxation frequency as the electric field interaction with material is too fast to influence the dipole rotation, as such the orientation polarisation disappears [24]. The Debye relaxation logarithm plots for the relaxation model parameters given in Table 2.3 is shown in Figure 2.20 and Figure 2.21 for methanol and ethanol solvents using (2.36) and (2.37) over a frequency range respectively.

Table 2.3: Debye relaxation model parameters of common solvent [67]

	Temperature (°C)	ε_s	ε_∞	τ **(ps)**
Methanol	25	32.5	5.6	51.5
Ethanol	25	24.3	4.2	163

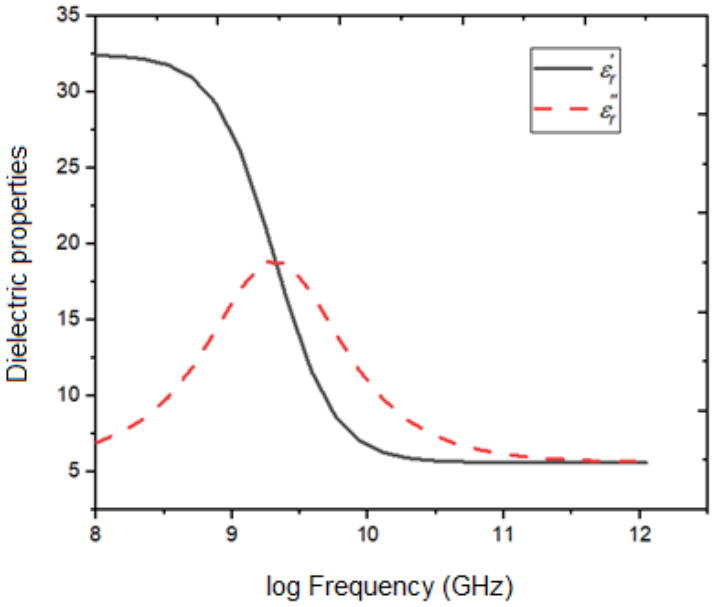

Figure 2.20 A typical Debye relaxation characteristic curve for methanol

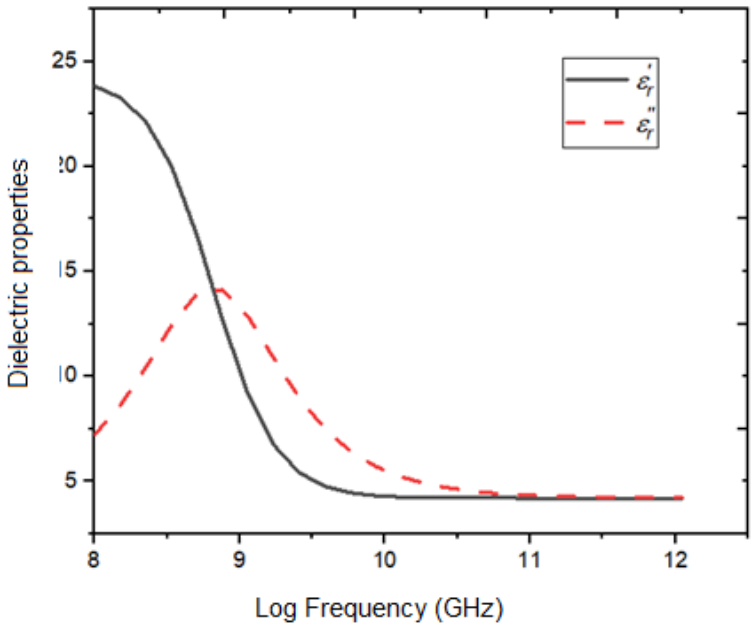

Figure 2.21 A typical Debye relaxation characteristic curve for ethanol

2.8 Cavity Perturbation Theory

The small change or modification in volume by introducing a small piece of a dielectric or metallic material in a cavity resonator is referred to as cavity perturbation [52]. The perturbation method is commonly used in the extraction of complex permittivity of the dielectric sample measured. They are considered to work better for measurement of low-loss and medium-loss dielectric material. However, the method is less useful if the material under measurement is of extremely low-loss dielectric property. This is because, for an empty cavity with low *Q*-factor the power dissipation may be much larger than the loss due material under measurement and this hardly affects the *Q*-factor. In this case, the extraction of the correct value of the loss factor or the imaginary part of the complex permittivity cannot be accurate [26]. The perturbation method is an approximate method arrived based on a number of assumptions as will be discussed later. The introduction of dielectric sample in a region of high electric field results in changes in resonant frequency

and the *Q*-factor associated to the polarisation and dielectric loss of the material, respectively [29]. The generalised approximate equation for the change in angular resonant frequency of the perturbed cavity due to the material perturbation based on Maxwell's curl equations is given by the expression [47], and this equation is based on the assumptions that the perturbation is small, and the cavity wall is perfectly conducting.

$$\frac{\omega_2 - \omega_1}{\omega_2} \approx \frac{-\int_{V_s}(\Delta\varepsilon E.E_o^* + \Delta\mu H \cdot H_o^*)\,dv}{\int_{V_c}(\varepsilon E.E_o^* + \mu H \cdot H_o^*)\,dv} \quad (2.39)$$

where ω_1 and ω_2 are the resonance frequency of the original cavity and perturbed cavity respectively. $E$and H are the perturbed field, whereas E_o, H_o are the original field.

The change in the permittivity ($\Delta\varepsilon$) and change in the permeability ($\Delta\mu$) are defined by

$$\Delta\varepsilon = \varepsilon_2 - \varepsilon_1\,, \Delta\mu = \mu_2 - \mu_1 \quad (2.40)$$

where μ_1, ε_1 and μ_2, ε_2 are permeability and permittivity before and after perturbation.

For small perturbation of the resonance cavity, the volume of the sample is very small compared to the volume of the cavity, and then we can assume that $E = E_o^*$. Similarly, we assume that the medium inside the cavity is air (vacuum) therefore $\varepsilon_1 = 1$, and $\mu_2 = \mu_1 = 1$.

For a non-magnetic component, equation (2.39) becomes

$$\frac{\omega_2 - \omega_1}{\omega_2} = -\frac{\varepsilon_r - 1}{2}\frac{\int_{V_s}E.E_o^* dv}{\int_{V_c}|E|^2 dv} \quad (2.41)$$

where, ε_r is the relative complex permittivity of the material (sample) defined as $\varepsilon_r = \varepsilon_2/\varepsilon_0$

The real resonant frequency and the *Q*-factor of a resonant cavity is associated with the angular frequency as complex quantity written as

$$\omega_n = \omega_{r,n} - j\omega_{i,n} \quad (2.42)$$

where $\omega_r = 2\pi f_r$ and the Q-factor is defined as $Q = \omega_r/2\omega_i$.

If we consider $\delta\omega/\omega = (\omega_2 - \omega_1)/\omega_2$ where ω_2 and ω_1 are complex with respect to (2.42); and we assume $\omega_{r1} \approx \omega_{r2}$ and $\omega_i \gg \omega_r$, then we have

$$\frac{\delta\omega}{\omega} = \frac{(\omega_{r2} - \omega_{r1}) + j(\omega_{i2} - \omega_{i1})}{\omega_{r2}\left(1 + \frac{j\omega_{i2}}{\omega_{r2}}\right)} \tag{2.43}$$

If we expand, simplify and further assume $Q_2 \gg 1$, we approximately have

$$\frac{\delta\omega}{\omega} \approx \left(\frac{f_0 - f_1}{f_0}\right) - \frac{j}{2}\left(\frac{1}{Q_1} - \frac{1}{Q_0}\right) \tag{2.44}$$

Equating (2.41) and (2.44) and for $\varepsilon = \varepsilon' - j\varepsilon''$ we have the perturbation formula

$$2\left(\frac{f_1 - f_0}{f_0}\right) = (\varepsilon' - 1)\frac{\int_{V_s} E.E_o^* dv}{\int_{V_c} |E|^2 dv} \tag{2.45}$$

$$\left(\frac{1}{Q_1} - \frac{1}{Q_0}\right) = \varepsilon''\frac{\int_{V_s} E.E_o^* dv}{\int_{V_c} |E|^2 dv} \tag{2.46}$$

Let

$$N = \frac{\int_{V_s} E.E_o^* dv}{\int_{V_c} |E|^2 dv} \tag{2.47}$$

The expression *N* is assumed to be constant, which is independent of the properties of the material constant term in cavity-perturbation for permittivity measurement. However, the perturbed field due to the presence of sample is dependent of the permittivity, shape and size in respect to (2.47). Therefore, the parameter *N* changes from case to case. The change in quality factor is related to both the real and imaginary part of the permittivity of the sample shown by (2.46). Therefore, in order to make the expression clearer, A and B are introduced to replace N and can be rewritten as

$$\varepsilon' = A^{-1}\frac{V_c}{V_s}\left(\frac{f_1 - f_0}{f_0}\right) + 1 \tag{2.48}$$

$$\varepsilon'' = B^{-1}\frac{V_c}{V_s}\left(\frac{1}{Q_1} - \frac{1}{Q_0}\right) \tag{2.49}$$

where f_1, f_0 and the coefficient constant A and B are determined by the shape, size configuration, location of sample and mode of excitation. They can be determined analytically or empirically using experimental calibration. These two equations are arrived at based on following three assumptions [68]:

- That introducing the sample does not change the electric field in the cavity and the energy stored remains the same with and without the sample;
- That the loss of the conductor wall is negligible;
- That the quality factors are measured at the same frequency.

However, the first two assumptions cannot be strictly fulfilled experimentally, while the third one provides a means of experimentally attaining the high accuracy without strictly fulfilling the first two assumptions.

The perturbation theory has been used over the years, since its first introduction by Bethe and Schwinger for complex permittivity measurement [69]. This method has conventionally been the most common approach use for resonator-based dielectric characterization of materials at microwave frequency range. The method is considered simple due to the easy calculation process of the dielectric properties. However, the formulation of the perturbation techniques assumes that the volume of sample under consideration is small compared to the volume of the cavity. The coefficient of A and B in (2.48) and (2.49) are determined based on configuration of the resonators. The traditional method of the perturbation theory is limited and therefore requires some modification to accurately evaluate the permittivity value of the material under test. To address these factors, the conventional cavity perturbation theory has been modified for various

geometry and for the measurements of low, medium and high loss materials over the years [70]. This is further discussed in Chapter 3.

2.9 Summary

In summary, this chapter has highlighted and discussed the principles of dielectric materials measurements within the microwave frequencies. The four (4) measurement techniques use in materials characterisation have been discussed and the methodology consider for this work have also been emphasised. This is based on resonant method using cavity resonator. The interaction of materials with EM field at microwave frequency has also been explained briefly. The measurements of materials considered in this work especially for the hydrocarbon liquids, the interactions of the material with EM field are based on electronic polarisation. Conventional cavity perturbation theory has been utilised for dielectric characterisation of materials in using conventional cavity structures as described in this chapter. However, it has some shortcomings due to number of assumptions associated with the expression and its limitations in terms of applications. A new approach is proposed for this work and will be discuss in subsequent Chapters.

CHAPTER THREE: LITERATURE SURVEY

This chapter presents the literature survey of cavity-based resonators for dielectric characterisation of materials. The survey covers the use of various conventional and unconventional cavity resonator structures at both lower and higher frequencies. A comparison in terms of frequency, quality factor, cavity geometry, applications, and fabrication method are given in Table 3.1. In addition, method of extractions of the dielectric properties, type of excitation and modes used for the material measurements has also been captured in the table. Some topologies of the cavity resonators discussed are also presented in Figure 3.1 to Figure 3.12. This chapter has therefore provided the trend, progress and challenges of cavity resonators for complex permittivity measurements over the years and how the research of this thesis comes in.

3.1 Background of Cavity Resonators

Cavity resonators have been utilized for dielectric measurements since it was introduced by Willis Jackson in 1941 and Penrose 1946 utilising electric field mode resonator and magnetic field mode resonator, respectively [71]. Following these advents, various geometries have been exploited in designing cavity resonator sensors in the microwave frequency range for complex permittivity measurements. For a waveguide cavity resonator, as the frequency increases the size of the cavity becomes smaller, making it difficult to realise. However, various approaches and techniques were utilized in designing cavity resonators for measurements up to 0.24 THz [26] as will be discussed in the subsequent Sections.

3.2 Cavity Geometries

3.2.1 Cylindrical Cavities for Materials Measurements

The most common type and widely used cavity is the cylindrical cavity resonator. For example, a cylindrical cavity using TM_{010} mode shown in Figure 3.1 (a) used for the measurements of moisture content and specific mass of MUT is presented in [72]. An analytical model was derived for the extraction of the complex permittivity for the $TM_{010,}$ which derives from a TM_{01} mode propagating in a cylindrical waveguide. In [43] a rigorous electromagnetic analysis using the Ritz-Galerkin method to convert the effect associated with insertion holes, sample holder (tube), and air gaps between the dielectric tube and sample insertion holes using cylindrical cavity has been reported. The authors have later in [73] verified their method in comparison with cavity perturbation to mitigate the challenges of calculation and sample positioning error associated with perturbation theory. The cavity structure is shown in Figure 3.1 (b). A through-hole radially placed samples for measurements at a position of high electric field assumes uniform distribution of the field, while this is not the case in practice. This non-uniformity of the field in the sensing region results in detuning of the resonant frequency that is not desired in some cases. For this, cylindrical cavity with metallic sheet of finite thickness placed symmetrically in the centre along the cavity diameter with at an aperture is reported [74].

Others include circular cylindrical cavity resonator for complex permittivity measurements of substrate materials using higher order TE odd modes [75]. This is to take the advantage of a high *Q*-factor, which offers better resolution and enable accurate loss factor measurement. An analysis of the perturbed mode and derivation of the expression for the relative permittivity and loss tangent measurements are provided. Few cavities with different dimensions were fabricated to demonstrate the proposed concept to cover

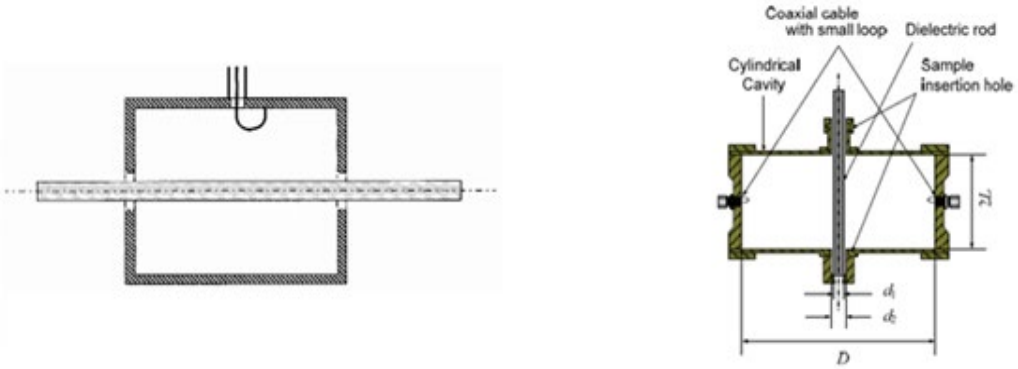

(a) (b)

Figure 3.1 Cylindrical cavity resonator structure: (a) radially placed sample [69] (b) axially placed sample [70]

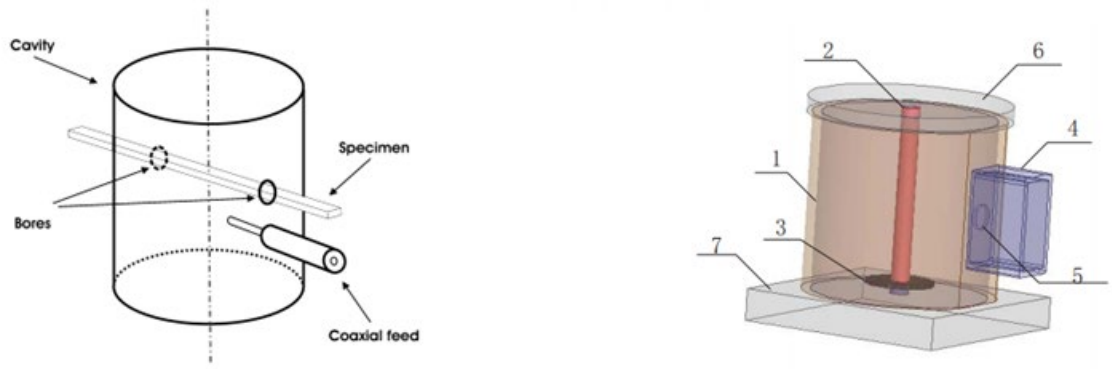

(a) (b)

Figure 3.2 Cylindrical cavity resonator structure with single port: (a) single port coaxial probe feedline [72] (b) single port waveguide feed line [73].

frequency range from 2 – 20 GHz [75]. The cavities were energised via an adjustable screw coupling method to meet the coupling factor of the diverse modes of TE_{111}-TE_{117} as shown in Figure 3.2 (a). Results obtained have shown excellent agreement with literature values for the substrate materials measured [75]. In order to avoid other interfering modes, the TE_{011} has been used to demonstrate the use of cylindrical cavity for dielectric

characterisation based on simulations [76]. As shown in Figure 3.2 (b) microwave-absorbing layer (no 3 in the figure) placed in the cavity was used to absorb the disturbing modes. Several liquids were simulated to illustrate the capabilities of the cavity for the intended usage.

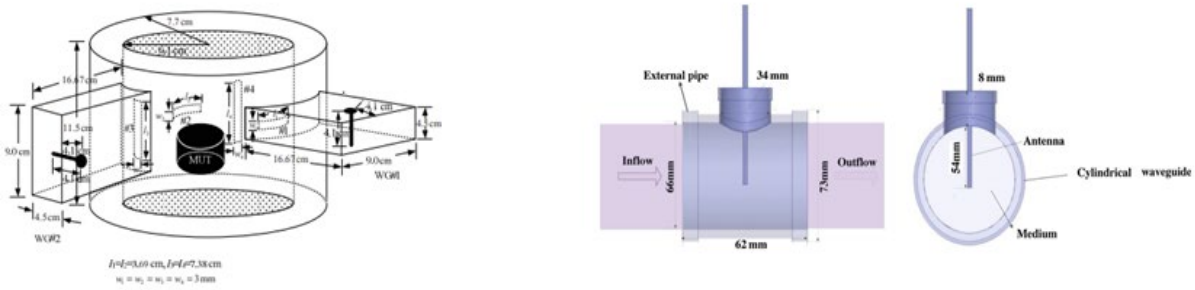

(a) (b)

Figure 3.3 Cylindrical cavity: (a) concentric cavity resonator [74] (b) both end open structure [75]

Another cavity resonator is the concentric cylindrical cavity that was utilized for both solid and liquid dielectric properties measurement in [77]. Both transmission and resonant frequency techniques were utilised in the measurements and results were compared. The resonant method is achieved by terminating one end of the probe with dummy load whereas the transmission techniques utilises both electric probe for the measurements. Figure 3.3 (a) shows the cavity geometry and how samples are placed for measurements. In [78] a novel cylindrical cavity structure with both end open has been reported for microwave materials characterisation. The cavity is designed in such a way that, liquids will be passing through the bulk of the cavity energised through a vertically placed feed antenna at one side of the cavity as shown in Figure 3.3 (b). The feedline is insulated with a thin layer to avoid any short-circuit due to charged ions from measured materials and corrosive substances. Concentration measurements have been demonstrated

and results were promising with some associated error for the intended use. However, the extraction of the dielectric properties of the materials involved has not been considered in their work [78]. In contrast to this, an open-ended cylindrical cavity has been proposed [79], the cavity is filled with a dielectric material of low permittivity (for better sensitivity) and the flat open end becomes the testing point as shown in Figure 3.4 (a).

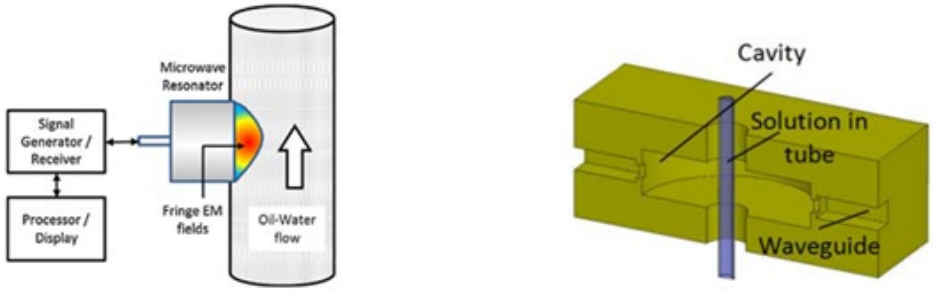

(a) (b)

Figure 3.4 Cylindrical cavity resonator: (a) one end open structure [76] (b) higher frequency cavity [77]

The electromagnetic fringing fields penetrate into the MUT when brought in contact with the open end and the resonance properties is measured. Although the concept has been validated using low loss materials (oils) with very low percentage of water content, however, due to it low *Q*-factor the application to water-liquid ratio measurement can be disadvantageous. This low *Q*-factor is attributed to the choice of the metal use in fabrication, radiation loss due to large opening and dielectric loss of the material filling the cavity [79]. In [80], a cylindrical cavity was used for dielectric measurement at higher frequency using the higher order mode of TM_{npq} mode, in contrast to the dominant TM_{010} mode widely used for the material measurements using cavity perturbation. This is to combat the challenge of cavity size, which becomes too small to be manufacture accurately as the frequency becomes high. The weaker electric field region was used to exposed the

sample in contrast to the conventional way of using the point of higher electric field for the perturbation of the MUT. The cavity structure is shown in Figure 3.4 (b).

3.2.2 Rectangular Cavities for Material Measurements

Rectangular waveguide cavities have also been extensively studied and used for dielectric material measurements. A detailed design and fabrication of a rectangular cavity for concentration measurements of liquid materials has been reported in [45]. The choice of rectangular cavity instead of cylindrical cavity which offers a high *Q*-factor is the ease of fabrication as claimed by the authors. Parametric study was carried out and the best location and length of the probes based on transmission configuration was chosen as shown in Figure 3.5 (a) to achieve the optimum *Q*-factor. Similarly, simulations were run to choose the appropriate inner diameter of the tube for the intended usage. As expected, large volume of MUT gives better sensitivity with higher frequency shift and the coefficient of transmission decreases accordingly. The cavity sensor was then validated with measurement of binary solutions [45].

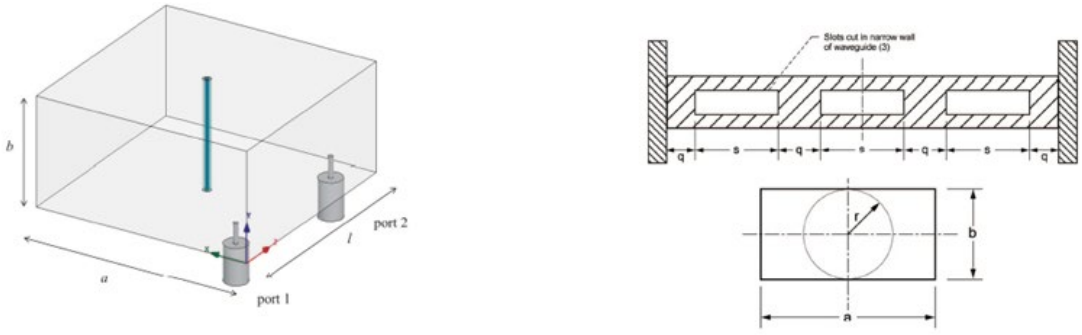

(a) (b)

Figure 3.5 Rectangular cavity: (a) liquid sensor waveguide [42] (b) Gas sensor waveguide [78]

An X-band rectangular cavity made of a stainless steel without coating has been used for dielectric measurements of gas [81]. Special semi-rigid coaxial cable and coaxial launcher that can withstand both temperature and pressure were used in connecting the sensor enabled by coaxial to waveguide transition. Slots covered with a stainless-steel mesh wire made at the narrow walls of the waveguide are used to allow gas flow into the cavity as shown in Figure 3.5 (b). Results obtained signifies the potential use of the method for gas sensing application [81]. In [82] a rectangular cavity has also been used to demonstrate the measurement of solid materials with an arbitrary cross-section. This was achieved using a hybrid electromagnetic method (combined extended spectral domain approach and mode-matching method) to evaluate the dielectric properties of the sample at X-band [82].

Others includes a reflection measurement based rectangular cavity for the extraction of dielectric properties of solid, liquid and powdered materials at millimetre wave presented in [83]. The measurement is in a way that, a section of WR-51 waveguide is filled with high density polyethylene (HDPE) plastic fixture. It is designed to contain a cylindrical shape sample placed at the centred as shown in Figure 3.6 (a). The measured dielectric properties of material agreed well with the literature values for the chosen mode. However, the choice of material filling the cavity has a significant effect on the *Q*-factor and also the suitability of the method for liquids and powdered samples which was the motive has not been shown. The authors [84] have demonstrated based on simulations the utilisation of an X-band and Ku-band frequencies for complex permittivity measurement using a rectangular cavity resonator. The cavities were designed to have three sections of waveguide, one section to serve as the sample holder. The section was filled with the MUT, and simulations were run to obtain the scattering parameters for the extraction of the

dielectric properties. The results were then compared with calculated values obtained using Debye equations and agrees well over the frequency range. Though the simulations results looks promising, however, practical utilisation of such designed presents a major challenge considering the sample insertion method [84].

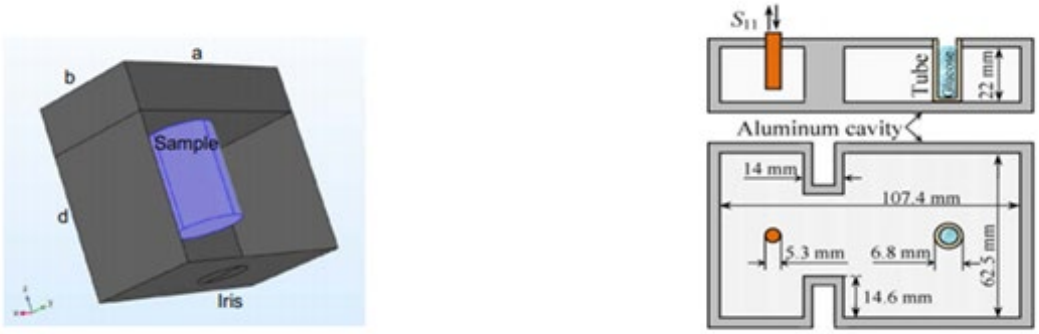

(a) (b)

Figure 3.6 Rectangular cavity: (a) sample inside waveguide; [80] (b) sampled in a one-open-end tube [82]

Another interesting rectangular cavity structure operating at 4.75 GHz based on reflection measurements method has been described [85]. The cavity was made using aluminium with an opening created at the top of the cavity where the sample is exposed. As an alternative of having a through-hole using both end open tube to pass in the samples, only one-end opening was made and a capillary tube with one open-end is utilised for the measurements as demonstrated in Figure 3.6 (b). One of the challenges associated to measurement at higher frequencies is the accuracy of the measurements. To improve the accuracy of permittivity measurements at higher frequency, higher order mode needs to be selected to use the perturbation theory. For this, an analysis and optimization of rectangular cavity resonator design have been given in detailed [85]. In [86] rectangular cavity for dielectric characterization in J-band has been reported. To combat the challenge of inserting sample into the cavity as the size becomes small with increase in frequency, a

different approach was adopted. The sample is placed in a close proximity and the electric field of the cavity is evanescently coupled to the sample through an opening at the top of the cavity as shown in Figure 3.7 (a). The measured results have shown a promising performance for dielectric materials characterisation. However, for higher values of dielectric constant, low frequency shift was observed as opposed to the expectation. This can be due to reduction in electric field strength resulting from the coupling and the dielectric of the materials under measurements [86].

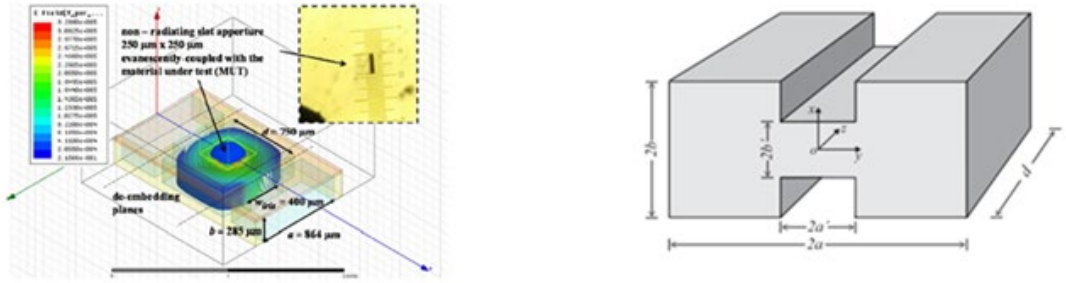

(a) (b)

Figure 3.7 Rectangular cavity: (a) Evanescently-coupled structure [83] (b) Doubled-ridged structure [84]

In [87], a doubled-ridged rectangular cavity was proposed to increase the bandwidth of the operational frequency in rectangular cavity Figure 3.7 (b). The novelty was to overcome the use of single-mode configuration, and thereby enabling multiple frequency measurements using a single device. Detailed derivation to arrive at the coefficient of proportionality based on the cavity geometry using cavity perturbation method has been presented. However, due to limitations of this technique resulting from number of assumptions associated with theory. The author has outlined and adopted two ways to improve the accuracy of the results of the measurement as detailed in the paper. This has led to the derivation of a modified measurements equation for the extraction of

the complex permittivity of the MUT. The device was then validated by permittivity measurements of solid materials using the three resonant modes of TE_{101}, TE_{102}, and TE_{103} and results agrees well with literature [87].

3.3.3 Spherical Cavities for Material Characterisations

Spherical cavity resonator presents higher quality factor compared to all other types of conventional cavity structure resonating at the same resonant frequency [88]. This has made them a good choice cavity resonator for dielectric characterisation in this regard, especially for very lossy materials. In [89], a spherical cavity resonator has been demonstrated as suitable geometry for materials characterisation as shown in Figure 3.8 (a). The authors have shown the used of Bragg effect as potential techniques to determine dielectric properties of materials using spherical resonator. However, sample preparation can be a big challenge in their utilisation for solid materials measurements. Perhaps they can be suitable for gas sensing [22]. Another interesting topology of spherical resonator is the quasi-spherical cavity resonator reported in [10]. The cavity sensor was used for the measurements of noble gases at various temperature and pressures with good accuracy in comparison with other method. In [90] a slightly compressed 3D printed spherical cavity resonator has been presented for dielectric measurement. Squeezing or compressing the cavity was to achieve a single mode with an axially aligned electric field to facilitate measurements as shown in Figure 3.8 (b). This way the other two degenerate modes supported by the spherical resonators are suppressed. A single port bent pin coupling was adopted and placed at a location where better excitation can be attained for the intended usage determined via simulations [90]. The cavity has been validated by concentration measurements of binary samples which shows a better accuracy as expected compared

with planar resonators for the same materials measured by the authors. However, owing to the size of the spherical cavity the measured *Q*-factor of the cavity reported is very low compared to the expected *Q*-factor at the resonant mode. This can be as a result of coupling and choice metallisation of cavity after printing even though the material used for the coating has not been reported.

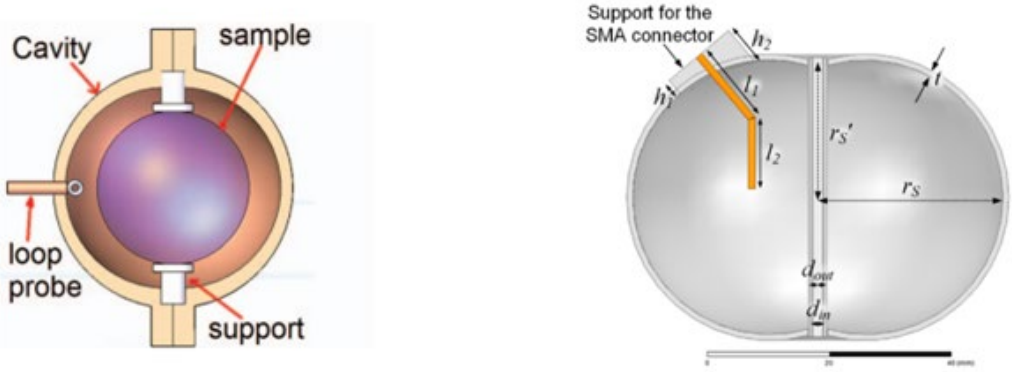

(a) (b)

Figure 3.8 Spherical cavity: (a) For solid samples [86] (b) quasi-spherical cavity for liquids sample [87]

3.3.4 Re-entrant Cavities for Material Characterisations

Re-entrant cavity is also a cavity structure that have been widely utilised for dielectric characterisation. This is due to their confined electric field at the gap region where materials are exposed for measurement as described earlier. In [91], a single re-entrant cavity resonator was designed and used for material measurements. An analysis for the selection of a suitable mode using a finite elements numerical modelling techniques for the intended use has been presented in detailed. This type modelling is now easy with simulations model such as the CST. The higher order mode was used for the dielectric materials measurements due its axisymmetric and uniformity in electric field at the sensing region. The cavity was built in two parts and was machined out of brass metals. To increase

the *Q*-factor and reduce insertion loss a choke was introduced at the mechanical join of the two parts. This is also to enforce the virtual short circuit [91].

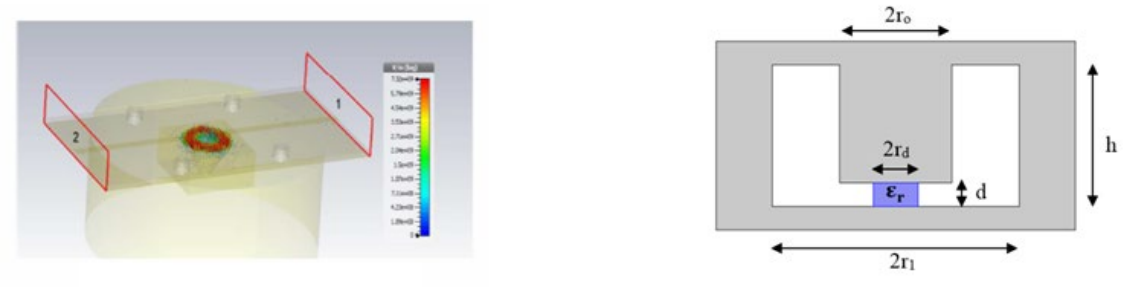

(a) (b)

Figure 3.9 Re-entrant cavity: (a) with microstrip feedline [89] (b) microfluidic sensor based [90]

A novel approach of rectangular cavity with conical central post forming a re-entrant cavity for measurements at S-band is presented in [92]. The cavity was coupled via microstrip feedline through an opening on top of the cavity as shown in Figure 3.9 (a). This is aimed at realising high-*Q* by reducing the effect of external coupling. However, high percentage decrease in *Q*-factor was recorded. This type of approach can be useful for dielectric characterisation at higher frequency when the size of the cavity becomes small and sample insertion becomes difficult [92]. In [93] a microfluidic sensor based on re-entrant cavity was used for low loss materials measurement. The design of the cavity is shown in Figure 3.1 (b) aimed at size miniaturising, high-*Q* and sensitive materials characterisation device at microwave frequency. This is in comparison with conventional cylindrical and rectangular cavity resonating at similar resonant frequency. An approximate formula based on perturbation theory was utilised for the extractions of the dielectric properties of the MUT. The results agree well with simulation results obtained using Debye parameters for each of the samples measured [93].

From the above described and discussed cavity structures, re-entrant cavity resonator is the choose of cavity for this work owing to their reduced size, high *Q*-factor and sensitivity enabled by confined electric field at the central point. However, certain modification would be made to further improve the *Q*-factor and mitigate current build up at the sharp corners of the cavity and post.

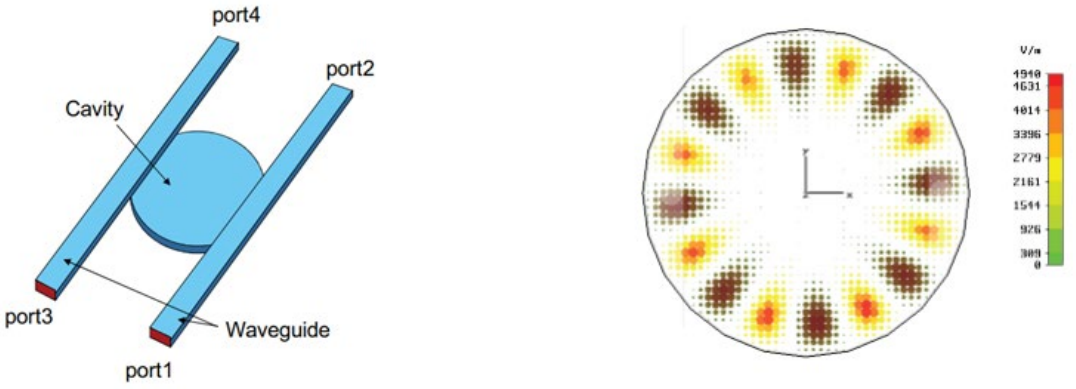

(a) (b)

Figure 3.10 Cylindrical cavity: (a) oversized structure (b) WG electric field pattern *[94]*

3.3 Electromagnetic Modes and Type Excitation

Generally, there are two types of electromagnetic modes in cavity resonator systems used for dielectric characterisations at microwave frequencies. These are pure transverse electric (TE), transverse magnetic (TM) modes [95] and the whispering gallery (WG) mode (for example the cavity structure shown in Figure 3.10) [94]. The choice in any of these modes largely depends on the geometry of the cavity, frequency of operation and applications scenario. The excitations of these resonant modes need a feeding/coupling network which also has an effect on both the resonant frequency and *Q*-factor. This effect results in modifying the resonance properties by shifting the frequency and lowering the *Q*-factor, depending on the degree of coupling [96].

In general, weak coupling is usually utilised to couple energy in and out of the cavity, such that the effect of the coupling becomes negligible, and the loaded *Q*-factor is approximately the same as the unloaded *Q*-factor. This can therefore avoid further and deeper analysis of the coupling coefficients. However, on the other hand, emphasis has always been on the *Q*-factor and not including the loaded frequency, for this an analysis of accurate permittivity measurements independent of coupling level based on coaxial resonator has been presented in detail [96] [97].

There are various number of ways to couple energy into and out of the cavity. The most common ones are the single port and dual ports coupling using coaxial probes for reflection and transmission type configurations, respectively. Others include fringing field method and waveguide coupling using inductive or capacitive iris. For example, two ports straight feed lines [45], two ports loops feeding network [93] and a Subminiature A (SMA) coaxial connector feeding network single port [98] have been used in cavity resonator sensors. Due to micro size of a cavity resonator for dielectric materials measurement at terahertz frequency, a waveguide coupling has been utilised [86]. Similarly, a microstrip feedline evanescently coupling a cavity through an aperture has also been reported [92]. To use an aperture for coupling waveguide cavity there is always a trade-off between sensitivity and better signal to noise ratio (SNR). Reducing the size of the coupling iris (aperture) increases the *Q*-factor, therefore better sensitivity to measure low dielectric loss materials is attained. While increasing the holes size gives rise of the coupling level (low *Q*-factor) and better SNR of the output signal is realised [87]. Therefore, the choice depends on application and type of cavity. In this work both the coaxial and waveguide coupling methods would be adopted based on the frequency of operations as will be fully

describe and discuss in Chapter 4 and Chapter 7 for low and high frequency measurements, respectively.

(a) (b)

Figure 3.11 Cylindrical cavity (a) solid rod placed at centre [40] (b) sample placed via form in the insert location [37]

3.4 Methods of Sample Insertion

Various approach for sample insertion has been demonstrated for materials dielectric measurement depending on the cavity structure and type of MUT. These materials can be solids (rods, bars, discs, slabs etc), liquids (oils, solvent, binary solutions, etc) using samples holder such as tube (made of polymer or glass) and gases which are usually contained within a cavity. In material dielectric measurements, the choice of samples insertion is also guided by the resonant mode excited in the cavity. The usual practice has been making a hole in the cavity, at a place where the electric field is maxima and then samples are placed for measurements. In [99] samples have been placed in a radial direction along the height of the cavity, as the field decay exponentially in the axial direction and TE mode was utilized for the measurements. On the contrary, an axial direction has been used by other authors for solid rod measurements [100] as shown in Figure 3.11 (a) and also for liquids dielectric characterisations using the TM mode [43].

In [82], measurements of arbitrary solid sample have been demonstrated by placing the sample inside a cavity as a different approach of sample placement in a cavity resonator. However, there are some challenges associated with samples placement in a cavity resonator that leads to measurements errors, this can come from a movement of the sample, air gaps and dielectric losses from the sample's holders such as tube for liquids measurements. In order to reduce the measurements errors resulting from these factors a new approach was adopted and reported in [40]. The authors have used cylindrical cavity made from three plates consisting of top, insert and bottom shown in Figure 3.11 (b) to demonstrate their concept. A low loss and low dielectric material (Rohacell Foam) was used as the specimen holder and the sample (powdered material) is held in the form. This has therefore avoided the movement of the sample and has also reduced the difficulty of sample preparation [40]. Another challenging factor is the cavity size which becomes small for a high frequency design, difficulty arises in placing the sample using any of the approach described earlier. For this the evanescently coupling approach has been adopted to fringe in the field via an aperture where the MUT is exposed and also utilizing the high Q-factor of the cavity for better sensitivity [86].

To this end, there is no particular or general approach for placing samples in a cavity resonator for dielectric measurements. This is determine based on the cavity structure and applications scenario. In this work, for dielectric characterisation of liquid materials two methods will be adopted: A glass tube to pass in the MUT as detailed in Chapter 4 and a new approach filling the entire cavity, using a closed end coaxial cavity resonator presented in Chapter 5. For solid materials measurement, also a modified method is proposed, this is by introducing a ring at the base (bottom) of the cavity where solid samples will be place and this is presented in Chapter 7.

3.5 Methods of Evaluating Permittivity from Measurements

Conventional cavity perturbation method is the most commonly used approach for the extraction of complex permittivity of dielectric materials in cavity resonators. The method is considered to work well for measurement of low-loss or medium-loss materials as already discussed in Chapter 2. The changes in resonant frequency and Q-factor (Δf, $\Delta(1/Q)$) due to material interaction with EM field are utilized in quantifying the complex permittivity of the sample being measured. A cavity perturbation model can be used for a cavity resonator, measuring the complex permittivity $\varepsilon = \varepsilon' - j\varepsilon''$ [29]. The perturbation model is developed based on the assumptions that the sample volume is negligibly small compared to the cavity volume as outlined in Chapter 2. However, in practice, due to the number of limitations the sample would have some finite volume. Therefore, this might affect the accuracy of the theory as the volume of the sample increases. The coefficient of the filling factor is determined by the field in the cavity, either analytically for a cavity with solvable field or experimentally using known dielectric properties. For this, various modifications of the theory have been presented in the literature.

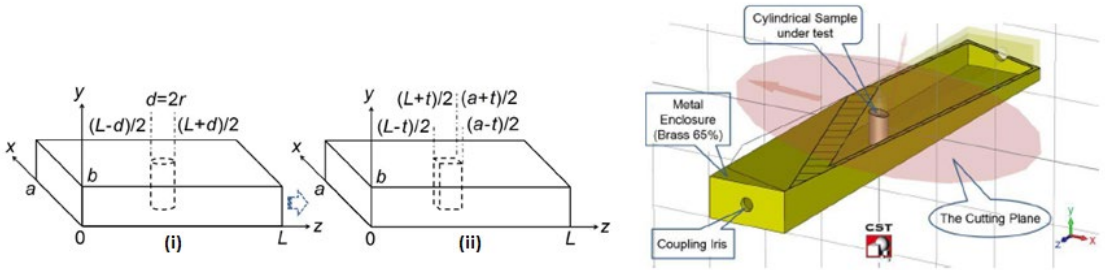

(a) (b)

Figure 3.12 (a) RC loaded with (i) cylindrical sample and (ii) bar sample placed at the centre of cavity (b) perspective view of modelled RC in CST loaded with sample at the centre

The authors [68] have presented a generalise approach for materials characterisation based on a rectangular cavity in detail as shown in Figure 3.12. Taking into consideration the effects of air gaps to modify the perturbation model. Besides modifying the empirical formula, the authors have presented and described a numerical optimisation technique. This is aimed at facilitating the measurements of materials with large physical dimensions and higher losses in contrast to ideal concept of conventional perturbation theory. Two samples geometry of cylindrical and rectangular bar are used for the analysis and the technique was validated by measurements of standard solid samples at X-band [68]. In [101] detail derivation of generalise cavity perturbation and filling coefficient based on rectangular cavity for a cylindrical shape sample have been reported. The relationships for evaluating the total relative error of the measurement results have also been described in their work. A further analytical model considering instances where samples cannot be made small due to technological difficulties using the superior modes in a second order cavity perturbation was also presented as modification to the formula. The results obtained using the modified model shows a good accuracy of using the second order perturbation for higher values of permittivity or large size samples [101]. Similarly, an analytical analysis for the explicit equations of evaluating the maximum sample volume of dielectric MUT based on the perturbation theory have been described in [102]. The authors have demonstrated the limits to the maximum volume ratio of the cavity and sample for various shapes of sphere, rod and disk. They have validated the expressions by measurements of both low loss and high loss dielectric materials. Their finding suggested that the maximum volume ratio of the cavity to sample depends on both geometry and the type of materials. It is also evident that, low dielectric loss materials can have large volume in contrast to high dielectric loss material making the former suitable for perturbation theory method.

On the other hand, factors such as temperature shows a linear decrease in the ratio (cavity to sample) as temperature increase irrespective of the sample's geometry [102].

In [70] Sheen and Weng have also presented a modified cavity perturbation technique for characterisation of laminated shaped samples. An analytical equation was derived for measurements of substrate materials with thin thickness. An X-band rectangular cavity was considered for the analysis and measurements. The new equations were validated by measurements of two substrate materials with varying width to demonstrate the effect of samples dimension. Result shows an increase in dimensions of the substrate increase the measurements errors using the conventional perturbation formula. This is in contrast with the modified perturbation formula which gives consistent results. However, it is also limited to certain dimensions, if the dimensions go beyond half of the wavelength, then measurements errors become obvious [70].

From the above-mentioned points, we can realise the need for the modification of the cavity perturbation model for both dielectric constant and dielectric loss measurements, with the later having high measurements errors when conventional model is utilised. In this work an analytical model were developed based on simulations of the designed cavity for the extraction of the dielectric properties of MUT based on the principle of perturbation theory for both liquids and solids measurement. Detailed derivation of the equations will be presented in Chapter 4 and 7 for liquids and solids measurements, respectively.

3.6 Applications

In terms of applications, cavity resonators have been utilised in many fields. This includes: the field of petroleum industry where they have been used for water content measurements because of their efficiency and stability in dielectric materials characterisation [78]. In

[79], an online water-oil ratio monitoring sensor using open ended cavity for applications such fiscal metering and custody transfer of crude oils in petroleum sector have been reported. Similarly, measurements of dielectric properties of heavy crude oils and their constituent components at temperature of up 300 °C have also been demonstrated [103]. The microwave measurement technique presented in [103] has established an opportunity to identify microwave absorbing phases in heavy oil processing in the oil industry. The technique is based on dielectric measurement for catalytic upgrading of the oils in a refinery and field settings.

Other application areas include the food industries, for example: measurements of wet mass and moisture content of grains for the purpose of storage and processing have been demonstrated using cavity resonant method [91]. More recently quality of honey against adulterations using a low-cost simple resonant measurement has been reported [104]. Though there was no novelty in terms of cavity geometry and choice of resonant mode, the results and extraction approach have shown good performance of the device. The authors have utilised the same cavity resonator for the analysis of Chinese liquor known as Baijiu to determine the amount of alcohol by volume through permittivity measurements as one of the most consumed spirits in the world [105]. Another application is the field pharmaceutical, where cavity resonators have also shown good measurement capabilities in blood glucose monitoring and detection of diseases such as diabetes [106]. Due to the limitations of techniques such coaxial probe and free space in measurements of some biological tissue with high losses such as the cornea covering the eye, a new method utilising the TE01n mode of cylindrical cavity resonator is reported in [107] for application in the field of medicine.

Dielectric characterisation of substrates material for high frequency communications and remote sensing to meet the demand of the ongoing transformation and development in communications industries using cavity resonator is another interesting application [86]. Monitoring industrial processes and the environment for high temperature, pressure and humidity cavity-based resonator are utilised. For example, in [81] the measurement of the permittivity of gases has been reported. Measurement of dielectric constant of nitrogen gas N_2 as a function of molar density and changes in concentrations of sulphur dioxide SO_2 gas were performed to demonstrate the measurement techniques [81]. These are some of the applications where cavity resonator sensors have made significant contribution in the field metrology. Their wider application areas make them one of the most utilised sensing approaches based on microwave measurements. For this, a lot of researchers are focusing on this aspect coming up with new and different design and measurements approach to key in, with some simple and cost-effective ways in materials measurements for various applications.

3.7 Summary

In summary, the use of these cavity resonators for material characterisation as described in detail in this chapter are generally aimed at some of the following key objectives either in terms of the device performance or applications:

- Better sensitivity and accuracy
- Simplicity in fabrication and measurement approach
- Easy extraction of dielectric properties
- Low-cost of making the device
- Simplicity of interpreting results

- Low power consumption
- Device miniaturisation

The accuracy and sensitivity of the measuring device using cavity resonator are attained by high electric field intensity at the point of measurements and high *Q*-factor. For this we have proposed the use of re-entrant cavity resonator as the main cavity structure for attaining the objectives of this work. However, the cavity structure would be modified. Details of the modification and its advantages over other conventional cavity structure for some of the outlined factors above will be discussed in the succeeding chapters. 3D printing additive manufacturing enabled by polymer and then coating it with copper material is consider for the fabrication of the cavities. This is due to their light weight, low cost and ability to fabricate complex structure. To overcome the approximation errors with cavity perturbation theory an analytical model based on simulation will be use for the extraction of dielectric properties of the material under consideration. All the various cavity resonators described and discussed as captured in various sections of this chapter are tabulated and compared in terms cavity geometry, frequency, *Q*-factor, applications and methods of extractions dielectric properties in Table 3.1.

Table 3.1: Comparison of Various Cavity Geometry for Material Characterisation at Microwave Frequencies

Cavity type	Freq. (GHz)	Q_w/Q_l *Q*-factor	Mode	Fabrication methods	Application	Extraction method	Excitation	Year/Ref.
Cylindrical	5.00	Ql = 500	TM010	CNC copper	Moisture content	Analytical derived expression	One-port loop feed	2000 [72]
Cylindrical	1 – 2.5	1100 – 15000	TM010 and TM020	CNC Copper	Solid rods	Rigorous analysis expression based on Ritz Galerkin	Two port straight feed line	2006 [73]
Cylindrical	2 – 20	7900 – 32000	TE111 – TE117	electro-silvering	Solid	Perturbation method	Adjustable One-port straight line feed	2005 [75]
Cylindrical	7.62	NA	TE011	Simulation-based	Liquid and solid	NA	One-port waveguide	2016 [76]
Cylindrical	2.52	63.25	TE	Simulation-based	Liquid and solid	Perturbation method	two-port waveguide	2019 [77]
Cylindrical	0.56	NA	TE01	Materialised steel metal pipe	Liquids	NA	One –feedline antenna	2016 [78]

Cavity type	Freq. (GHz)	Q_u/Q_l Q-factor	Mode	Fabrication methods	Application	Extraction method	Excitation	Year/Ref
Cylindrical	4 – 7	50	TM010 TM011	Stainless steel CNC	Liquid	Perturbation method	One-port straight	2018 [79]
Cylindrical	100	2762	TE221	CNC gold	Liquid	NA	Waveguide port	2011 [80]
Rectangular	1.92	3800	TE010	CNC –Aluminium	Liquid	Perturbation theory	two-port straight feed line	2013 [45]
Rectangular	10	QL-600	TE10	CNC-Stainless steel	Gas		Two port coaxial feed	2018 [81]
Rectangular	15-34	165 – 232	TE102 – TE121	CNC –Aluminium	Solid	Mode matching	one-ports waveguide	2018 [83]
Rectangular	240	600	Fringing e-field	Silicon-wafer etched DRIE-gold coated	Solid	Perturbation	Two-ports waveguides	2017 [86]
Doubled-ridged	3 - 8	2881 – 3797	TE101 – TE105	CNC copper	Solid rod	Perturbation method	Two-port waveguide	2016 [87]

Cavity type	Freq. (GHz)	Q_u/Q_l *Q*-factor	Mode	Fabrication methods	Application	Extraction method	Excitation	Year/Ref
spherical	13.8	22000	Bragg mode	-	Solid	-	Two-port probe	2014 [89]
Spherical	4	QL=321	TM011	3D printed VAT photo polymerisation	Liquid	Developed analytical model	One-port bent probe	2020 [90]
Re-entrant	8	2872	TM011	CNC- brass	Solid	NA	Two-port waveguide	2003 [91]
Re-entrant	2.14	750	Evanescent mode	CNC	NA	NA	Microstrip feedline	2016 [92]
Re-entrant	2.40	1250	TM010	CNC- Aluminium	Liquids	Perturbation	Two-port loop probe	2018 [93]
Rectangular	4.75	NA	TE011	CNC –Aluminium	Liquid	NA	One-port waveguide	2012 [106]
Rectangular	10	5500	TE107	CNC aluminium	Solid	Perturbation	Waveguide aperture	2014 [68]
Cylindrical	40	16070	TMm10	CNC	Liquids	Perturbation method		2009 [94]

CHAPTER FOUR: RE-ENTRANT CAVITY RESONATOR SENSOR FOR LIQUIDS MEASUREMENT

This chapter presents a microwave resonant dielectric metrology technique using a new unified analytical model to extract complex permittivity of low-loss liquid materials. A new structure of re-entrant cavity resonator enabled by additive manufacturing technique is demonstrated here. The main design drive of the modified re-entrant cavity is to confine the electric field and therefore enhance the interaction with the material under test while maintaining high *Q*-factor of the cavity. This enables high sensitivity when measuring complex permittivity of low loss materials. The fabrication of the resonator was made easy by using stereo-lithography (SLA) 3D printing. The measured resonant frequency of the fabricated cavity is 2.09 GHz and the *Q*-factor is 5250. The device was first validated using several common solvents. A unified analytical perturbation model based on simulations is developed for the extraction of the complex permittivity. The influence of the dielectric constant on the loss-tangent model has been considered. Results obtained agree very well with literature values. The device has subsequently been used in the measurement of crude oil samples and the correlation between permittivity measurement and crude oil category has been established. This work has been published in Sensor and Actuator A: Physical journal. Furthermore, the cavity has been used for measurement of binary and ternary solution at two resonant frequencies of 2 GHz and 6 GHz demonstrating the use of harmonics in dielectric characterisation using cavity resonator.

4.1 Re-entrant Cavity

In conventional re-entrant cavities, as shown in Figure 4.1 (a), there is a significant trade-off between the field concentration and the *Q*-factor because of the flat base of the centre post. While the electric field increases with a reducing gap *g*, the resistive loss increases too due to excessive concentration of the field around the sharp edges giving a reduced *Q*-factor. In this work a modified re-entrant cavity geometry is proposed as shown in Figure 4.1 (b). The modification is to confine the electric field intensity at the central point where MUT is placed for measurement, while maintaining high cavity *Q*-factor for the sake of sensitivity (refer to Figure 4.2 and Figure 4.4)

The round base avoids the electric field build-up over corners and edges. The field is effectively focused on the tip. Detailed comparison between the flat and curve post will be given in Section 4.2. Although this is a simple geometry change, the machining of the rounded post is not straightforward for conventional milling. So, an additive manufacturing technique based on stereo-lithography (SLA) 3D printing is used to produce the device.

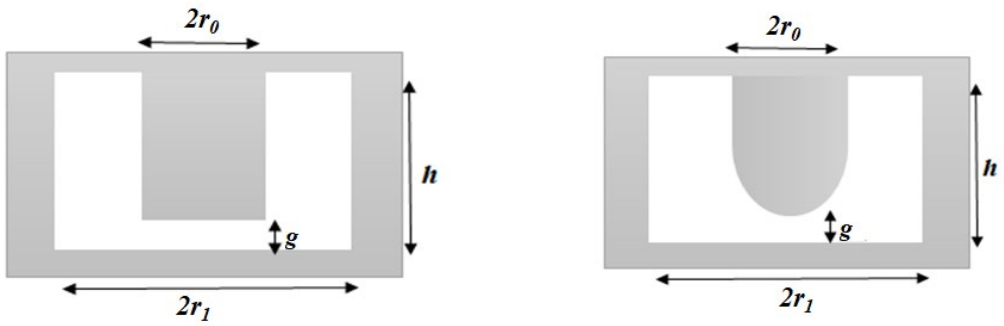

(a) (b)

Figure 4.1 Re-entrant cavity: (a) Conventional structure and (b) Modified structure

Table 4.1: Eigen mode analysis results of the cavities

Gap, *d* (mm)	**Post profile**	**Freq. (GHz)**	**Quality factor**	**Electric field strength (V/m)**	**Cavity geometry dimensions**		
					h **(mm)**	r_1 **(mm)**	r_0 **(mm)**
2	Flat	2.072	4432	4.50×10^8	13.35	25.00	11.25
2	Curve	2.072	6104	6.75×10^8	24.00	25.00	11.25
2	Flat	2.072	4731	5.75×10^8	11.85	25.00	7.50

4.2 Eigenmode Analysis of Re-entrant Cavities

The two geometries of Figure 4.1 were analysed and compared using eigenmode solver by Computer Simulation Technology (CST) software [108]. The gap *g* between the top post and cavity adjusts the mode of frequency and traps the electric field within the gap. The dominant TM010 mode as in [109] is utilized in this design.

In the parametric study, the radius (r_0 in Figure. 4.1) of the post (both flat and curved designs) and that of the cavity (r_1) are kept the same. The height of the cavity is varied to maintain the same gap *g* for the same resonant frequency as in the cases of row 1 and 2 of Table 4.1. In the case of row 3 (flat post) both the height and the post radius were adjusted whist keeping the cavity radius r_1 and the gap *g* for the same resonant frequency. In both cases, the modified (curve post) geometry shows higher magnitude of electric field strength of 6.75×10^8 V/m and higher *Q*-factor of 6104 based on simulation than those with the conventional re-entrant cylindrical cavity. Reducing the radius of the flat post or changing the gap *g* may increase the volume of the cavity and in turn increases the *Q*-factor, but this

will lower the electric field strength and therefore the sensitivity. A further study reveals that the curve post geometry gives a higher *Q*-factor irrespective of the post radius under the same resonance frequency, as shown in Figure 4.2. In this parameter study, the height *h* of the cavity is adjusted while keeping the cavity radius r_1 and the gap *d*. The highest *Q*-factor of 5800 is recorded for the flat post at a post radius of 5 mm, which is about 5 % less than that of the curved post as presented in Figure 4.2.

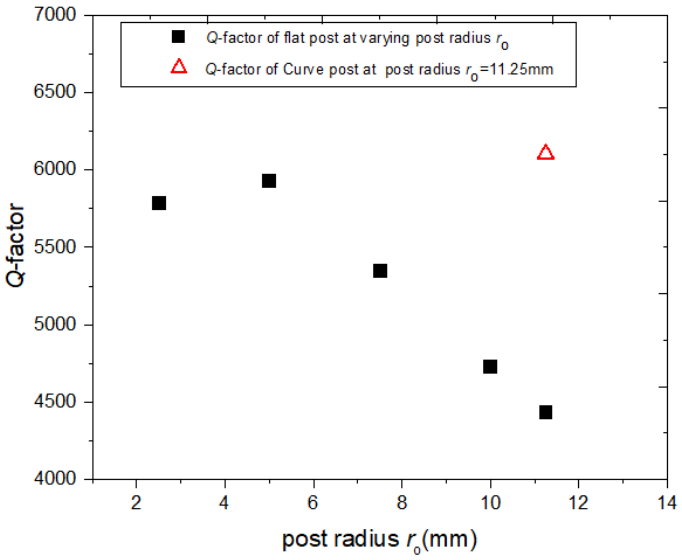

Figure 4.2 Simulated *Q*-factor plotted against radius of the post

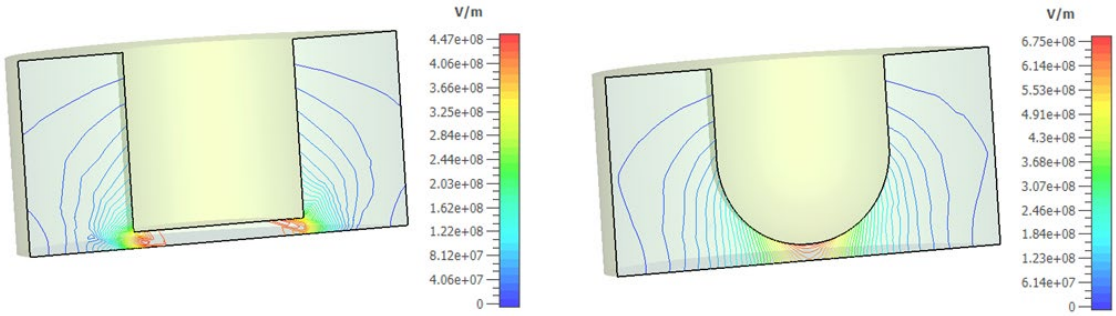

(a) (b)

Figure 4.3 Electric field patterns: (a) conventional re-entrant cylindrical cavity (b) modified (curve post) cavity

The electric field patterns of the conventional and modified geometry are illustrated in Figure 4.3. The high-quality factor and concentration of electric field at the post tip of the modified cavity resonator is highly desired for the increase of device sensitivity [110]. The emphasis on the *Q*-factor and its relevance in this work is further described in Section 4.4.

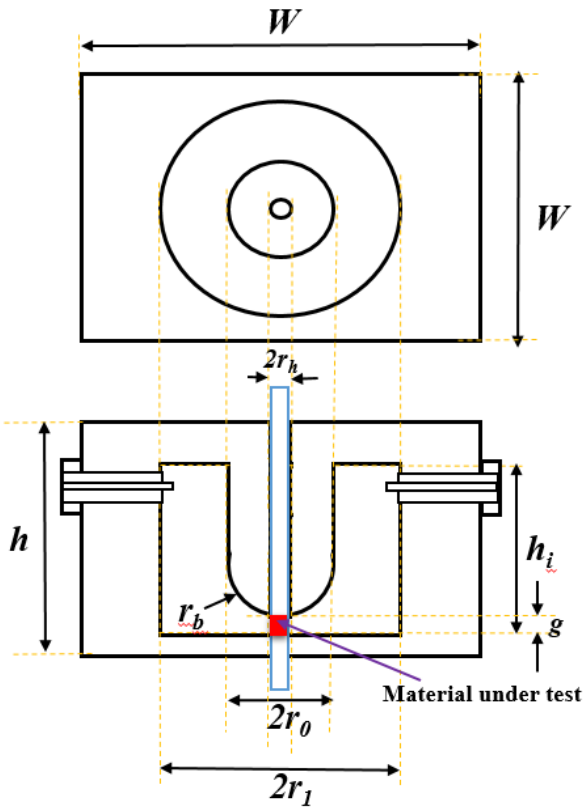

Figure 4.4 Top and cross-sectional view of the re-entrant cavity. The dimensions in millimetre are: *W=70, h=24, ho=45, r1=25, r0=11.25, rh =3.4 rb=11, g=2.*

4.3 Sensor Design and Fabrication

The measurement cavity was designed to operate at a centre frequency of 2.0 GHz. It has a radius, $r_1 = 25$ mm and a height, $h = 24$ mm. The post has a radius, $r_0 = 11.25$ mm and the gap, $g = 2$ mm. The base of the post was rounded by a curvature with a radius, $r_b = 11$ mm as shown in Figure 4.4. A hole of a diameter of $2r_h = 3.4$ mm was made at the centre

of the post where a tube would be inserted as a sample holder as illustrated in Figure 4.4. A transmission-type configuration is adopted for the measurement. The external coupling is via the probe of the Subminiature A (SMA) coaxial connectors placed on the side walls of the re-entrant cavity frame in a rectangular shape to predominantly couple the electric field to the resonator. The two ports are made identical, and the probes have a diameter of 1.3 mm and a length of 2.9 mm penetrating into the cavity. The probes are positioned toward the joint between the post and the cavity where the electric field intensity is low. This reduces the external coupling level and minimizes the loading effect of the probes.

These design parameters give a simulated resonance frequency of 2.082 GHz, a loaded quality factor of 5920 and insertion loss of 28.8 dB without the tube insertion hole. The CST frequency domain solver was used with adaptive mesh refinement for the simulation. Following the introduction of the hole into the design, there was a slight increase in frequency to 2.089 GHz and the loaded quality factor had a negligible change as will be discussed further. The insertion loss is 28.6 dB at 2.089 GHz. The S_{21} response of these two responses is shown in Figure 4.5. The material under test fills the entire tube, but only interacts with the E-field in the gap g between the post and the base of the cavity as shown in Figure 4.4. The coupling into and out of the cavity is made weak (i.e. large external Q-factor Q_e) to achieve the insertion loss of over 20 dB [56, 50]. The relationships between loaded, unloaded and external Q-factor of the resonator are given in Section 2.4 of Chapter 2.

The unloaded Q-factor Q_u is attributed to the conductor loss, radiation loss through the hole, dielectric loss of the tube and loss due to the sample under test in this case. These are represented by Q_c, Q_r, Q_t and Q_s, respectively and relate to Q_u by [50].

$$\frac{1}{Q_u} = \frac{1}{Q_c} + \frac{1}{Q_r} + \frac{1}{Q_t} + \frac{1}{Q_s} \tag{4.1}$$

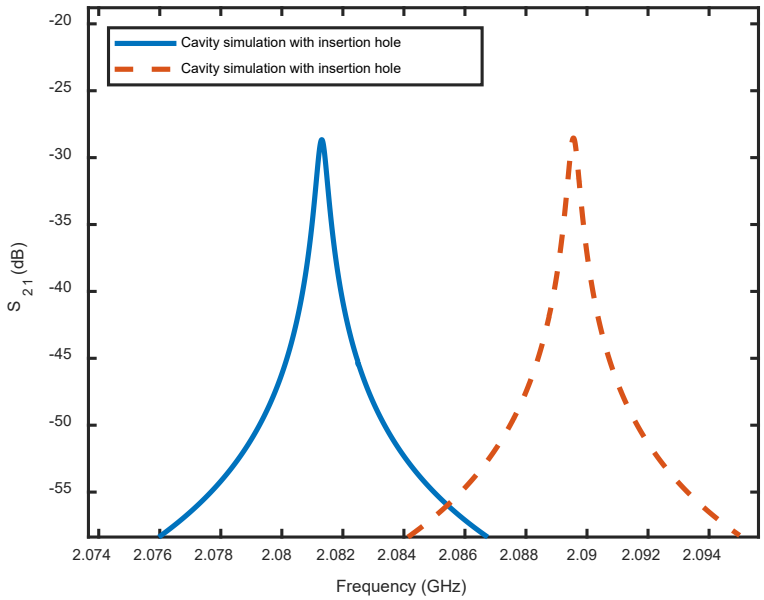

Figure 4. 5: Simulation S_{21} response of cavity with and without tube insertion hole

This relationship and the previous equations in Chapter 2 on Q-factor (2.28) to (2.31) has been utilised in the computation of the losses as will be described subsequently. The contributions from all these different losses are computed using a series of simulations and the equations mentioned above based on the following steps:

Table 4.2: Nominal dielectric properties of the three glass tubes [111]

Tube	**Dielectric constant, ε'**	**Loss tangent, $tan\delta$**
Quartz glass tube	3.75	0.0004
Borosilicate glass tube	4.30	0.0047
Soda Lime glass tube	6.00	0.0200

a) Starting with a shielded cavity model with copper walls and external energy coupled in and out of the cavity but with no tube hole giving no radiation or dielectric loss. The loaded Q-factor, based on (2.33) and the magnitude of S_{21}, in dB, can be read from the simulation results. Using (2.31), the external Q-factor of the resonator, which includes the input and output loading effects, can be estimated.

b) Now that Q_l and Q_e are known, the unloaded Q-factor can be calculated using (2.29) or (2.30). Since the only source of internal loss is from the copper conductor in this simulation model, $Q_u = Q_c$ can be deduced from (4.1).

c) A hole is then introduced into the cavity model. An open boundary simulation gives a new loaded Q-factor. Since the difference between this Q_l and the one from Step a) is solely a result of the hole and the associated radiation, the radiation loss Q_r is deduced using (2.28) and (4.1) as Q_c is known.

d) Now, a tube is inserted into the sample insertion hole. From the change of the unloaded Q-factor which has the combined effect of tube and radiation, the Q-factor due to the tube Q_t can be extracted accordingly as Q_r is known (which is also negligibly small).

e) This cavity model, with copper walls, a hole and a tube, under open boundary condition, is used as the reference model to represent the experimental configuration before inserting samples.

Table 4.3: Values of quality factors contribution based on simulation

Simulated *Q*-factors	***Q*-factor values**
Q-factor due to conductor Q_c	6126
External *Q*-factor Q_e	1.63×10^5
Q-factor due to radiation Q_r	2.03×10^6
Q-factor due to Quartz glass tube Q_{tq}	43776
Q-factor due to Borosilicate glass tube Q_{tb}	3420
Q-factor due to Soda Lime glass tube Q_{ts}	600

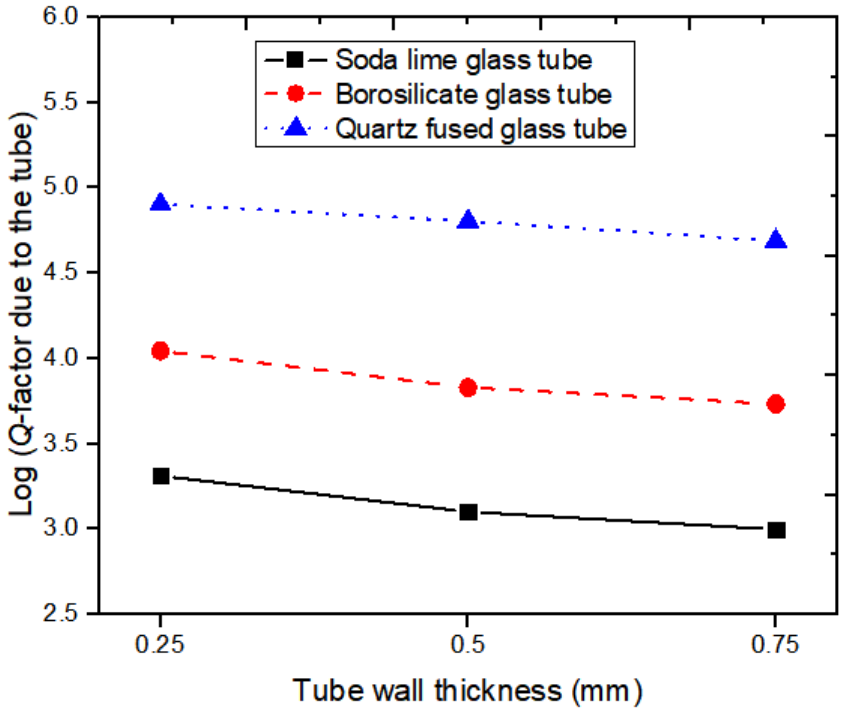

Figure 4. 6: Q-factor due to the tube with respect to tube wall thickness. The outer diameter is 3 mm in all cases

4.4 Tube Consideration

The tubes that are used to hold samples could also have an important impact on the *Q*-factor. Three types of tubes were considered - borosilicate, quartz fused and soda lime glass tubes. The choice of glass tubes is for easy cleaning and its re-usability irrespective of the type of material passing through it. The rigidity of glass tubes would also help with the placement of the sample and the repeatability of the measurement as compared to polymer tubes. A parametric study using simulation is carried out on each of the tubes with varying wall thickness. The dielectric properties of the tubes used in the simulation are given in Table 4.2 [111]. The change of *Q*-factor as a function of wall thickness is shown in Figure 4.6. The quartz tube has much higher *Q* than the other two types. As also expected, the *Q* decreases with increasing wall thickness. The *Q*-factors corresponding to the tubes of 3 mm outer diameter (O.D) and 1.5 mm internal diameter (I.D) are given in Table 4.3 for comparison with all the other *Q*-factors computed. As given in Table 4.3, both $Q_{e,}$ and Q_r are significantly larger than Q_c and therefore have negligible loading and radiation effect on the cavity. The practical choice of the tube will be discussed in the next section. The device was fabricated using stereo-lithography (SLA) 3D printing technology. The additive manufacturing process allows the accurate fabrication of the irregular shapes and surfaces quickly and easily. The device was made from Accura 25+ polymer and coated with 25 μm copper which is 15 times the skin depth. This is to ensure completeness in the coating and to avoid wear and tear of the plating. The prototype photo is shown in Figure 4.7. The cavity is framed in a block of rectangular shape with a minimum wall thickness of 10 mm. A separate base plate was bolted to the main cavity. Considering the surface current concentrates at the point where the post joins the cavity, the split was made on the base away from the post so that the current disturbance was kept to a minimum as

shown in Figure 4.8. The parts were assembled via fourteen 3 mm × 50 mm threaded rods to ensure good contact as shown in Figure 4.7 (b).

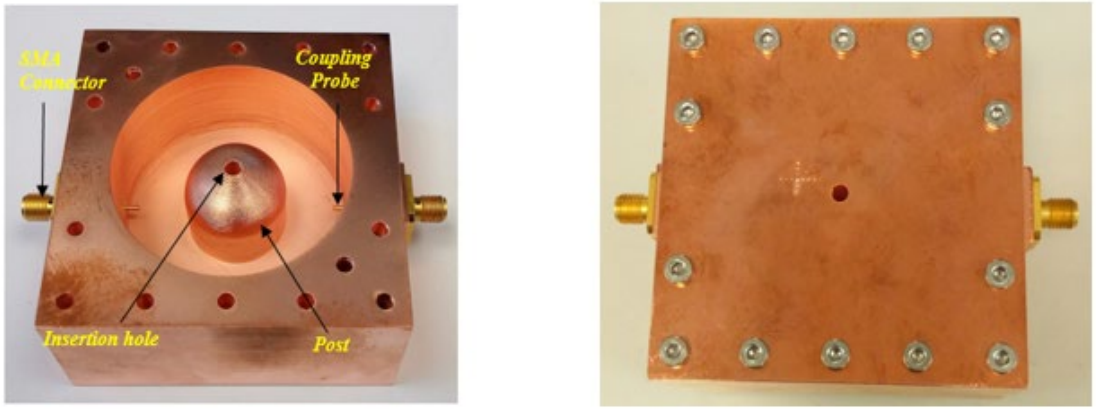

(a) (b)

Figure 4. 7: Photographs of the 3D printed prototype (a) cavity internal structure (b) assembled cavity

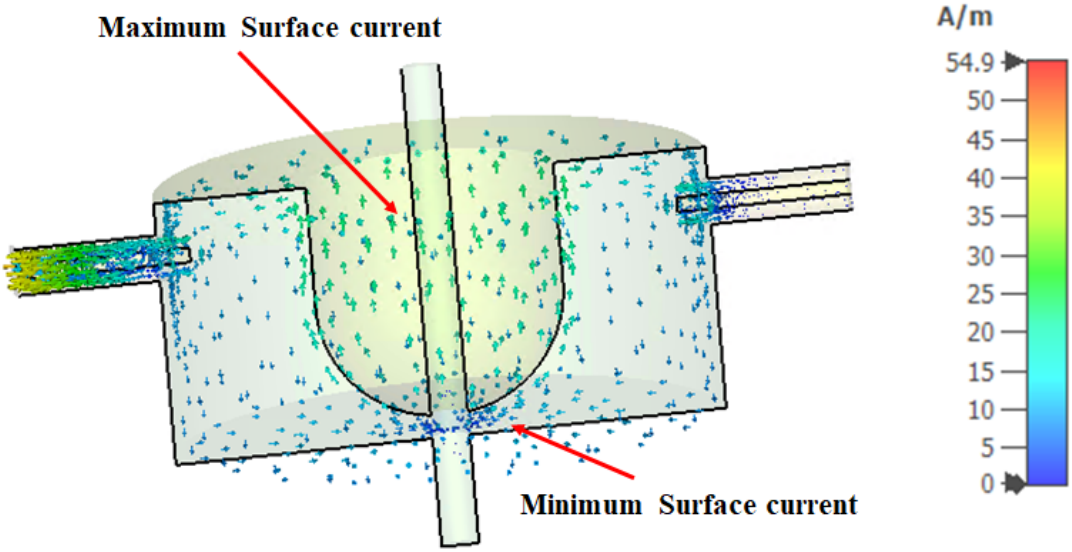

Figure 4. 8: Simulation response showing the intensity of surface current of the cavity resonator

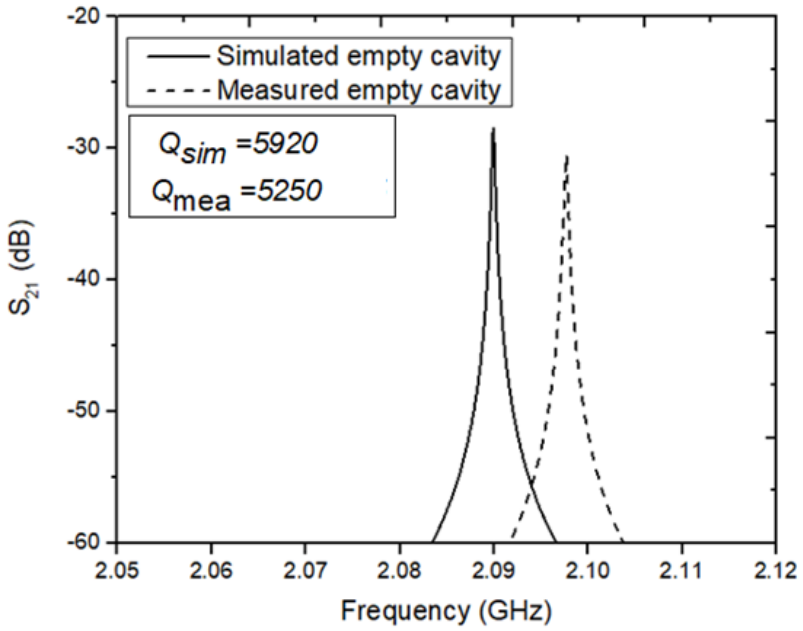

Figure 4. 9 Measured and simulated S21 response of the empty cavity, while the simulated and measured loaded Q-factors of the cavity are denoted by Qsim and Qmea respectively

Table 4.4: Dimensions and associated *Q* of the three measured glass tubes

Tube	**Outer diameter (mm)**	**Inner diameter (mm)**	**Wall thickness (mm)**	**Associated *Q* from measurement**
Quartz glass	3.00	1.50	0.75	126867
Borosilicate glass	3.00	2.98	0.01	52618
Soda Lime glass	1.80	1.24	0.28	3355

4.5 Measurement Set-up

Measurements were carried out using a PNA network analyser (Agilent Technology E8382C) which was calibrated with 85052D kit based on the standard two port calibration method using short-open-load-thru (SOLT) procedure. The measured resonance frequency of the empty cavity with the hole, but no glass tube, is 2.094 GHz, with a loaded quality factor of 5250 and insertion loss of 29.3 dB. The measured conductor *Q*-factor neglecting radiation loss is 5436. As shown in Figure 4.9, the measurement and simulation agree very well with a small frequency shift of 5 MHz (0.28 %) and difference in *Q*-factor of 670 (11.3 %). This is probably due to the fabrication tolerance of around 10 μm and imperfect cavity assembly as well as imperfect copper. The uncertainty analysis of all possible factors of errors will be presented in the next section.

Three commercially available tubes have been experimentally examined for their contribution to the *Q*-factor. Their dimensions are given in Table 4.4. The measured *Q*-factors before and after the tube has been inserted into the hole of the cavity resonator is used in computing the *Q*-factor associated with the dielectric loss of the tubes. These are also given in Table 4.4. Both the quartz tube and the thin-wall borosilicate tube exhibit higher *Q*-factor value than the conductor and this would have little effect on the overall *Q*-factor of the resonator. However, the thin-wall tube has been found to be too fragile to handle and have large inaccuracy in its dimensions. To this end, the quartz fused tube with 3 mm O.D and 1.5 mm I.D was chosen for this work.

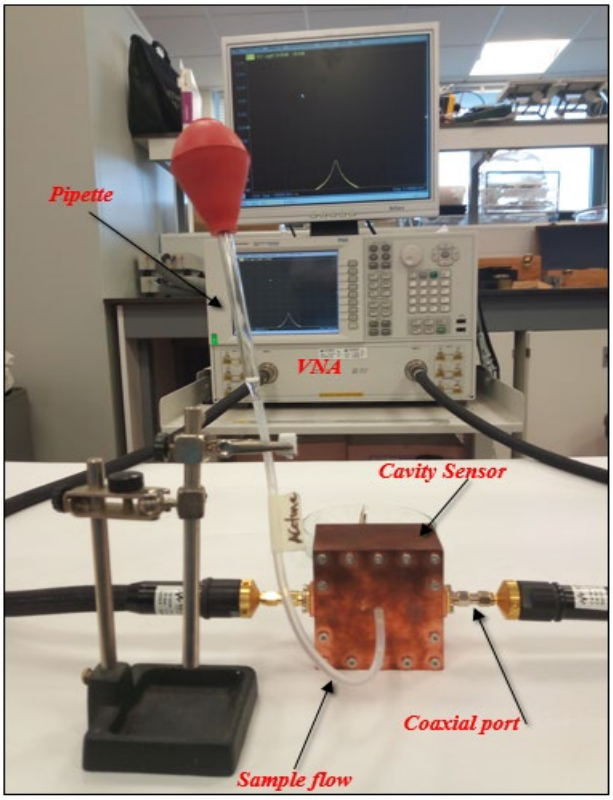

Figure 4.10 Photograph of the measurement set-up

To test the performance of the sensor, three common solvents, ethanol (99% purity), acetone (95% and 99% purity), and methanol (99% purity) from Sigma Aldrich Company Ltd. were measured and analysed as reference liquids. The liquid samples are passed to the quartz glass tube via a silicone tube with a pipette as shown in the measurement set-up in Figure 4.10. The silicone tube is connected at both the inlet and outlet of the quartz tube. As the liquid begins to flow out, the outlet of the silicone tube is sealed. This is to allow static measurement of the liquids and avoid the effect of flow rate. The tube was washed with isopropanol solvent and dried by gentle heating for 5 minutes before taking any new measurement. New pipettes and silicone tubes are used for each measurement while making sure there were no air bubbles visible as the liquids flows through the transparent tube. All samples are measured 5 times to ensure repeatability of the measurement and to

determine the associated measurement errors. The measured S_{21} responses of the cavity, the cavity with the tube and the common solvents are shown in Figure 4.11. The changes in Q-factor signify how lossy the samples are, as demonstrated by the respective Q-factor due to samples shown in Figure 4.11. The results obtained will be discussed in Section 4.8.

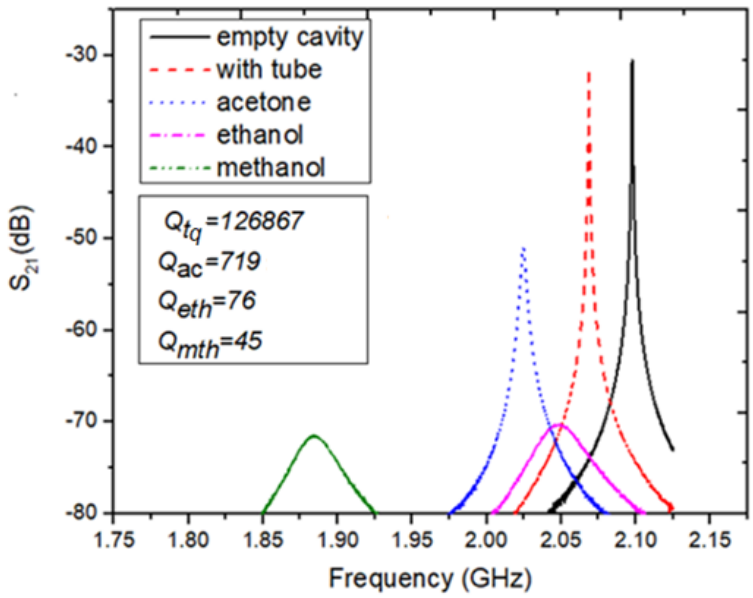

Figure 4. 11 Measured S_{21} response of the empty cavity, cavity with the tube and with common solvent. The measured Q-factors due to quartz tube, acetone, ethanol and methanol are denoted by Q_{tq}, Q_{ac}, Q_{eth}, and Q_{mth} respectively

4.6 Extraction of Complex Permittivity

The perturbation method is commonly used for the extraction of complex permittivity of dielectric samples in cavities. The method is considered to work well for measurement of low-loss or medium-loss materials as discussed in Section 2.8 in Chapter 2 [29]. The changes in resonant frequency and Q-factor (Δf and $\Delta(1/Q)$) due to material insertion are utilized in quantifying the complex permittivity of the sample being measured. A cavity perturbation model can be used for a cavity resonator measuring the complex permittivity $\varepsilon = \varepsilon' - j\varepsilon''$ [112].

$$\varepsilon' = A^{-1}\frac{V_c}{V_s}\left(\frac{f_1 - f_0}{f_0}\right) + 1 \tag{4.2}$$

$$\varepsilon'' = B^{-1}\frac{V_c}{V_s}\left(\frac{1}{Q_1} - \frac{1}{Q_0}\right) \tag{4.3}$$

where ε' and ε'' are the real and imaginary part of the complex permittivity. V_s is the sample volume exposed to E-field, and V_c is the volume of the cavity. The coefficient *A* and *B* are influenced by the shape, size, and location of the sample as well as the mode of excitation. The resonant frequency and *Q*-factor of the cavity before and after insertion of the sample are f_o, Q_o and f_1, Q_1, respectively. The coefficients in (4.2) and (4.3) can be mathematically determined only for cavity structures with high symmetry and analytically solvable fields such as the conventional cylindrical cavity [29]. However, this is not the case for the cavity used in this work. Therefore, we have developed a model based on simulations as discussed below.

The change in resonant frequency with varying ε' over the range from 1 to 80 at a fixed loss tangent, $\tan\delta$, is established by simulation and plotted in Figure 4.12. This is used to model the real part of the permittivity. It should be noted, that increasing the loss tangent up to a value of 0.1 has negligible effect on the relationship between ε' and $\Delta f/f_c$ as can be seen from Figure 4.12 where three curves are overlapping each other. A quadratic curve fitting gives the following relationship for the extracted real part of the complex permittivity.

$$\varepsilon_r' = 12257.96\left(\frac{\Delta f}{f_c}\right)^2 + 762.1\frac{\Delta f}{f_c} + 1.05 \tag{4.4}$$

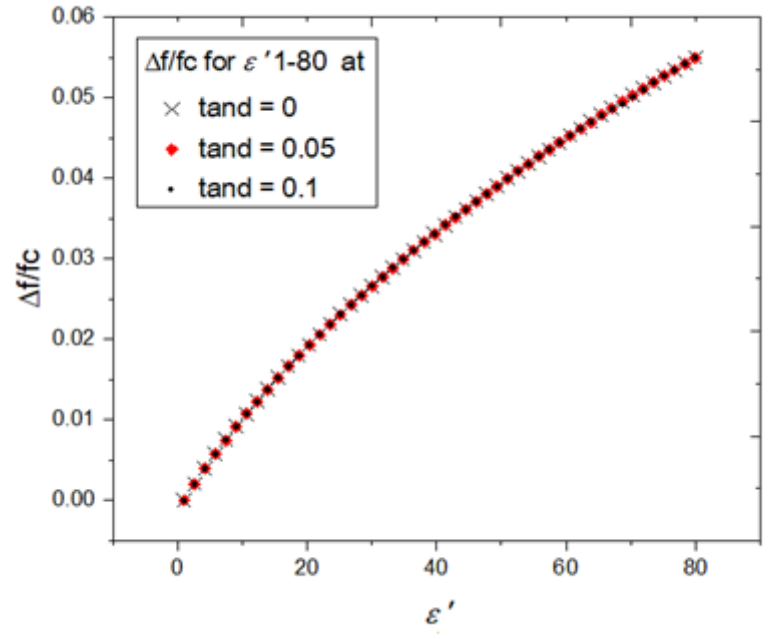

Figure 4. 12 Relationship between change in resonance frequency and permittivity

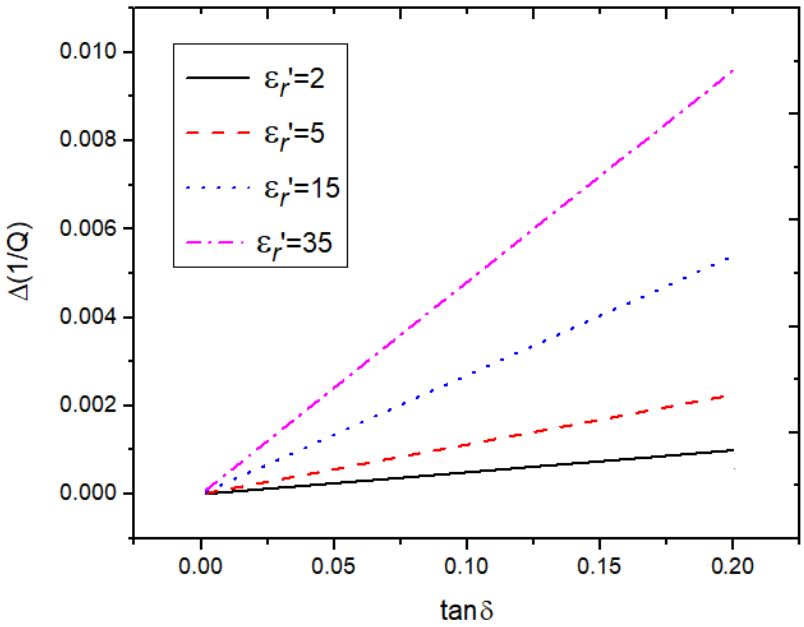

Figure 4. 13 Relationship between the change in quality factor of the material under test and loss tangent at different permittivity values

The model for the imaginary part (i.e. the dielectric loss) is more complicated as the change of the dielectric constant as well as the loss tangent will have an impact on the cavity quality factor. This is because the change of the dielectric constant alters the field. Therefore, a fixed perturbation model will not apply to different materials with significantly different dielectric constants [110]. To deal with this, we first obtained results by simulating the change in $1/Q$ due of the sample as a function of a varying $\tan\delta$ from 0.001 to 0.2 for a number of ε_r' values. As shown in Figure 4.13, a linear relationship was observed. However, as ε_r' increases the slope increases. From the data obtained we can derive,

$$\Delta(1/Q) = P(\varepsilon_r') \cdot \tan(\delta) + M \tag{4.5}$$

where P is a function of ε_r' and M is treated as a constant close to zero. The dependence of P on ε_r' is then investigated at a fixed tan δ. The simulated relationship between ε_r' and $\Delta(1/Q)$ for a fixed $\tan\delta = 0.2$ is plotted in Figure 4.14. A polynomial fitting of Figure 4.14 gives

$$\Delta(1/Q)|_{tan(\delta)=0.2} = A_1\varepsilon_r'^4 + A_2\varepsilon_r'^3 + A_3\varepsilon_r'^2 + A_4\varepsilon_r' + C \tag{4.6}$$

where

$$\begin{cases} A_1 = -3.75 \times 10^{-10} & A_2 = 8.3 \times 10^{-8} \\ A_3 = -7.23 \times 10^{-6} & A_4 = 4.36 \times 10^{-4} \\ C = 1.82 \times 10^{-4} \end{cases}$$

The function $P(\varepsilon_r')$ can then be deduced from

$$P(\varepsilon_r') = \frac{\Delta(1/Q)|_{tan(\delta)=0.2} - M}{0.2} \tag{4.7}$$

Substituting (4.7) into (4.5) we can arrive at a unified relationship for determining the loss tangent as

$$tan\delta = \frac{0.2\left(\Delta\left(\frac{1}{Q}\right) - \mathrm{M}\right)}{\Delta(1/Q)|_{tan(\delta)=0.2} - \mathrm{M}} \tag{4.8}$$

where the constant $M = 3.27 \times 10^{-7}$ can be taken as negligible. The imaginary part can be calculated based on the results obtained in (4.4) and (4.8) using the equation

$$\varepsilon_r'' = \varepsilon_r' \times tan\delta \tag{4.9}$$

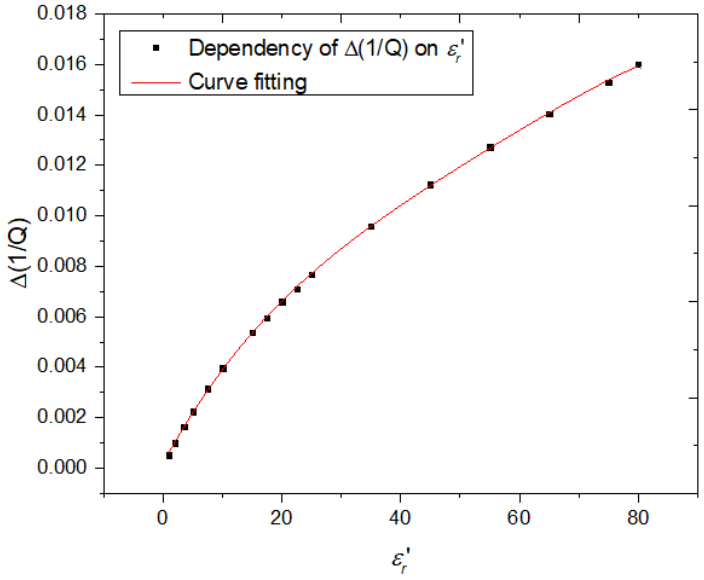

Figure 4. 14 Relationship between changes in quality factor as a function of permittivity when tan δ = 0.2.

The coefficient of determination also known as R-squared [113], a measure of the accuracy of the curve fitting, is 0.9999 in all the curve fittings of the mathematical models above indicating good fit of the equations (4.4) and (4.6) with the simulated results. On the other hand, due to fabrication tolerance, the designed cavity cannot be accurately made to its exact dimensions. So, there would be some difference between the design cavity in CST and the fabricated device. However, based on the very small difference between the measured and simulated results as presented in Section 4.5, additional calibration of the

model is not required in this case. The curve fitted extraction model is based on the difference between two values (before and after sample insertion) rather than the absolute values. Therefore, the discrepancy (very small in this case) between the absolute measurement and simulation will be largely cancelled out. However, any residual error due to this factor is included in the error analysis as would be describe in the next section.

4.7 Error Analysis and Uncertainty Evaluation

In relative permittivity and loss tangent measurement using the designed cavity sensor, there are a number of sources for errors. These include dimensional errors of the tube; the hole; the cavity dimensions; and system errors in the model described in Section 4.6.1. Others include measurement uncertainties due to temperature instability and random errors from the S-parameter measurements (including calculation of the Q values). There is also measurement repeatability of the device and the set-up. These errors combine together, and estimation of their effect is discussed below.

The uncertainties resulting from the abovementioned factors were determined separately in relation to changes in frequency (for dielectric constants) and quality factor (for loss tangents) based on simulations and measurements. The procedure given in [114] is adopted to compute for individual uncertainty as well as the expanded standard uncertainty and results presented in Table 4.5.

4.7.1 Dimension Errors

CST simulation is utilized to arrive at the uncertainty influenced by the potential dimensional errors. The nominal tolerances of the tube, hole, and cavity, given by the manufacturer (Table 4.5), were used to obtain separately the potential change in frequency

and quality factor resulting from the variations in dimensions. The individual standard uncertainty is then computed.

4.7.2 Temperature Variation

The effect of temperature change was determined based on measurements taken at different temperatures within a variation of ± 1.0 °C from three data sets (n = 3). The standard uncertainty in frequency and quality factor resulting from the changes in temperature were determined accordingly.

4.7.3 Measurements Error

The measurement repeatability was evaluated using methanol as the reference sample by taking several repeated readings and the standard uncertainty for both change in frequency and *Q*-factor were evaluated.

4.7.4 Extraction Model

The model developed for the extraction of the dielectric properties based on curve fitting from simulations data has some discrepancy between the data and estimation model. The measure of this, is the residual sum of square. The change in frequency is related to (4.4) and *Q*-factor is associated with (4.8). This source of error is considered and included in Table 4.5.

The combined uncertainty in dielectric constant and the loss tangent were evaluated and the expanded uncertainty assuming a normal probability distribution using a coverage factor value $k = 2$ was computed accordingly [114]. This signifies a confidence level of approximately 95 % [114]. The expanded uncertainty on the dielectric constant is taken

Table 4.5: Uncertainty analysis based on simulation and measurements

Sources of Uncertainty		**Temp.**	**Cavity dimensions (fabrication tolerances)**	**Outer Diameter of the tube dimension**	**Inner Diameter of the tube dimension**	**Hole dimension**	**Residual sum square of developed model**	**Meas. repeatability**	**Combined**
Tolerance		±1°C	±0.01mm	±0.02mm	±0.02mm	±0.05mm	-	-	-
Uncertainty of resonance frequency and quality factor	$\Delta f/f$	6.17×10^{-3}	2.95×10^{-3}	4.90×10^{-3}	2.20×10^{-3}	2.72×10^{-4}	8.56×10^{-6}	1.82×10^{-4}	8.70×10^{-3}
	$\Delta(1/Q)$	7.45×10^{-7}	5.79×10^{-6} .	8.01×10^{-6}	5.10×10^{-5}	1.78×10^{-6}	9.72×10^{-6}	1.55×10^{-3}	1.55×10^{-3}
Covering factor (k=2)	**Expanded uncertainty on ε_r' is 1.74×10^{-2}**						**Expanded uncertainty on $tan\ \delta$ is 3.10×10^{-3}**		

into consideration, while that of the loss tangents is considered negligible and not included in the results of the measurements (Table 4.6 and 4.8).

In order to minimize some of these errors, certain measures were taken as described below. A tube with measured outer diameter of 3.020 mm (using micrometre screw gauge) is used as sample holder. As the dimensions of the tube may vary along the length of the tube, measurements were only taken while maintaining its position relative to the cavity. However, the inner diameter was not measured. To minimize the measurement error, a large number of sweep points (6401), over a bandwidth about five times the 3dB bandwidth, were used. An IF bandwidth of 50 Hz for high loss materials and 500 Hz for low loss materials is used to reduce effect of noise in the response. All samples were measured four times and the average was used in computing the dielectric properties. All measurements were carried out within an ambient temperature of 21.0 ± 1.0 °C.

4.8 Model Verification

The real parts of the complex permittivity were extracted using (4.4) for the three common solvents and the imaginary parts were obtained using (4.8) and (4.9). The measured and reported complex permittivity of the common solvents is compared in Table 4.6. There is a close agreement between the results especially for methanol with the lowest difference of 1.5% with the literature results. Acetone and ethanol recorded a slightly higher difference of 5.2% and 3.9% respectively. It should be noted the small difference could potentially be because the liquids have slightly different purity. The measured results between the two acetone samples with different purity suggest how sensitive the device is to minor changes of concentration or purity. Generally, Table 4.6 shows our method has

Table 4.6 Comparison between measured and literature values of permittivity of common solvent at s-band

Samples	Measured	Literature	% Difference in Magnitude between measured and literature
Acetone (99.9% purity)	22.09 ± 0.38 – j0.84	21.40 – j1.02 [115]	3.2
Acetone (95.5% purity)	22.52 ± 0.38 – j0.97	-	5.2
Ethanol (95.5% purity)	8.58 ± 0.15 – j7.42	8.26 – j7.91 [67]	3.9
Methanol (99.9% purity)	25.22 ± 0.44 – j10.8	24.84 – j12.28 [67]	1.5

produced good agreement with those reported in the literature. This has validated the model developed for the extraction of complex permittivity.

4.9 Measurement of Crude Oil

Further measurement of three different samples (S1, S2 & S3) of crude oil as classified by the parameter, American Petroleum Institute (API) gravity were carried out [116]. The crude oil samples were chemically characterised in terms of density, viscosity and weight percentage of asphaltenes before the microwave measurements.

An Anton Paar DMA 35 digital density meter was used to measure the specific gravities of the oils, from which the API gravity was calculated. The viscosity was measured using Bohlin Instruments CVO 50 NF rheometer (Malvern Instruments Ltd., UK) at 25 ºC using a shear rate of 100 s^{-1} and a steel parallel plate with 100 µm gap. The asphaltene in the oils was precipitated in accordance with ASTM D2007 [117], by mixing 40 ml n-heptane solvent and 1 g of crude oil sample. The mixture was stirred for about 4

hours using magnetic stirrer and allowed to settle for 24 hours. The asphaltene was then filtered as solid from the oil/precipitant mixture using a standard funnel filter system. The filter paper with the content (asphaltenes) was dried and then weighted. As shown in Table 4.7, the samples are in the categories of light, medium and heavy crude oil based on their API gravity values. About 15 wt % of asphaltenes was obtained for the heavy oil while only 1 wt % and 2 wt % were obtained for the light and medium crude oils respectively. The deasphalted liquid was then separated from the n-heptane by evaporation at 30 ºC. The dielectric constant and the loss factor of the crude oil, deasphalted oil, and asphaltenes (for heavy oil only) were measured and are presented in Table 4.8. The properties of asphaltenes for the light and medium oil could not be determined due to low quantities of collected asphaltenes. For the microwave measurement the samples were passed through the tube using the set-up explained earlier except in the case of asphaltenes which is in solid form. For this, the asphaltenes were ground and put into the tube. Compression was applied and sample was measured and re-measured after further compression to reduce effect of air gap. The measured packing density of the crushed asphaltenes is in the range of 0.5 – 0.6 g/cm^3. However, complete removal of air cannot be ascertained.

The results of dielectric constants of the original crude oils show a clear distinction between the three classifications. The dielectric constant increased as the density of the crude oil increased from light to heavy oil (Tables 4.7 and 4.8). The trend is similar for the loss factor and was also observed in [118]. The loss factor of the crude oil and the deasphalted are very similar, suggesting less effect of asphaltenes on the loss factor, as also reported by [103]. However, this is contrary to an earlier suggestion [119] that asphaltenes made a significant contribution toward the loss factor of heavy oils. The dielectric constant of the crude oil is higher than that of the asphaltenes in the heavy oil, which agrees well

Table 4.7: Properties of the three crude oil samples

Crude Sample	Sample weight (g)	API Gravity (°)	Viscosity @ 25°C (mPa-s)	Asphaltene (wt%)	Specific gravity
S1: Light Crude	2.00	40.58	2.30	1.00	0.8223
S2: Medium Crude	2.00	27.35	9.38	2.00	0.8908
S3: Heavy Crude	28.00	12.80	1483	14. 60	0.9806

Table 4.8: Comparison between measured and literature values of permittivity of crude oil samples

Samples and crude oil categories		Dielectric constant ε_r'			Loss factor ε_r''			Literature values of crude oil [118] [103]	
		crude oil	Asphaltenes	Deasphalted Oil	crude oil	Asphaltenes	Deasphalted Oil	Dielectric constant ε_r'	Loss factor ε_r''
S1	Light oil	2.06 ± 0.04	-	2.37 ± 0.04	0.0141	-	0.010	2.16	0.021
S2	Medium oil	2.25 ± 0.04	-	2.45 ± 0.04	0.0148	-	0.016	2.31	0.020
S3	Heavy oil	2.72 ± 0.05	2.26 ± 0.04	2.52 ± 0.04	0.0159	0.0028	0.018	2.47	0.015

with earlier reported values [120]. This is also in agreement with results obtained for dielectric constant of asphaltenes extracted from vacuum distilled residue (VDR) heavy oil [103, 121].

It has to be said that the results are not conclusive as the extracted asphaltene sample in our study may not have the full density. The deasphalted oil has not been further separated in this work to obtain the fractions of saturates, aromatics and resins. This therefore recommended for future work. The difference in asphaltenes dielectric properties with the earlier reported data can also be attributed to composition of the crude oil which changes according to source, maturity, thermal chemical sulphate reduction and biodegradation [118].

4.10 Measurement of Binary and Ternary Solution at Discrete Resonance Frequencies

The fundamental TM_{010}-like mode and the first higher order mode of a re-entrant cavity resonator have been utilised for the measurement of binary and ternary samples that contains the mixture of ethanol, sucrose and deionised water. The objective is not to analyse the samples but to further validate the measurement method and demonstrate the use of higher order mode for the extraction of dielectric properties of material.

The re-entrant cavity sensing device used and described in previous sections is utilised for this measurement. However, the cavity external coupling is modified for 6.6 GHz resonance. This was achieved by reducing the length of the probes connected at two identical ports of the cavity. The length of conductor penetrating into the cavity is made 1.0 mm instead of 2.9 mm. This is to achieve the insertion loss of at least over 10 dB at the resonance mode. This also reduces the effect of external coupling. The broadband response

of S_{21} given in Figure 4.15 shows the resonance at 5.95 GHz is not affected by the presence of materials. This is due to the absence of E-field at the central position where the sample is expose at this resonance modes as shown by the respective E-field patterns in Figure 4.16. Thus, we can use this resonance peak as a way of calibrating the device for accurate measurement.

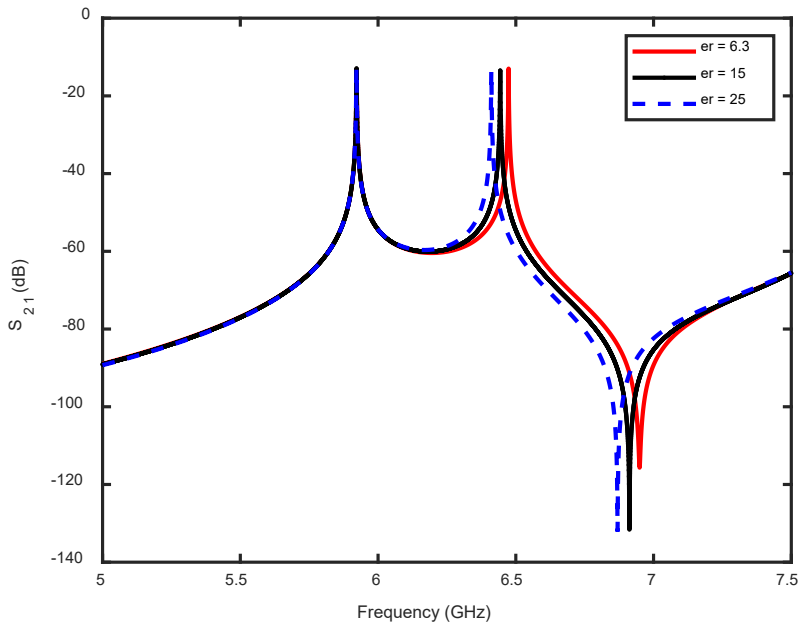

Figure 4. 15 S_{21} Simulation response of the varying □r values for measurements at higher order mode

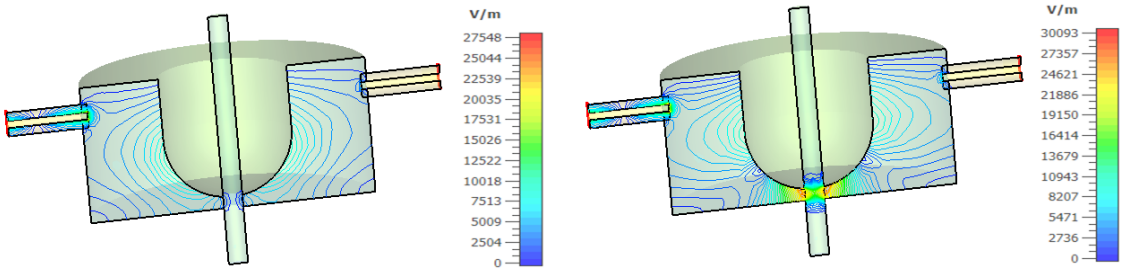

(a) (b)

Figure 4. 16 E-field pattern (a) 5.94 GHz resonance (b) 6.6 GHz resonance

4.10.1 Composition of Binary Solution and Measurements

The composition of binary solutions consider for measurements are describe as follows: First is the solution of 10 % of ethanol diluted in 20 ml with deionized (DI) water ranging from 10 – 50 %; the second solution is a mixture of different amount of sucrose ranging from 1 g to 20 g added to 20 ml of DI water and the third samples is made of varying percentage of Alcohol by volume (ABV) of ethanol ranging from 60 – 100 % with an interval of 10 %. That is, high percentage of ethanol in DI water as compared to the first one. The measurement setup and procedures described in Section 4.5 was adopted for measurements at both 2.0 GHz and 6.6 GHz resonant frequencies. The S-parameter S_{21} response of the measured binary samples at 2 GHz are given in Figure 4.17 to 4.19 for the three sets of binary solutions measured. To validate the measurement at higher order mode using the cavity resonator two of the three sets of the binary samples (60 – 100 % ABV of ethanol and water-sucrose solutions) were considered for the measurements at resonant frequency of 6.6 GHz. The S_{21} response of ABV of ethanol and 15 g and 20 g of sucrose in DI water are given in Figure 4.20 and Figure 4.21, respectively.

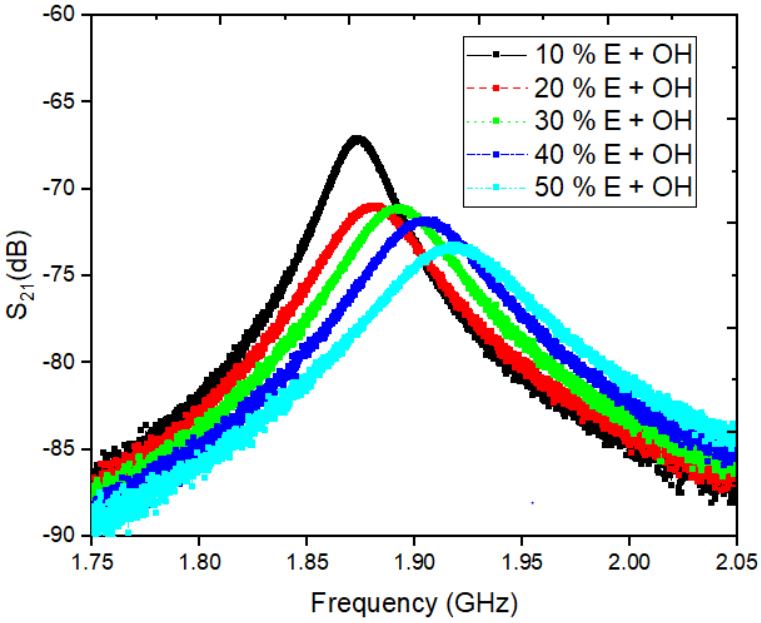

Figure 4. 17 S_{21} response of the varying percentage of ethanol with deionised water measured at 2 GHz

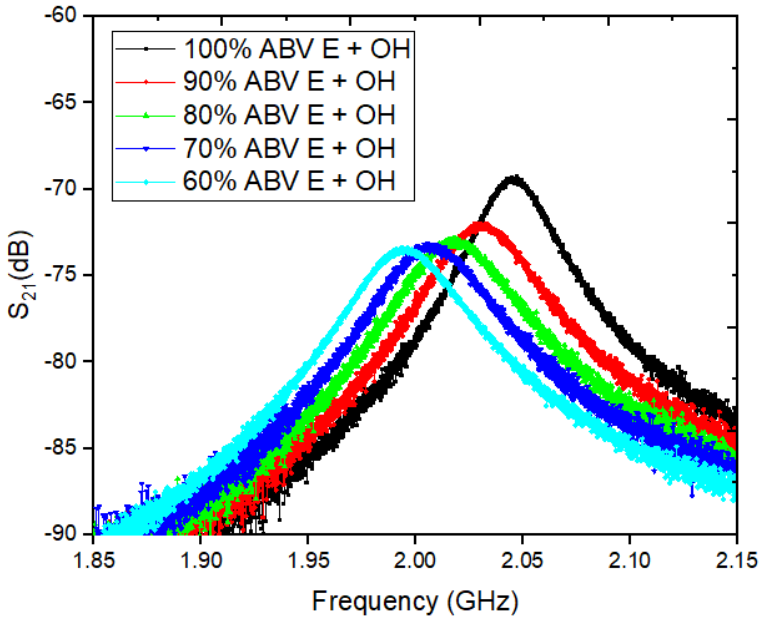

Figure 4. 18 S_{21} response of the varying percentage of alcohol by volume of ethanol measured at 2 GHz

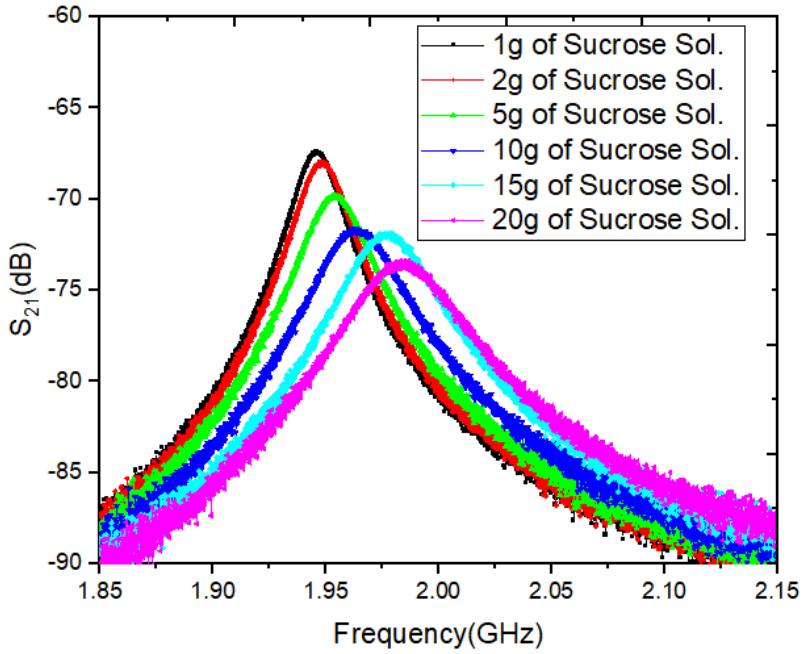

Figure 4.19 S_{21} response of the varying amount of sucrose dissolved in deionised water measured at 2 GHz

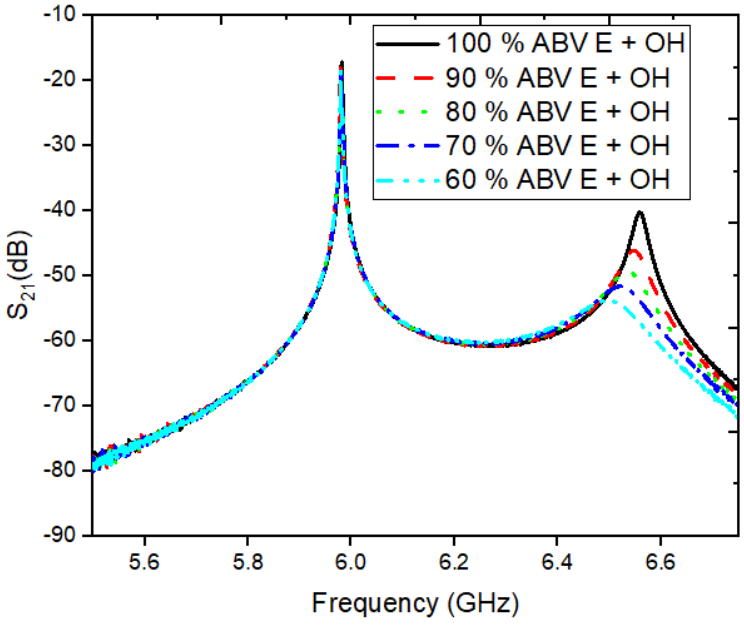

Figure 4.20 S_{21} response of the varying percentage of alcohol by volume of ethanol measured at 6.6 GHz

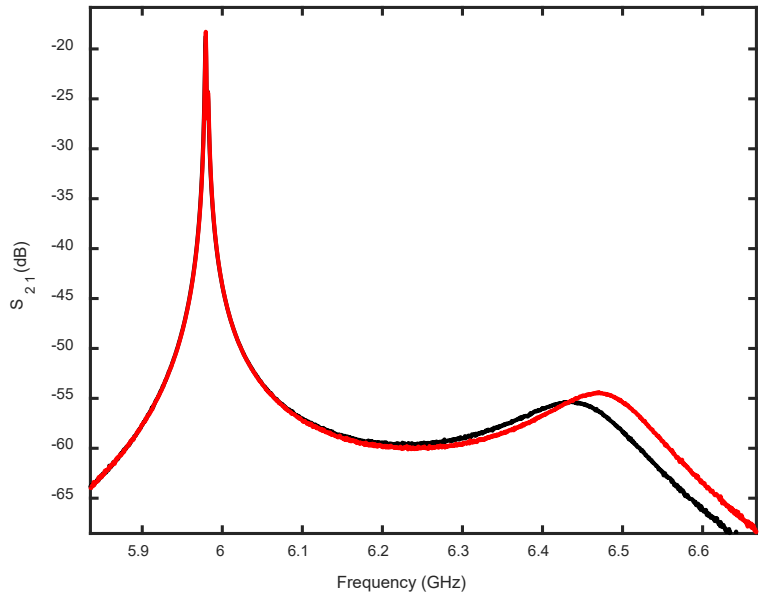

Figure 4. 21 S_{21} response of 15 g and 20 g of sucrose in DI water measured at 6.6 GHz

Table 4.9: Ternary sample composition

Samples	% Deionised water	% Ethanol	Sucrose mass (g)
Sample 1	90	10	10
Sample 2	90	10	4
Sample 3	50	50	10
Sample 4	30	70	2

4.10.2 Ternary Samples

The ternary solution consists of water-ethanol-sucrose in different mixing ratio as detailed in Table 4.9. All samples are prepared in 20 ml volume and the measured S-parameter response is given in Figure 4.22.

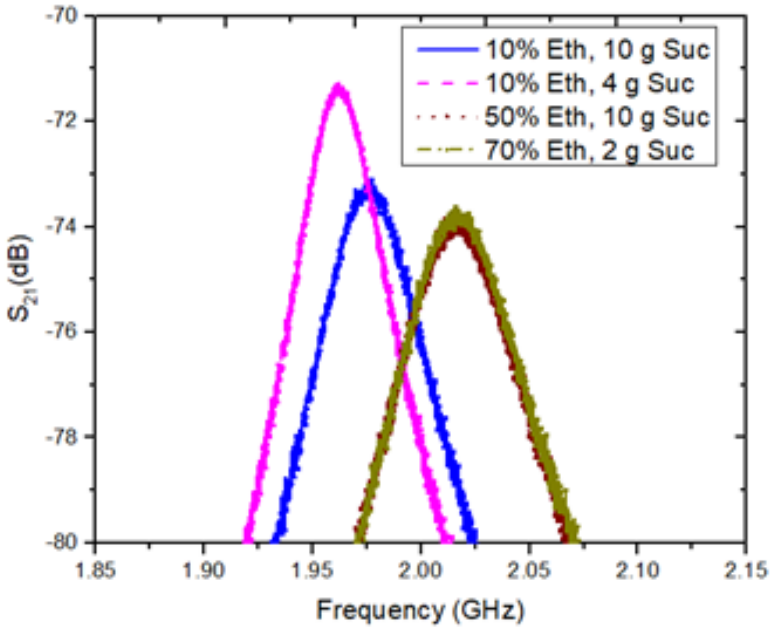

Figure 4. 22 S_{21} response of the measured ternary samples as given in table 4.9 at 2 GHz

4.10.3 Extraction of Complex Permittivity of Binary and Ternary Solutions

To extract the complex permittivity of the measured solutions, the average measured change in frequency and *Q*-factor from five readings is use. The analytical formula developed (4.4), (4.8) and (4.9) as used in Section 4.7 are utilised for the evaluation for measurements at 2 GHz resonant frequency. The results of the complex permittivity and loss tangent together with measured frequency, unloaded *Q*-factor are given in Table 4.10 to 4.12 for all the binary samples. While the results of the ternary solution at 2 GHz resonant frequency is captured in the Table 4.13

Table 4.10: Measured results of % of ethanol in DI water at 2 GHz

Sample	Frequency (GHz)	Unloaded *Q*-factor	Complex permittivity	tan δ
50 % Ethanol	1.9829	44.7025	50.14 – j 18.80	0.37
40 % Ethanol	1.9731	52.4442	58.58 – j 16.85	0.29
30 % Ethanol	1.9641	59.5024	66.82 – j 15.61	0.23
20 % Ethanol	1.9560	65.4632	74.64 – j 14.80	0.20
10 % Ethanol	1.9508	93.7825	79.85 – j 10.56	0.13

Table 4.11: Measured results of % ABV of ethanol at 2 GHz

Sample	Frequency (GHz)	Unloaded *Q*-factor	Complex permittivity	tan δ
100 % ethanol ABV	2.0461	61.4115	8.83 – j 7.91	0.90
90 % ethanol ABV	2.0316	46.8865	16.29 – j 12.06	0.74
80 % ethanol ABV	2.0192	44.4117	23.62 – j 14.28	0.60
70 % ethanol ABV	2.0084	44.0465	30.73 – j 15.73	0.51
60 % ethanol ABV	1.9954	42.8760	40.16 – j 17.78	0.44

Table 4.12: Measured results of deionised water – sucrose solution at 2 GHz

Sample	Frequency (GHz)	Unloaded *Q*-factor	Complex permittivity	tan δ
1g Sucrose Sol.	1.9464	91.0425	84.38 – j 11.07	0.13
2g Sucrose Sol.	1.9486	85.0356	82.10 – j 11.73	0.14
5g Sucrose Sol.	1.9543	68.0216	76.32 – j 14.27	0.18
10g Sucrose Sol.	1.9643	54.0055	66.64 – j 17.06	0.23
15g Sucrose Sol.	1.9765	52.0754	55.60 – j 16.52	0.27
20g Sucrose Sol.	1.9841	45.0354	49.14 – j 18.24	0.33

Table 4.13: Measured results of the ternary sample at 2 GHz

Sample	Freq. (GHz)	Unloaded *Q*-factor	Complex permittivity	tan δ
Sample 1	1.9757	54.1545	59.16 – j 16.28	0.275
Sample 2	1.9621	57.5569	71.82 – j 16.50	0.230
Sample 3	2.0166	37.1342	27.43 – j 18.04	0.658
Sample 4	2.0177	38.5437	26.71 – j 17.18	0.643

For the extraction of complex permittivity at 6.6 GHz resonant frequency, a new mathematical model is develop using similar procedure of the 2 GHz formulation. The change in resonant frequency due to material insertion for dielectric constant from 1- 80 established using simulation for tan $\delta = 0$ is used to generate the formula by curve fitting.

Table 4.14: Measured results of percent of ABV of ethanol at 6.6 GHz

Sample	**Freq. (GHz)**	**Unloaded *Q*-factor**	**Dielectric constant**
100 % ethanol ABV	6.5580	250.7136	5.30
90 % ethanol ABV	6.5453	128.0554	9.09
80 % ethanol ABV	6.5309	86.5042	13.41
70 % ethanol ABV	6.5150	65.6572	18.19
60 % ethanol ABV	6.4860	49.5819	26.96

Table 4.15: Measured results of deionised water-sucrose mixture at 6.6 GHz

Sample	**Freq. (GHz)**	**Unloaded *Q*-factor**	**Dielectric constant**
15g Sucrose Sol.	6.4161	39.0005	48.34
20g Sucrose Sol.	6.4559	45.3545	36.13

A second order polynomial curve fitting provide the new extraction formula given by

$$\varepsilon_r' = 1528.8\left(\frac{\Delta f}{f_c}\right)^2 + 1953.5\frac{\Delta f}{f_c} - 0.0062 \tag{4.10}$$

while the loss tangent equations are not derived in this case. For this, only the results of the dielectric constant of the samples measured at 6.6 GHz with their respective average measured resonance frequency and unloaded *Q*-factor for the two measured binary sample of ABV of ethanol and mixture of DI water and sucrose are given in Table 4.14 and 4.15, respectively.

4.10.4 Results Discussion of Concentration Measurements

The results of dielectric constants and loss tangents of the binary samples measured at 2 GHz resonant frequency are compared using a line plot as shown in Figure 4.23. It can be observed that, decreasing the percentage in amount of ethanol in DI water, ABV of ethanol and the amount of sucrose in DI water increases the dielectric constant, as expected and vice versa. While the loss tangent tends to decrease as the amount of concentration is decrease. On the other hand, the frequency dependency of the binary sample is determined, the results of the of measurement ABV of ethanol and mixture of DI water-sucrose solutions at 2.0 GHz and 6.6 GHz resonant frequencies are compared and presented in Figure 4.24. The results show frequency dispersion as the permittivity of the material decreases with increasing frequency. Similar trend has been observed from a reported results of percentage of ethanol in deionised water [122].

In the measurements of ternary samples even though only few samples were measured, the results of (sample 1 and 2 as detailed in Table 4.9) shows that the amount of sucrose in a solution of deionised water and ethanol decreases the dielectric constant and increases the lost tangent and vice versa. Similarly, in sample 3 which has high percent of DI water than sample 4, higher value of dielectric constant is expected. However, similar dielectric constant was recorded due to the large amount of sucrose in sample 3. This shows the complexity when three constituents interact to form a solution. Therefore, dielectric metrology is promising method for determination of concentration levels even in ternary solutions. The results obtained for both binary and ternary samples are in conformity with data reported in literature [122] [123].

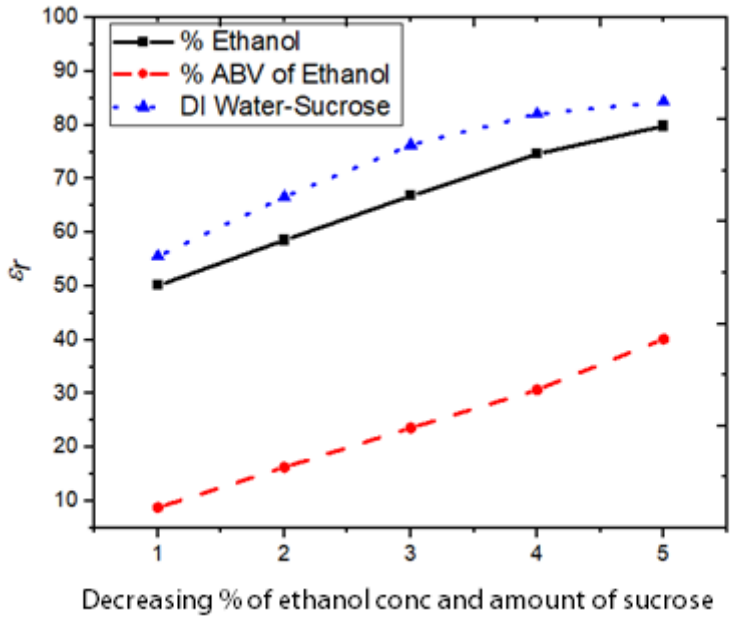

(a)

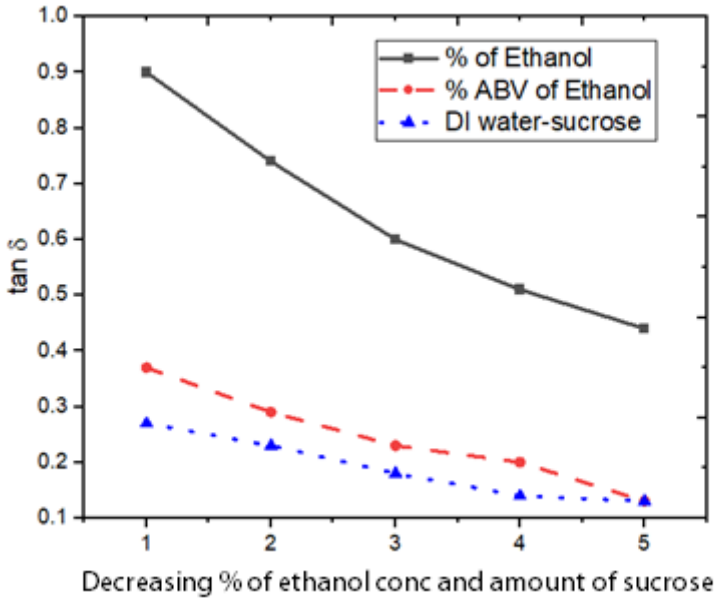

(b)

Figure 4. 23 Comparing results of binary samples measured for five sample at 2 GHz (a) dielectric constant (b) loss tangents

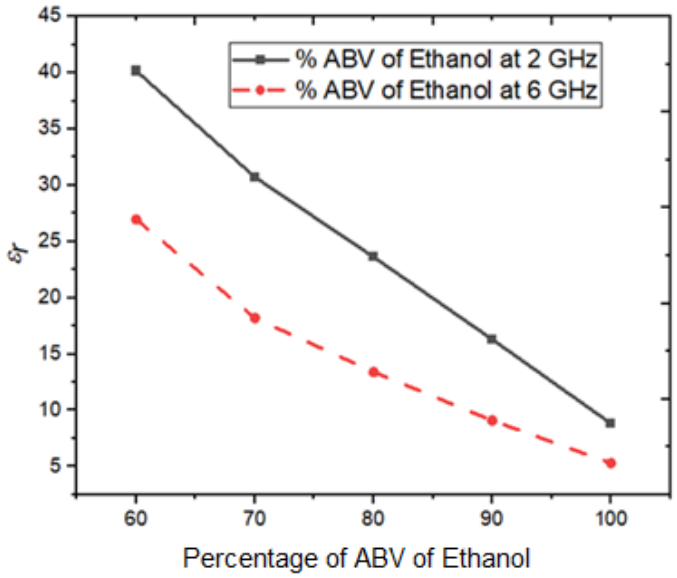

(a)

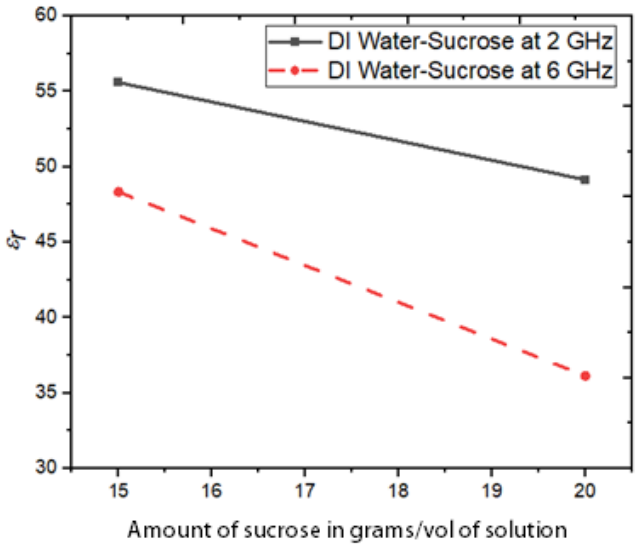

(b)

Figure 4. 24 Comparing results of measured dielectric constant ε_r' at 2 GHz and 6.6 GHz

(a) % ABV of Ethanol (b) DI water-sucrose

4.11 Summary

A modified re-entrant cavity resonator has been realized for complex permittivity measurement of liquids sample at 2.0 GHz. A unified analytical formula was developed based on simulation to accurately extract the complex permittivity of the samples. The influence of the dielectric constant on the loss-tangent model has been fully considered. The cavity has the advantage of high-quality factor and confined electric field. Experimental tests have been carried out to demonstrate the sensing capabilities of the sensor using several common solvents. Results obtained verified the device capability in permittivity measurement and its sensitivity in purity measurement as seen in the case of acetone. The device has also been used to measure the dielectric properties of three different crude oils as classified by API gravity - light, medium and heavy oils. The correlation between dielectric permittivity and the crude category has been established. The results obtained from the measured dielectric properties reveals that the presence of asphaltenes has less effect on the dielectric loss of the crude oil than other components. A lower dielectric constant than the original oil was obtained in the case of asphaltenes as against earlier reported findings using technique other than cavity perturbation. However, this investigation and comparison is not conclusive due to potential influence from the sample density. This study has now opened up the need to investigate further the asphaltenes properties in relation to crude oil density and viscosity using microwave sensing techniques. In addition, the cavity has been used to demonstrate the use of discrete frequency for dielectric metrology and was validated by measuring several binary and ternary solutions.

CHAPTER FIVE: COAXIAL MICROWAVE RESONATOR SENSOR FOR DIELECTRIC MEASUREMENT OF LIQUID

This chapter presents a coaxial resonator for dielectric measurements of low and medium loss liquids at multiple resonance frequencies up to 8 GHz with the fundamental transverse electromagnetic (TEM) resonant mode at 2 GHz. The measurement is by filling the entire resonator cavity with the material under test and the permittivity of the material is easily extracted using simple equations**.** This technique provides an easy and accurate extraction method of dielectric properties without any analytical approximation and dedicated software algorithm as used in broadband open coaxial probes or the complex perturbation formula in resonator-based methods. This significantly reduces the risk of systematic errors from the model approximation. The measured *Q*-factor of the resonator is 2650 – 3500 depending on the resonant mode. This allows for the measurement of samples with loss tangents up to 0.05 (Acetone tanδ taken as reference). The device was made by 3D printing and verified by measurements of several common solvents at all four resonance frequencies. The results obtained agree well with values reported in literature. Further measurements of crude oil samples were carried out to determine the effect frequency dispersion and results confirmed with values obtained using other techniques. This work has been published in Microwave and Optical Technology Letter.

5.1 Background of Materials Measurement using Coaxial Resonator

Coaxial cavity resonators have been widely utilised in the measurements of dielectric permittivity material [124]. One of the most common types is the coaxial probe, also

referred to as open-ended coaxial line for liquids, solids and gels materials [125]. In this type of measurement, the sample is place in contact with the open-end of the resonator to determine the reflection coefficient or transmission coefficient over a broadband depending on the port-type [126]. The resonance frequency shifts, and quality factor of the cavity changes as the electric field fringes into the material under test MUT. These quantities are then utilised in the extraction of the dielectric properties. Based on this principle various design approaches have been reported in the literature.

An open coaxial resonator with RF transceiver with microcontroller as measuring instrument was presented for moisture monitoring for industries such as paper, textile, and foil processing [127]. In order to reduce the effect of air gap associated with open-ended resonator the authors introduce a spring supported inner conductor [127] [128]. Detailed design process of coaxial resonator has also been reported by [129] and the author later used the design approach for rain sensing using glass cover at open-end [130]. A coaxial-feed open-ended cut-off circular waveguide resonator have been utilized for dielectric measurement using a reflection type measurements approach [126] and was later verified in comparison with other methods [131]. More recently, Zhu *et al*. reported a hollow coaxial cable Fabry-Perot resonator that is made for dielectric constant measurement at low-cost for the first time. The concept is to replace the insulator in the cable with air and create an opening in the hollow coaxial cable. The opening groove allows the liquid into the cavity and the reflected signal is measured [49].

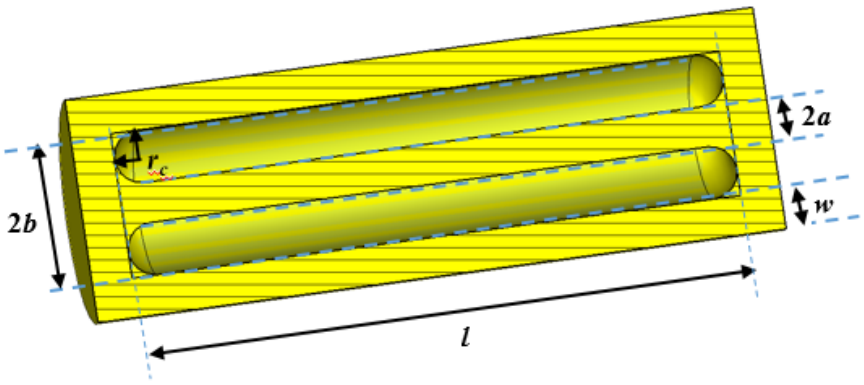

Figure 5.1 Illustration of half-wave coaxial resonator internal structure with design dimensions in millimetre (mm*): a = 5, b = 17.9, l =74.59, w = 5 and* r_c *= 3.25*

In this work a closed-end coaxial cavity resonator is proposed for the measurement of low and medium loss liquids material for the first time to the best knowledge of the author. The design is in such way that the entire cavity would be filled with the MUT and easily extract the permittivity of the material using simple equation as against cavity perturbation formula, thereby reducing a great deal involved in computation of the dielectric properties. What's more, multiple resonances are used to establish the dielectric property as a function of frequency up to 8 GHz.

5.2 Design and Fabrication

The half-wavelength air-filled coaxial was made short-circuited at both ends to facilitate the support of the central conductor. As shown in Figure. 5.1, the diameter of the inner conductor of the coaxial resonator is a = 5 mm while the outer cavity diameter is b = 17.95 mm, which is approximately 3.59 times the inner radius to ensure the optimum quality factor (Q-factor) [132]. The length of the coaxial resonator l is 74.59 mm, half of the wavelength at the fundamental frequency. To increase the Q-factor and mitigate effect of

losses resulting from sharp corners in the cavity we have introduced round corners in the coaxial cavity resonator. Simulation shows a corner radius r_c of 3.25 mm resulted in 2.5% increase in Q-factor compared to the one without round corners. A 3 mm hole was created to enable liquid sample insertion. The coaxial resonator is coupled based on a transmission configuration and the coupling into and out of the resonator was deliberately made weak to attain insertion loss of over 10 dB in all the resonance modes. The resonator is excited with two identical 50 Ω Subminiature A (SMA) connectors. The SMA open probe has a conductor diameter of 1.3 mm with 1 mm penetration length into the cavity. These design parameters provide frequency operation based only on TEM modes up to 8 GHz with a fundamental transverse electromagnetic (TEM) mode resonance of 2 GHz. The 8 GHz limit is determined by the onset of the first high-order non-TEM mode (TE_{11}) and it covers four TEM-mode resonances within the frequency range.

Besides the fundamental TEM modes, there are other TE and TM modes in the coaxial resonator that could be utilised for the measurement of dielectric properties of materials. However, an added complexity with the use of these higher order modes lies in the tracking of the mode after filling the liquid. This is possible but not considered in this work. In order to maintain the use of only TEM mode resonances but extend the operation frequency range, the limit of the upper frequency by TE_{11} mode could be pushed higher by reducing the dimension of the inner and outer conductor while maintaining the ratio b/a = 3.59 for the optimum Q-factor. Also, as the length of the resonator determines the frequency of the first fundamental TEM mode, increasing the length of the resonator will be able to generate more modes (and therefore more measurement points) within the frequency range. This work only uses four TEM-mode up to 8 GHz to ease fabrication within reasonable dimensions.

The coaxial resonator is closed at both ends. To ease fabrication and assembly, the device has to be cut. However, cutting along the radial direction of the coaxial disturbs the currents and increases the losses. To minimise this effect, the cutting has to be made at a point where the current density is not at its maximum for all the concerned resonance modes. To this end, the current distributions in all four resonance modes are studied and shown in Figure 5.2, based on eigen-mode simulation in CST Microwave Studio. Cutting the device in the middle or at the ends may significantly disturb the current of at least two modes, as it cuts through the current maxima. To avoid these maxima, the device was conveniently cut at distance l_1 = 28.827 mm from one end. At this cutting position, we have considered the trade-off between all four modes. This to a large extent will not have much effect on the overall performance of the device, as later confirmed by the experiment. It is noted that further trade-off may have to be made if more resonances are used either to extend the measurement frequency range or the number of data points. Having said that, as the extraction of the dielectric property relies on the differences in frequency before and after the liquid filling rather than the absolute frequency values. The impact of the cutting is not expected to be significant. The depth and round geometry of the coaxial structure presents a big challenge for CNC machining. Therefore, the device was manufactured by stereo-lithography (SLA) 3D printing with Accura 25 plastic materials. The device was then copper plated inside and out with a 10 μm thickness.

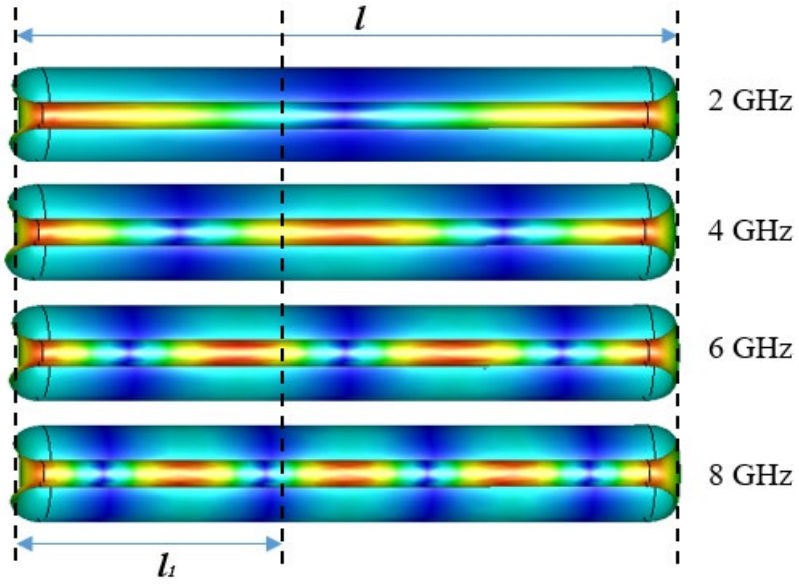

Figure 5.2 Coaxial cavity resonator current density field strength

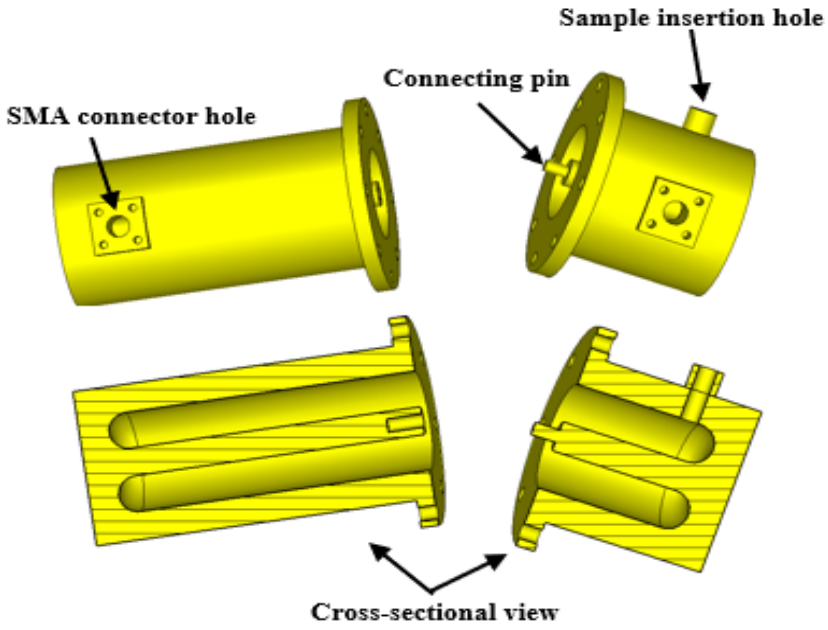

Figure 5.3 Coaxial resonator (a) 3D CST model (b) cross-sectional view of the model

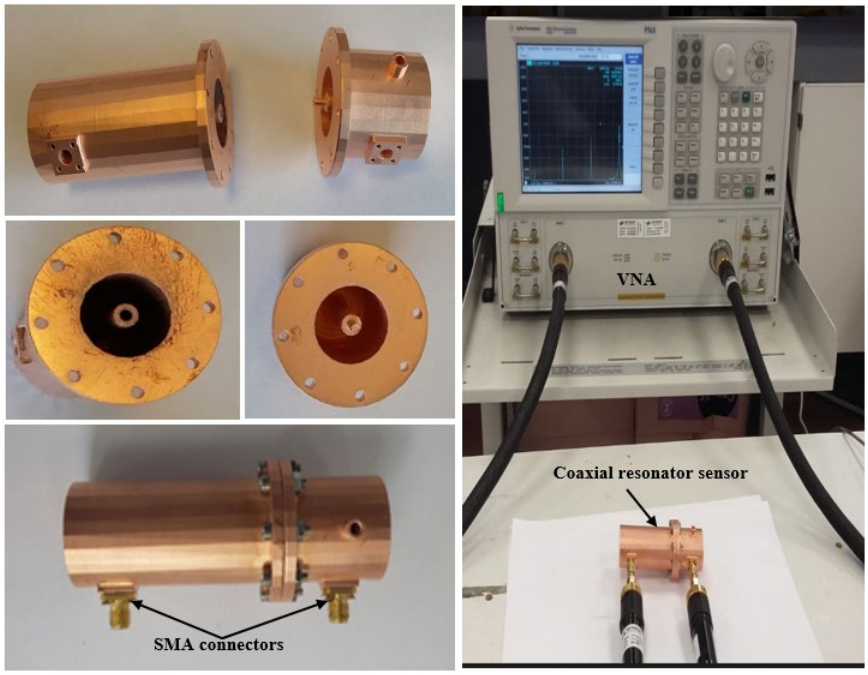

(a) (b)

Figure 5.4 Coaxial resonator photograph (a) prototype (b) measurement setup

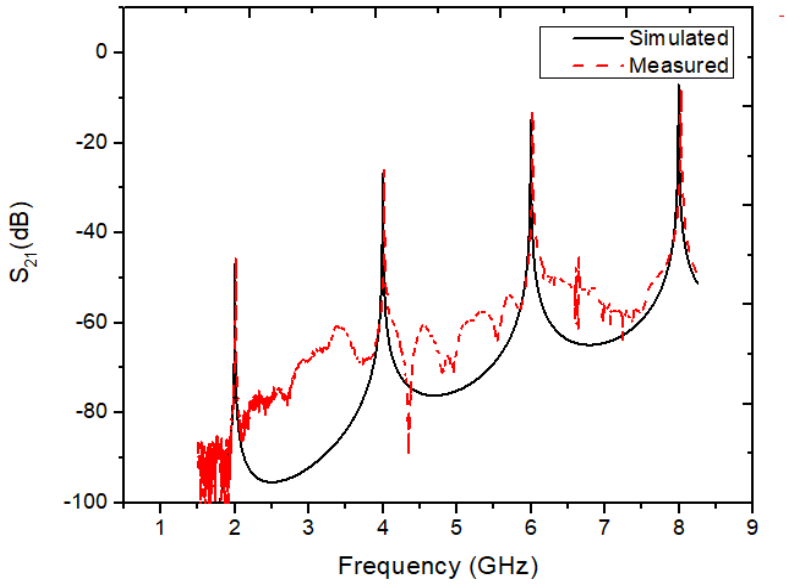

Figure 5.5 Broadband S_{21} response of measured and simulated empty coaxial resonator

5.3 Test and Measurements

The coaxial resonator cavity was tested after assembling the device with eight 2.5 mm screws as shown by the photo of the prototype and the measurement setup in Figure 5.4. The measurement procedure begins by calibrating the device using 85052D calibration kit over a frequency range of 250 MHz to 8.50 GHz. An IF bandwidth of 500 Hz was used with 6401 sweep point to better the accuracy of the *Q*-factor measurement using the 3dB method. The measured and simulated broadband transmission coefficient S_{21} response of the empty coaxial resonator is given in Figure 5.5 and Figure 5.6 (for each resonance mode). There is a close agreement between the two results with a frequency shift of around 10 MHz (0.50%) at 2 GHz, 19 MHz (0.48%) at 4 GHz, 26 MHz (0.43%) at 6 GHz and 30 MHz (0.38%) at 8 GHz. These small shifts are a result from the fabrication tolerance of about 10 µm. The measured *Q*-factor is 2650-3500 for the four resonances, which is in very good agreement with the simulated *Q* of 2900-3850. This demonstrated good fabrication accuracy of the SLA and plating quality.

5.4 Material Measurement

To verify the device for dielectric property measurement, the coaxial resonator was filled with different samples using a glass pipette through the 3 mm hole opening as shown in the measurement set-up in Figure 5.4 (b). Three common solvents of n-heptane Analytical Reagent AR grade, hexane HPLC grade (purity 95%) from Fisher Scientific, and pentane reagent grade (purity 98%) from Sigma Aldrich Ltd were used as standard sample to calibrate the device. The cavity is emptied after every measurement and was allowed to

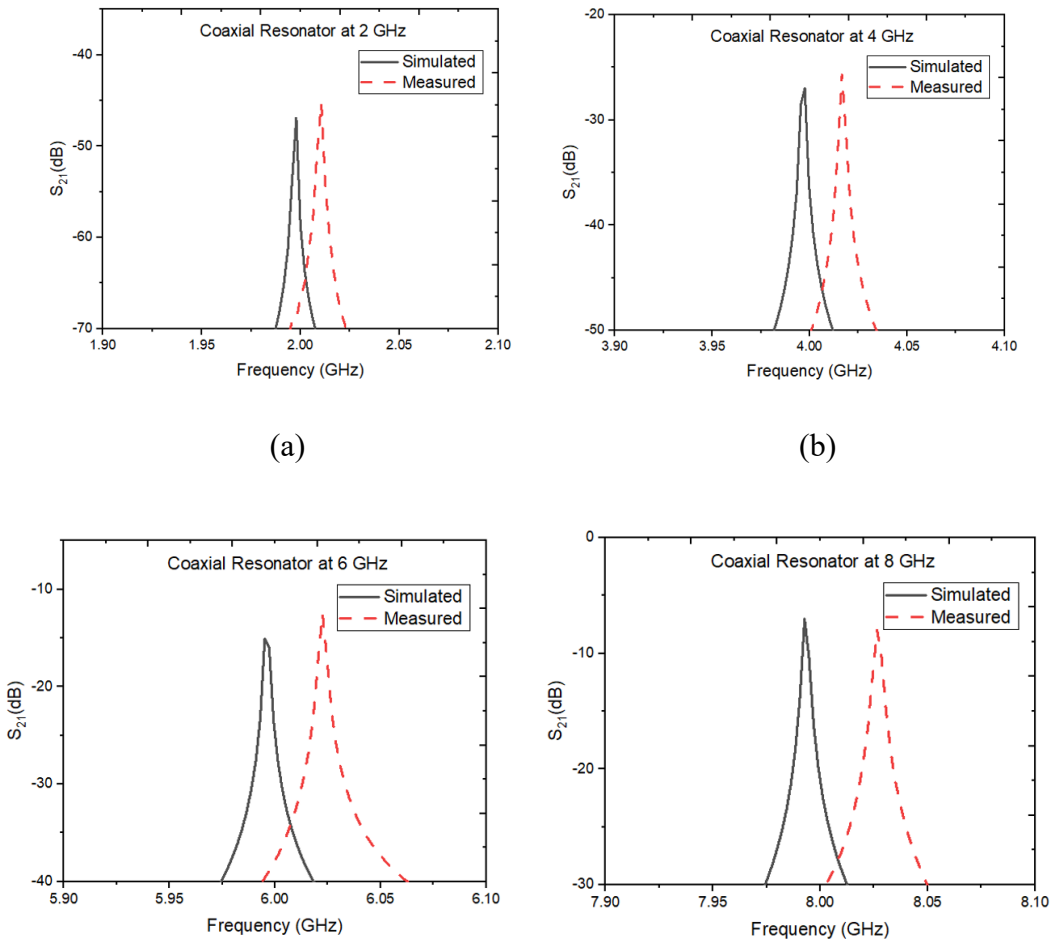

Figure 5.6 S_{21} response of measured and simulated empty coaxial resonator at (a) 2 GHz (b) 4 GHz(c) 6 GHz (d) 8 GHz

evaporate. The cavity was further heated gently with an electric air heater dryer. The device is then cool to the ambient temperature. The empty cavity is then measured again at all the four resonant modes before putting in a new sample and measured accordingly. The S_{21} response of the empty cavity after cleaning following the measurement of pentane and hexane is shown in Figure 5.7. There is very little change in the response. Further measurements of dielectric properties of light and medium crude oils as classified by American Petroleum Institute API gravity were carried out. Acetone as a medium loss sample was also measured. Following the measurement of light crude oil, the cavity was

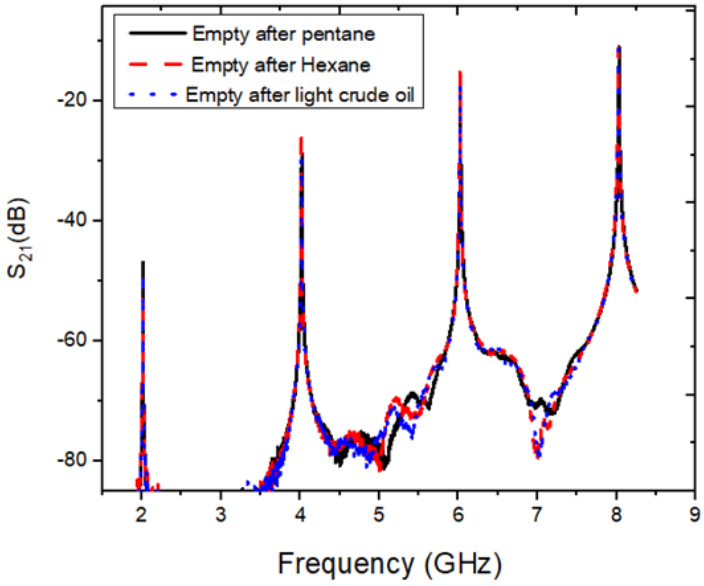

(a)

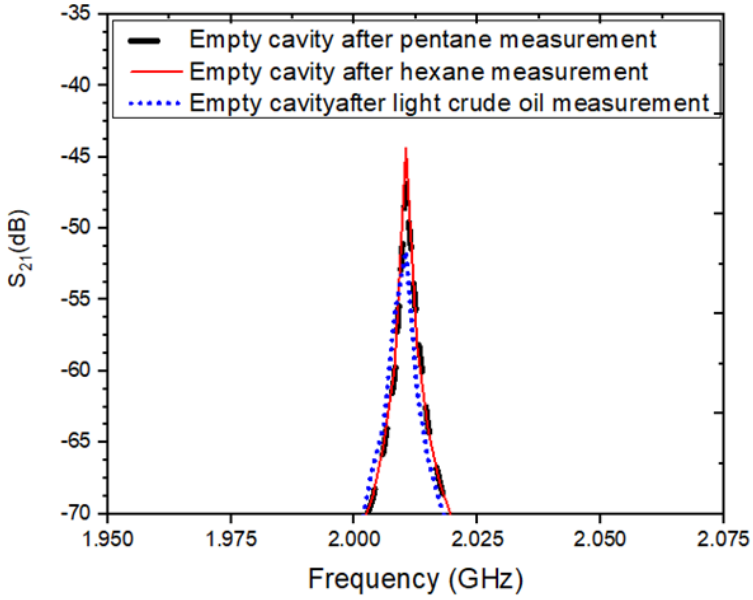

(b)

Figure 5.7 Measured S_{21} of the coaxial resonator: (a) Broadband response of empty cavity after measuring different sample of pentane, hexane and light crude oil (b) response at 2 GHz

cleaned with isopropanol. However, this time the *Q*-factor of the cavity reduced by 7.5 % due to cavity contamination which is about 7 dB difference. The resonance frequency barely changes as shown in Figure 5.7. Further measurements of dielectric properties of acetone, light and medium crude oil as classified by API gravity as known and unknown samples were carried out respectively. The broadband S_{21} response of common solvents and crude oil materials measured is depicted in Figure 5.8 and 5.9 respectively. We can clearly observe the peak of the response, the magnitude of S_{21} and its change over the broadband.

5.5 Extraction of Dielectric Properties

The resonance frequency and *Q*-factor before and after the samples was put into the cavity were measured. The resonance frequency was used to evaluate the magnitude of the dielectric constant based on the relationship given by [133]

$$\varepsilon = \left(\frac{f_r}{f_s}\right)^2 \tag{5.1}$$

where f_r is the resonance frequency of the empty cavity and f_s is the resonance frequency with the sample. The measured *Q*-factor was used in extracting the dielectric loss tangent tan δ of the material. Filling the cavity with dielectric medium affects the unloaded *Q*-factor, which is determined by dielectric losses and conductor losses as given in the relation (2.28) in Chapter 2.

$$tan\delta = \frac{1}{Q_d} \tag{5.2}$$

The loaded Q-factor before and after the cavity is filled with liquid samples are measured. The unloaded Q-factors were extracted using equation (2.16) in each case. The Q-factor due to radiation Q_r was estimated to be 2.4×10^6 based on simulation using (2.15).

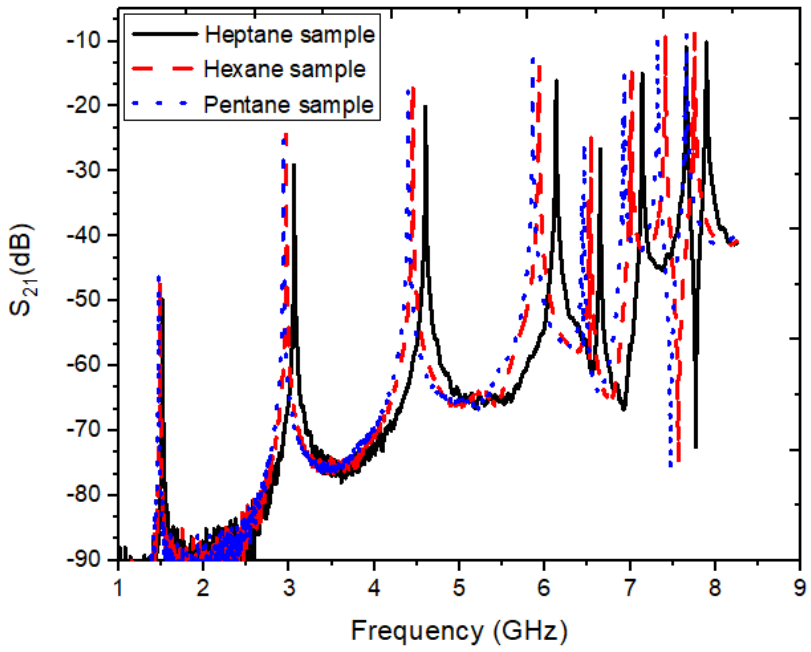

Figure 5.8 Measured broadband S_{21} of the common solvents

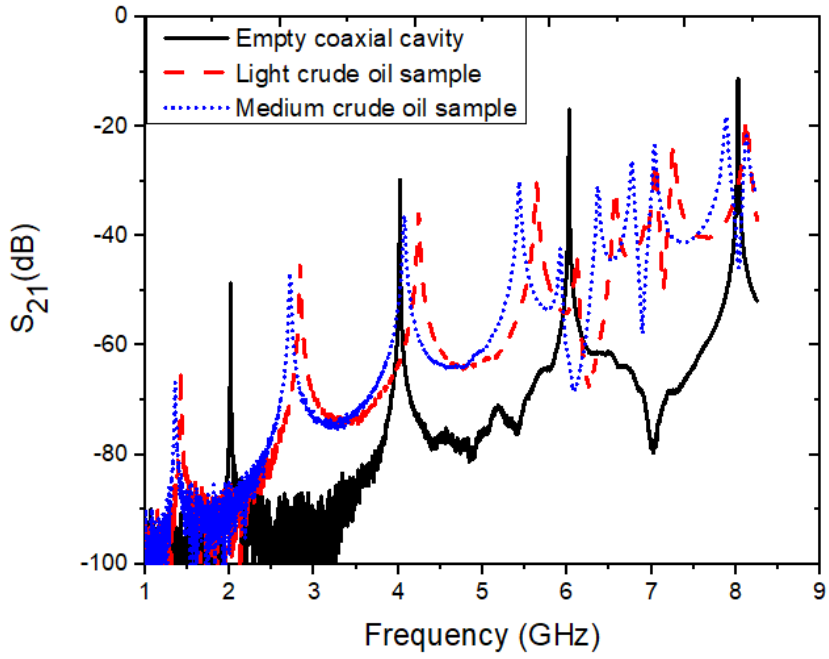

Figure 5.9 Measured broadband S_{21} of the coaxial resonator of Crude oil samples

Neglecting Q_r, $Q_u \approx Q_c$ when the cavity in empty. The loss tangent is then evaluated using (5.2) and (2.28). The results of all the measured samples at all the resonance modes are given in Table 5.1 and is discussed in Section 5.7.

5.6 Sources of Error and Condition of Accuracy

The errors in measurements of the dielectric properties (ε_r and $tan\ \delta$) using coaxial cavity resonator depend not only on the accuracies of the measured resonance frequency and loaded quality factors but also on several other factors. This includes

- Error resulting from temperature instability
- Error due to air bubbles/air gap in the cavity resonator
- Mismatch due to coupling probe

Minimising the influence of these factors is essential for obtaining accurate results. For this, special measures were taken. The errors in reading and recording the values of resonant frequency and *Q*-factor has been mitigated by the measures outlined in the calibration and evaluation process in Section 5.4. To overcome the effect of air gap/air bubbles, as the inner cavity of the resonator is not visible, air bubbles were removed by pushing the air out in way of tilting the device to ensure adequate removal of air by means of pressure. However, it is difficult to ascertained complete removal of the air bubbles. The effect of air gap was then analyse using CST simulation by introducing an air gap varying from 0.5% - 7.55 % of the sample volume over ε_r of 2 - 10 in step of 2 using the first resonant mode. An air gap of 0.5 % will results in change in dielectric constant ($\Delta\varepsilon_r$) of 1.45 % and this will go higher as the percentage of air gap and ε_r value increase. Therefore, 0.5 % air gap is consider as the uncertainty and was reflected in the results of the measurements. Microwave heating can be a big challenge in cavity resonator which is usually addressed by taking a quick measurement within some seconds. However, for coaxial cavity resonator taking reading over a broadband can take time and may results into microwave heating depending on the power, thereby affecting the accuracy of the measurement. However, in this case the input power is too low for a significant microwave heating.

5.7 Results Discussion

As given in Table 5.1, the measured dielectric properties of the samples under consideration are in close agreement with literature values and in consistence to each other at all resonant frequencies. The maximum variation among the four modes is about 1.25%

for all the measured samples with reference to the fundamental mode results. This has strongly validated the measurement method. Similarly, the results of the low and medium crude oil samples presented earlier in Chapter 4 (light crude oil ε=2.06 and medium crude oil ε = 2.20) are in conformity with the results presented in Table 5.1. However, one question lies in the re-usability of the resonator. The cavity has to be open, clean and re-assemble after every measurement. Depending on the type of material measured, the cavity is subject to potential contamination or even damage. However, as the measurement of the dielectric constant depends only on the ratio of resonant frequency before and after the sample, this may not have a significant effect on the results. This has been further verified by measuring hexane sample at all the resonant modes following cavity contamination (with heavy crude oil) and measured fundamental resonant frequency of the empty cavity being 1.988 GHz and *Q*-factor of 564. Results obtained (e.g. hexane ε_r =1.878 at 2 GHz) are still in consistence with the earlier results given in Table 5.1 for the dielectric constant and in conformity with the values in literature. However, the *Q*-factor due to dielectric loss of the material in this case cannot be correctly evaluated. The measured *Q*-factor is far below the initial measured *Q* of 2650 and therefore, does not represent the actual ratio of energy stored and dissipated due to the dielectric loss of the material. For this, the loss tangent is not extracted in this case. Therefore, from our experience and the results of investigation presented here, it is believed that reopening the cavity is less of the problem. The main issue in this case is the degradation of the metal coating on the 3D printed part. This is a relatively well-known challenge for plastic 3D printing. However, it can be mitigated by using other fabrication method such as 3D metal printing.

5.8 Summary

A coaxial half-wavelength cavity resonator was designed to undertake dielectric measurement of low-and medium dielectric loss liquids over a broadband up to 8 GHz. Four resonance modes are utilised. The device was fabricated by 3D printing. The change in resonance frequency and the *Q*-factor of materials under measurement were measured by filling the entire cavity. The dielectric properties were extracted using a simple and accurate formula. The results obtained have validated the capability of using the device for dielectric metrology. The re-usability of the device remains a challenge for the closed coaxial resonator especially as to the extraction of loss tangents. However, the technology provides an easy and accurate extraction method of dielectric properties without using any dedicated software algorithm as in the broadband open coaxial probes or using complex cavity perturbation formula in the resonant method. The risk of system error due to analytical approximation is therefore mitigated.

Table 5.1: Dielectric Constant and Loss Tangent of MUT at Four Resonant Modes

Samples	**2 GHz**		**4 GHz**		**6 GHz**		**8 GHz**		**Literature**		**References**
	ε_r	**tan δ**	ε_r	**tan δ**	ε_r	**tan δ**	ε_r	**tan δ**	ε_r	**tan δ**	
Heptane	1.81	0.00013	1.81	0.00017	1.82	0.00024	1.83	0.00033	1.92	0.00041	at 8 GHz [39]
Pentane	1.84	0.00010	1.84	0.00013	1.83	0.00017	1.84	0.00023	1.84	0.00025	at 8 GHz [39]
Hexane	1.88	0.00011	1.88	0.00014	1.88	0.00019	1.88	0.00026	1.89	0.00031	at 8 GHz [39]
Acetone	20.98	0.016	20.81	0.031	20.97	0.043	21.02	0.055	21.40	0.047	at 2 GHz [115]
Light crude oil	2.00	0.0055	2.01	0.0055	2.02	0.0051	2.03	0.0049	2.16	0.0097	at 2 GHz [118]
Medium crude oil	2.20	0.012	2.18	0.010	2.19	0.0092	2.20	0.0085	2.31	0.0064	at 2 GHz [118]

CHAPTER SIX: 60 GHZ HIGHER ORDER MODE RE-ENTRANT CAVITY RESONATOR FOR LIQUID CHARACTERISATION

In Chapter 4 re-entrant cavity has been used for liquid measurements within the S-band frequency range and good performance was demonstrated. In this chapter the use of re-entrant cavity structure for measurements of dielectric properties at higher frequency such as the V-band is proposed. As discussed in Chapter 2, for cavity resonator structures, as the frequency increases the size of the cavity becomes small. This therefore presents a challenge in fabricating and utilising the cavity for dielectric measurements, using the technique described and used in Chapter 4. That is, inserting or placing the sample at the centre of the cavity. However, there exist some higher order modes which can be utilised for dielectric measurements of liquid materials at higher frequencies. Having described the advantage of re-entrant cavity over other cavity structure in the preceding chapters and the growing interest in dielectric characterisation at millimetre wave [134], a 60 GHz cavity resonator sensor for material measurements is presented here. To design cavity resonator at 60 GHz and to use its fundamental mode for measurement makes the cavity very small and the Q-factor is also very low. For this, the higher order mode is considered and can be utilised to achieve higher frequency measurement with high-Q. It is also less sensitive to fabrication tolerances. The design of the re-entrant cavity is given in Section 6.1 with detail comparisons of the E-field of re-entrant cavity and cylindrical cavity for the mode of interest. Simulations were run to determine the measurement capability and limit to which dielectric properties of materials can be characterise using the proposed cavity. The results of the investigation are presented in Section 6.2. The final design and fabrication of the cavity is highlighted in Section 6.3. The measurements set up and results of the

measurements are presented and discussed in Section 6.4 and Section 6.5, respectively. The summary of this chapter is given in Section 6.6.

Table 6.1: Cavity dimensions

Description	Dimension (mm)
Radius of cavity, ***R***	5.00
Height of cavity, ***H***	5.00
Post radius, ***r***	2.50
Post height, ***h***	4.00
Gap region, ***g***	1.00

6.1 Field Pattern Analysis of Cylindrical and Re-Entrant Cavity Transverse Mode

The proposed higher order mode re-entrant cavity is examined in comparison with cylindrical cavity resonator in terms of their field pattern in the transverse magnetic (TM) modes. The cavities were simulated using the dimensions given in Table 6.1 for the purpose of analysis and examination of the higher order mode within the V-band frequency range. The simulations result of 22.95 GHz resonant frequency for cylindrical cavity and 10.10 GHz for re-entrant for the fundamental TM_{010} mode were obtained. The cross-sectional view of the cavities and their dimensional labels are shown in Figure 6.1. The design and dimensions of the proposed 60 GHz will be presented in subsequent Sections

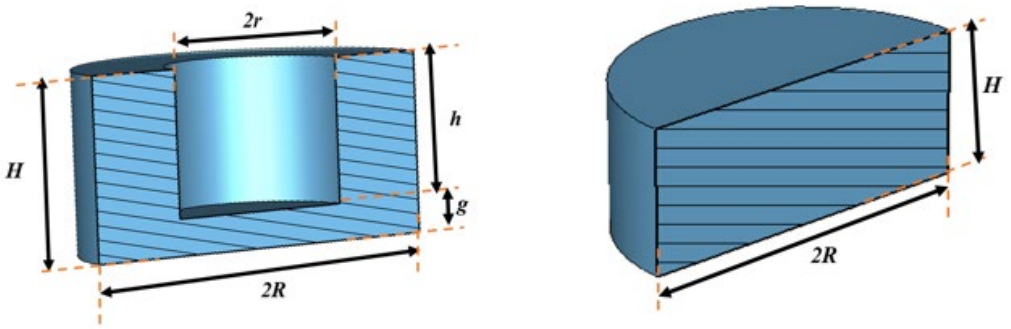

Figure 6.1 Cross-sectional view: (a) a re-entrant cavity (b) a cylindrical cavity: Dimensions as given in Table 6.1.

The fundamental and first higher order TM modes of a re-entrant cavity have analogous field patterns to that of a cylindrical cavity as shown in Figure 6.2 and 6.3, respectively. The standard re-entrant cavity mode transforms into cylindrical cavity by simply removing the central post, and this can be viewed as a perturbed TM_{010} mode. In a re-entrant cavity, as discussed earlier, most of the electric energy is retained in the gap region with the stronger field at the central position. This confined electric field at the central post can be utilised for the measurement purpose, making the cavity sensitive to small changes. The objective of the comparison is to demonstrate the analogous form of the field pattern in the two cavities at the desire modes. Moreover, cylindrical cavity at higher frequency have been reported for dielectric measurement in [80] based on cavity perturbation technique. However, the use of a re-entrant cavity for dielectric materials characterisation at higher frequencies has not been reported in the literature using similar technique.

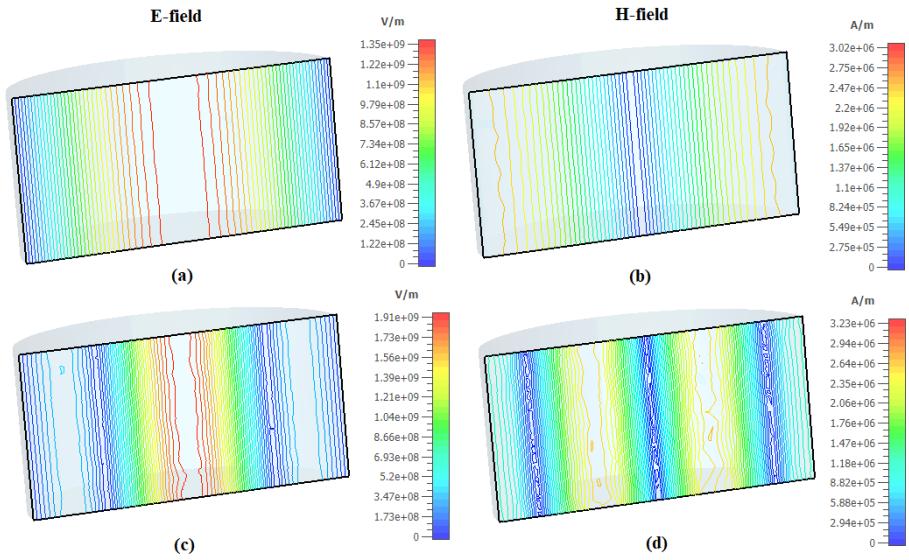

Figure 6.2 Electric and magnetic field pattern of the cylindrical cavity: (a & b) fundamental TM_{010} mode at 22.95 GHz; (c &d) Higher order TM_{020} mode at 52.68 GHz

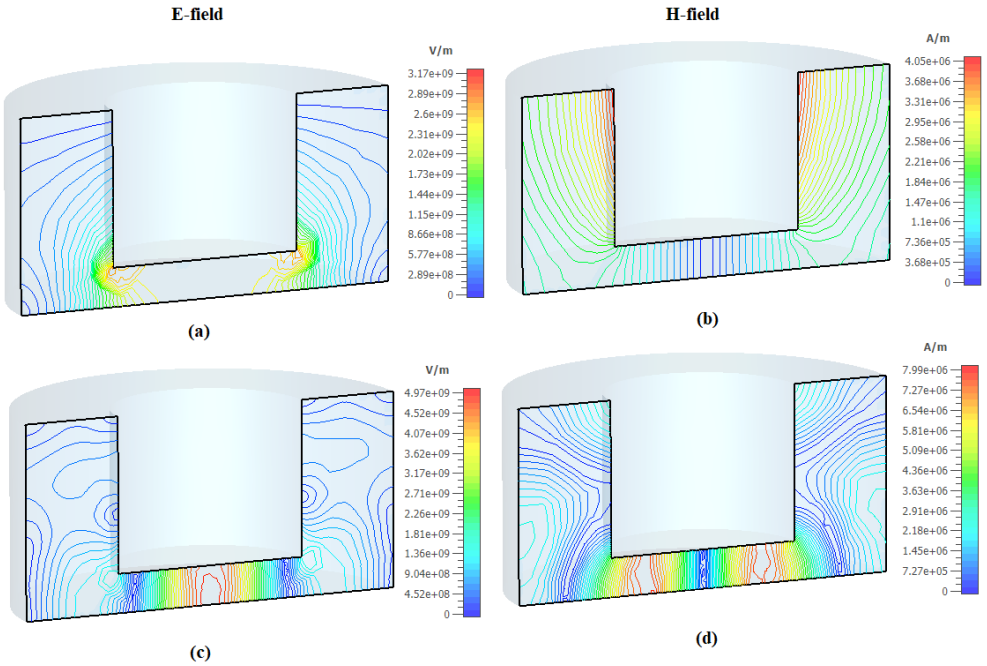

Figure 6.3 Electric and magnetic field pattern of the re-entrant cavity: (a & b) Fundamental TM_{010} mode at 10.10 GHz; (c &d) Higher order TM_{020} mode at 54.54 GHz

Table 6.2: Dimensions of the waveguide and coupling iris of the re-entrant cavity

Designation	Dimensions (mm)
Waveguide width, w_w	3.76
Waveguide height, w_h	1.88
Waveguide length, w_l	3.00
Coupling iris height, C_h	1.034
Coupling iris width, C_w	1.316
Coupling iris length, C_l	0.75

6.2 Design of V-band Re-entrant Cavity

The re-entrant cavity in this chapter is design to operate at 60 GHz higher order resonant mode. The cavity has the following dimensions: a radius r = 4.583 mm and height h = 4 mm with a gap g =1 mm between the cavity and the post. Due to small size of the cavity a waveguide coupling was adopted to couple energy into and out of the cavity. This was enabled via two V-band (50 to 75 GHz) WR 15 waveguides. The dimensions are shown in Figure 6.4 as given in Table 6.2. The two ports are made identical, placed directly opposite to each other. The broadband S_{21} response of Figure 6.5 shows two peaks at 56.83 GHz and 60.00 GHz corresponding to TM_{210} and TM_{020} modes based on their electric field patterns as shown in Figure 6.6, respectively. There is no presence of the electric fields at 56.83 GHz resonant frequency, and therefore will not respond to presence of materials under test. However, the presence of some undesired peaks both anti-resonance and spurious mode besides the mode of interest (the higher order TM020) are observed.

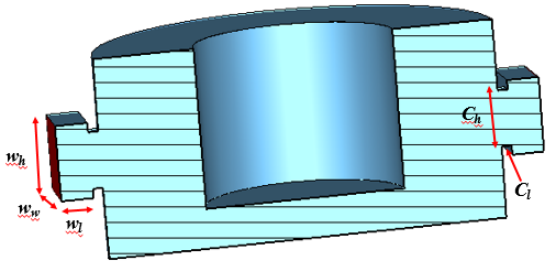

Figure 6.4 Cross-sectional view of the waveguide-coupled re-entrant cavity resonator showing waveguide and coupling iris dimension as given in Table 6.2

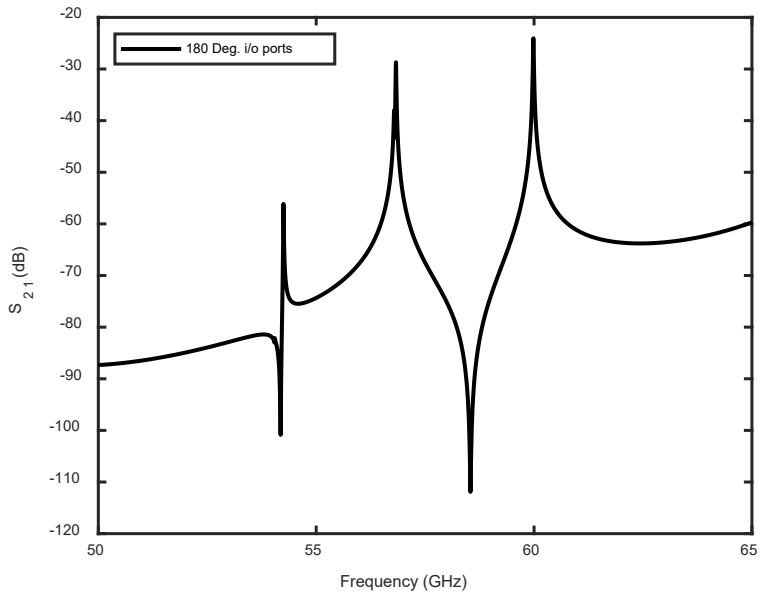

Figure 6.5 Broadband S_{21} response of the re-entrant cavity resonator

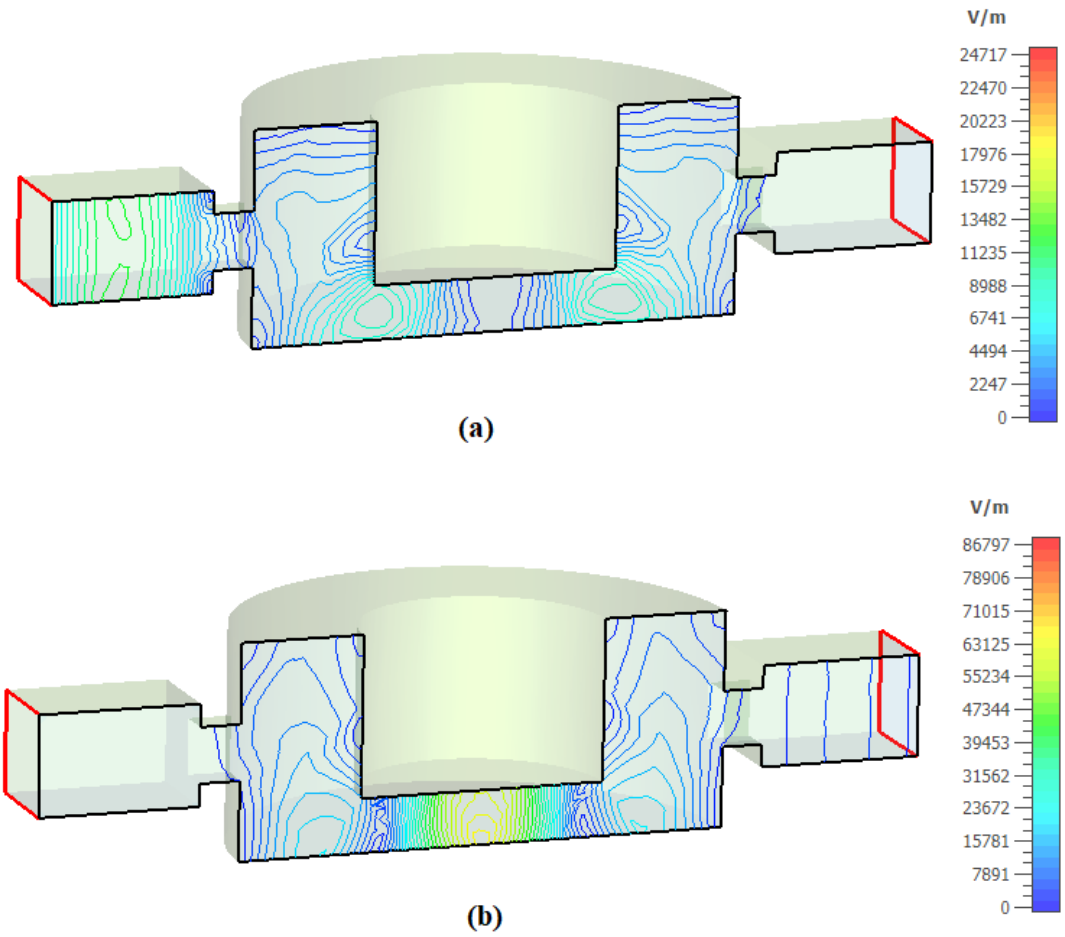

Figure 6.6 Electric field pattern for (a) TM_{210} 56.83.35 GHz (b) TM_{020} 60.00 GHz

In order to suppress the undesired peaks, the position of the coupling was changed. The two waveguide ports are then placed 90° apart instead of 180° as shown in Figure 6.7. The corresponding S_{21} broadband response of this coupling arrangement and the previous one are compared in Figure 6.8 with the anti-resonace mode greatly suppressed even though the spurious mode is still present. However, the spurious mode can be suppressed by reducing the dimensions of the coupling iris. But this presents some fabrication challenges. Since the resonance at this frequency does not respond to the presence of material because of the absence of electric field, it will not pose any challenge in tracking the resonance properties. One good advantage of this coupling arrangement is that the

frequency difference between the two resonance peaks of TM_{020} and TM_{210} mode is well spaced. This would therefore avoid any interference or compusion in tracking the desired frequency response during measurements.

6.2.1 Re-entrant Cavity Modification

The cavity is further modified by introducing curve post instead of a flat one similar to the 2 GHz cavity in Chapter 4. Additionally, another curvature is introduced where the cavity and post joined as shown by the cross-sectional view in Figure 6.9. This will further improve the *Q*-factor and facilitate good plating considering the cavity size. The dimensions of the cavity radius and post radius were varied to attain 60.0 GHz resonant frequency for TM020 mode while keeping all other dimensions as follows: cavity radius of r_c = 4.325, mm h = 4 mm post radius r_p = 2.1625 mm with gap d = 1 mm as shown in the Figure 6.9. The dimensions of the waveguide and coupling irises were maintained as given in Table 6.2. The broadband S_{21} response is given in Figure 6.10 and the electric field pattern corresponding to the two peaks alongside their frequencies and resonant modes are also shown in Figure 6.11.

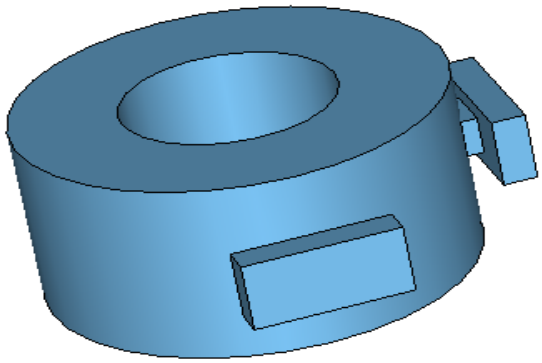

Figure 6.7 90^o placed coupled re-entrant cavity resonator keeping same dimensions

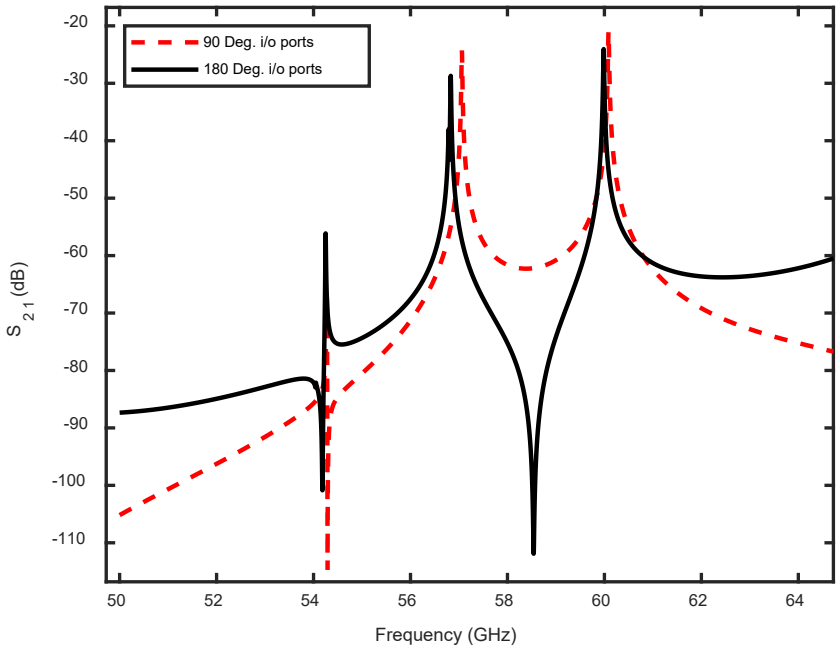

Figure 6.8 Broadband S_{21} response of the re-entrant cavity resonator with coupling ports placed 90° apart and 180° apart

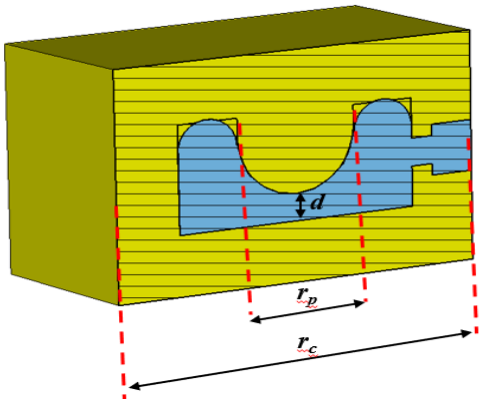

Figure 6.9 Cross-sectional view of cavity with spherical head post

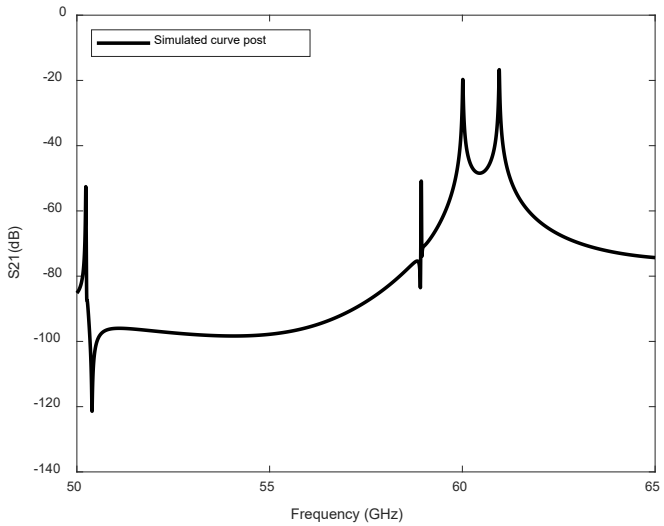

Figure 6.10 Broadband S_{21} response of re-entrant cavity with curve post

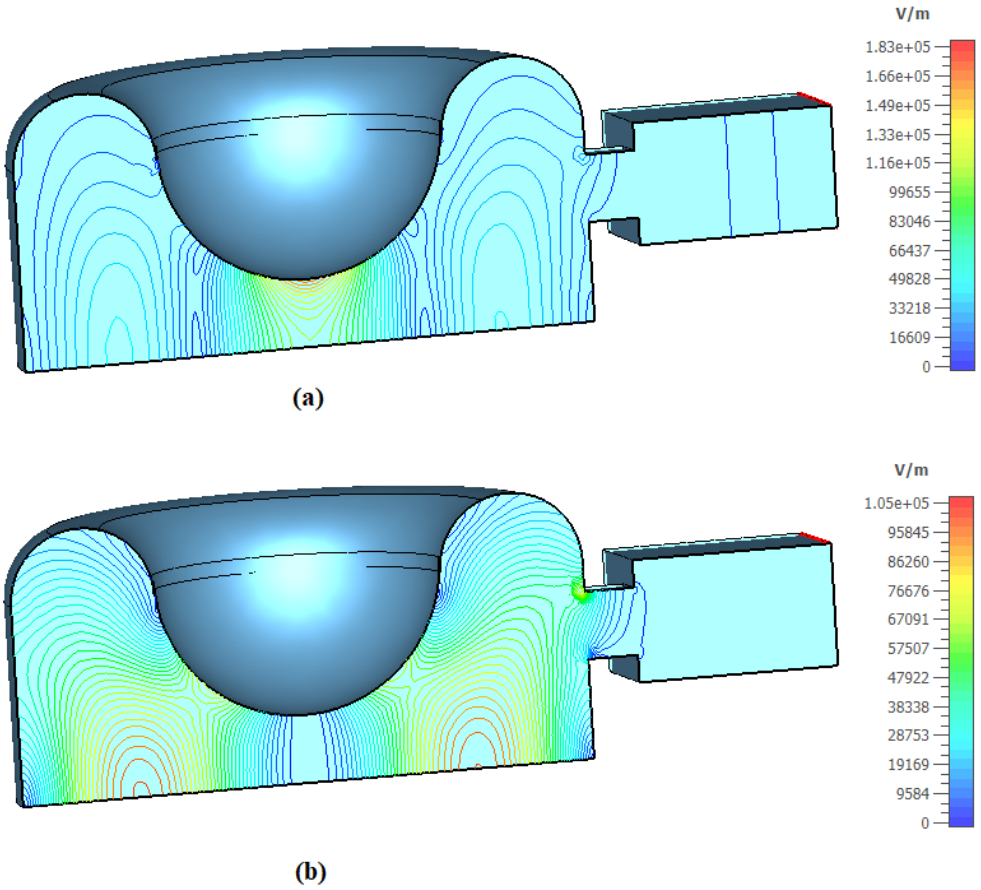

Figure 6.11 Electric field patterns of the curve post cavity (a) at 60.00 GHz (TM020) (b) at 61.34 GHz (TM210)

6.3 Simulation Based Analysis of the Designed Cavity Using Liquids for Dielectric Constant Measurements

The designed cavity resonator is used in analysing the measurements capability by parametric simulations for dielectric constant ε_r from 1 to 50 in steps of 7.0 while keeping the loss tangent $\tan\delta = 0$. This is to determine the measurements limit in terms of dielectric constant within the V-band frequency range. It is important to note that this depends on the size of tube used in the measurements. The chosen tube for this measurement is Polytetrafluoroethylene (PTFE) tube with outer diameter (O.D) of 0.76 mm and inner diameter (I.D) of 0.31 mm which has nominal dielectric properties of $\varepsilon_r = 2.1$ and $\tan\delta = 0.0001$ (taken from CST library). The choice is to allow for easy sample insertion via a normal syringe rather than the use of pump or pressure syringe. A hole of 1.0 mm was made at the centre of the cavity where the tube will be place as shown in Figure 6.12. Simulation for the said parameter of ε_r was carried out and the S_{21} broadband response of the parameterisation is given in Figure 6.13. It is interesting to observe that the TM_{210} mode is not affected by the dielectric property of the materials. This is expected, because this mode has an electric field minimum at the position where materials are exposed (Figure. 6.11). In contrast, the TM_{020} mode is highly sensitive to the change of ε_r. Due to large frequency shift resulting from the high sensitivity of the resonator and the volume of the sample, higher dielectric constant value of $\varepsilon_r > 50$ causes the resonance shifting to go below the lower frequency limit of the nominal V-band. This would therefore limit the ability of device in measuring higher dielectric constant as shown in Figure 6.13. Similarly, a parameter sweeps of loss tangent $\tan\delta$ from 0.0001 to 0.1 for a fixed dielectric constant of $\varepsilon_r = 5$ was carried out and the change in Q-factor over the range is plotted in Figure 6.14.

The S_{21} response indicates a significant reduction in Q-factor as tanδ increase. These two parametric studies demonstrate the measurement capability and possible utilisation of this cavity for dielectric metrology.

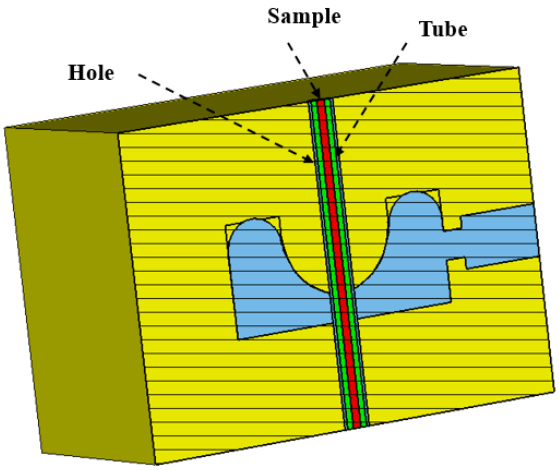

Figure 6.12 V-band cavity with hole, tube and sample placed in the centre

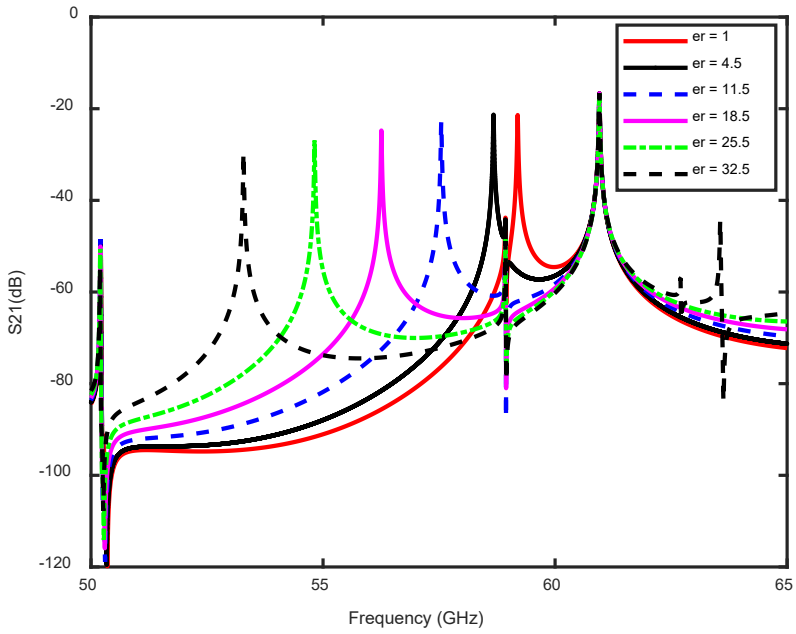

Figure 6.13 Broadband S_{21} response of re-entrant cavity for varying ε_r values at tan $\delta = 0$ using PTFE tube of 0.76 mm O.D and 0.31 mm ID

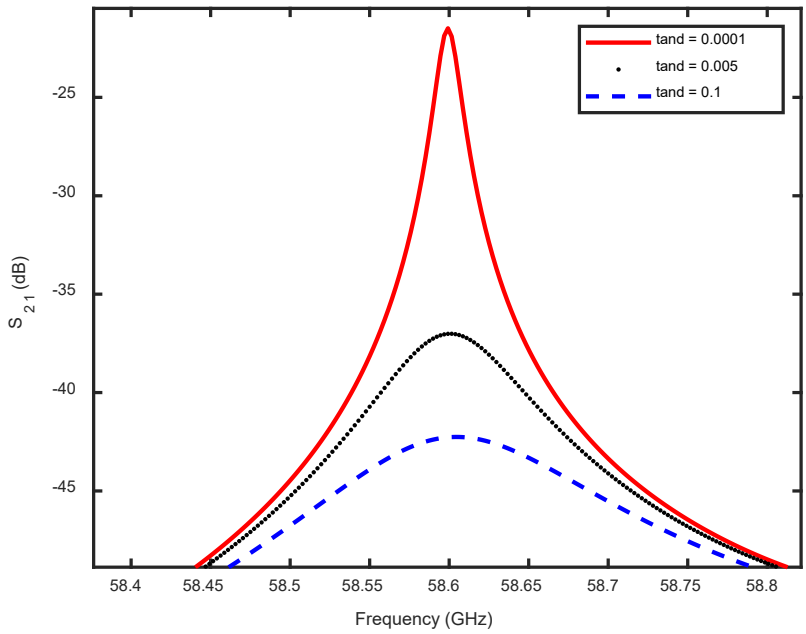

Figure 6.14 Change of Q-factor due to loss tangent from 0.0001 to 0.1 for $\varepsilon_r = 5$

6.4 Final Cavity Design, 3D Modelling and Fabrication

The re-entrant cavity was finally modelled to enable connection into V-band waveguide to coaxial adapter. The dimensions of the standard round cover flange were used in the design, and the WR 15 waveguide coupling energy into the cavity was extended to facilitate easy connection of the flanges for measurement as shown in the 3D model in Figure 6.15. The device was split into two parts to aid plating as shown in the model figure. Like all previous cavities, this cavity was also printed by SLA 3D printing technology using Accura+ polymer and then coated with copper material of 10 µm thickness as shown in Figure 6.16, respectively.

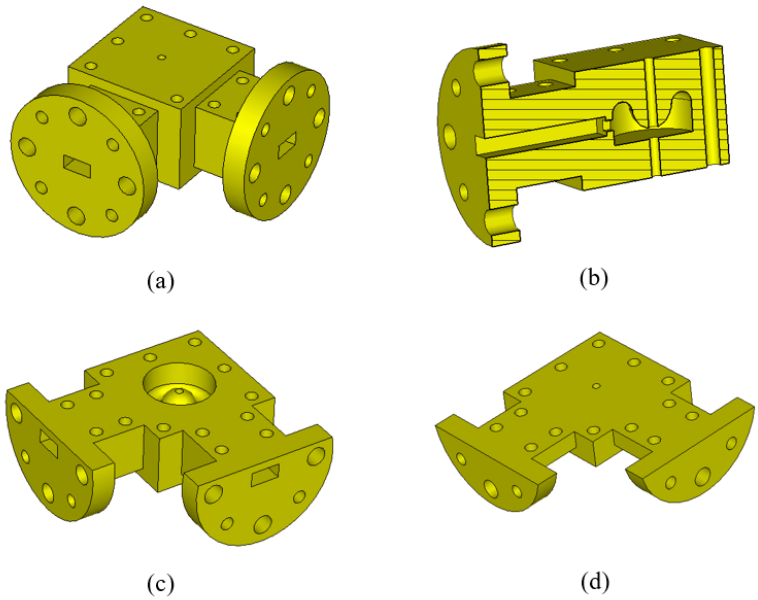

Figure 6.15 3D model of the 60 GHz re-entrant cavity: (a) complete Cavity; (b) cross-sectional view; (c) main cavity (top part); (d) cavity base (bottom part)

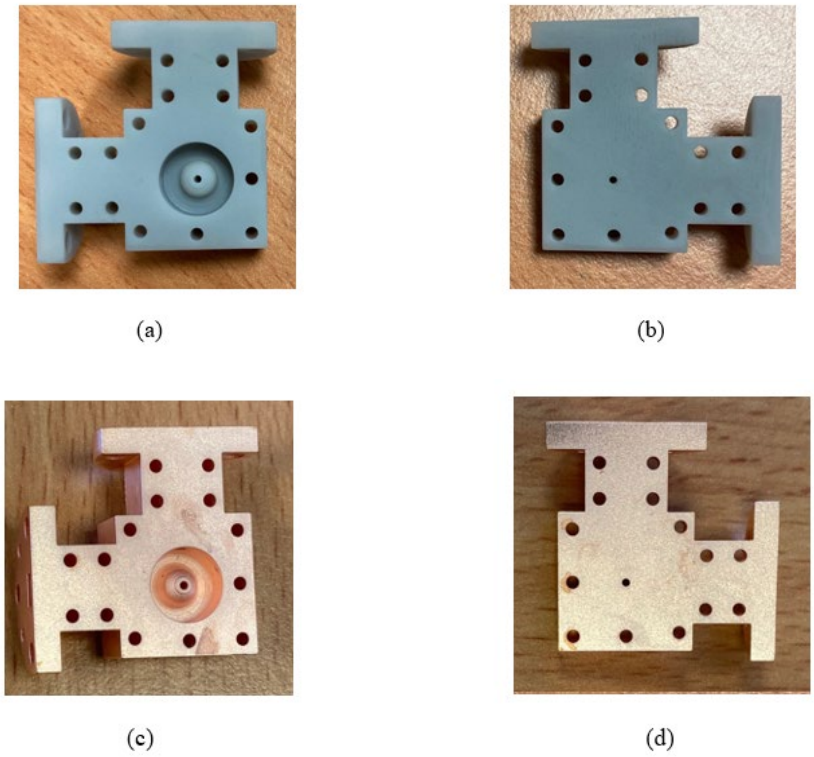

Figure 6.16 Prototype 3D printed re-entrant cavity top and bottom parts: (a & b) before plating; (c & d) after plating

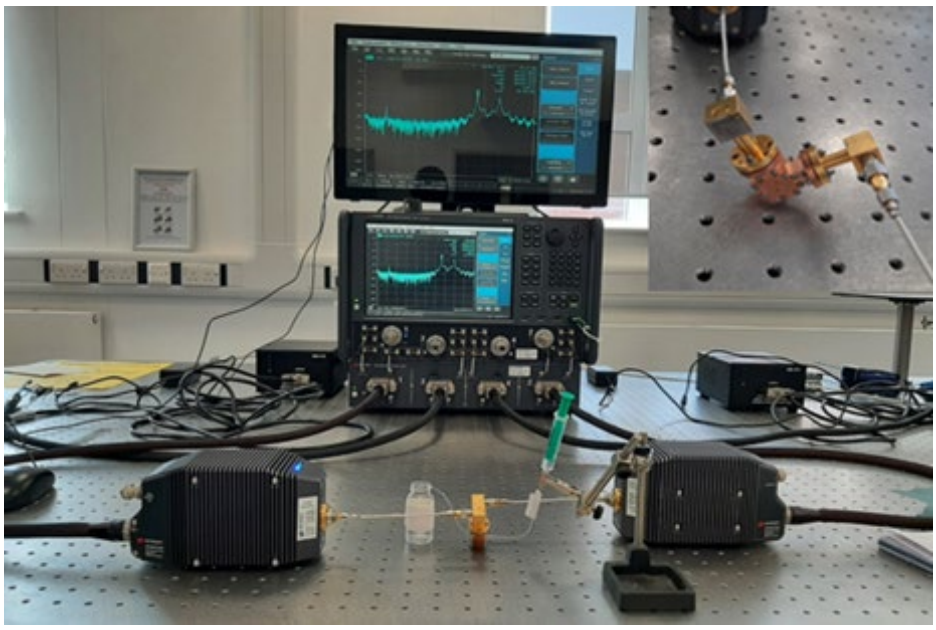

Figure 6.17 Set-up of 60 GHz re-entrant cavity for liquid measurements

6.5 Measurement and Validation of Cavity for Sensing Application

The cavity was measured using Keysight N5247B PNA-X (10 MHz to 67 GHz) network analyser as shown in the set-up in Figure 6.17. The instrument was calibrated over 50 - 65 GHz with the assistance of a pair of coaxial-to-waveguide adaptors. The measured average resonance frequency and *Q*-factor of the empty cavity are 60.58 GHz and 2157 with an insertion loss of 31.78 dB for five repeated measurements. The measured and simulated S_{21} responses are compared in Figure 6.18. There is a frequency shift of about 10 %. This can be attributed to fabrication tolerance and cavity assembly. The simulated *Q*-factor using copper conductivity of 5.8×10^7 S/m is 4095 which is nearly twice the measured value. This reduction in *Q*-factor can result from the surface roughness of the cavity, as well as the type of the copper coating used as discussed in previous chapter. The device surface roughness and dimensions were measured using Alicona microscope. The average

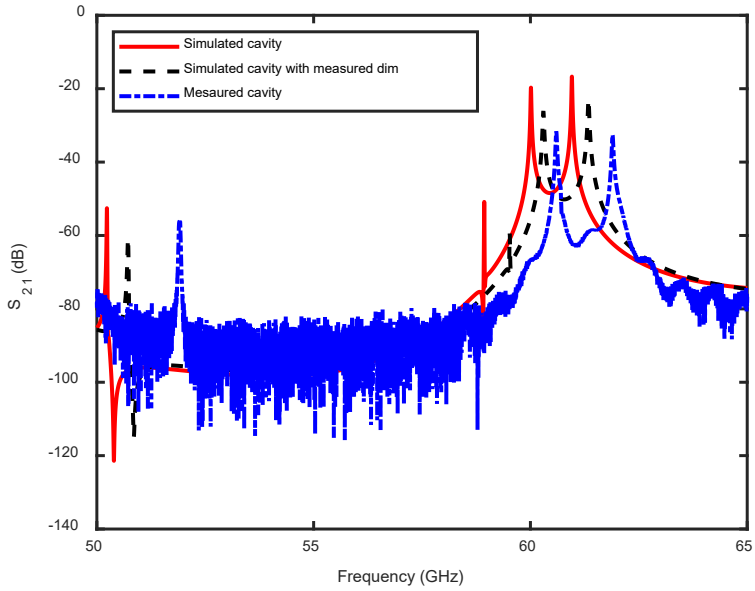

Figure 6.18 Simulated and Measured S21 response of empty re-entrant cavity

height of the selected area (Sa) value of the roughness is 1.25 µm from the measurements at three different points. This amount of surface roughness will effectively change the conductivity of the materials (copper) from 5.8×10^7 S/m to 1.48×10^7 S/m at the resonant frequency of 60 GHz. The cavity diameter was measured to be 8.632 mm which is 18 µm less than the actual dimension. The height of the cavity could not be measured due to the difficulty presented by the round curvature. A new simulation was run using the measured diameter of the cavity and the new value of conductivity. The S_{21} response of the simulations and measured empty cavity are compared in Figure 6.18. A resonance frequency of 60.28 GHz and *Q*-factor of 2257 is obtained from the new simulation taking into account fabrication tolerance and surface roughness. The result agrees well with the measured resonance parameters. To validate the sensing capability of the 60 GHz cavity, a PTFE tube of 0.76 mm O.D and 0.31 mm inner diameter consider for the simulations was purchased from Fisher Scientific and used for the measurement. N-hexane sample, an Alfa Aesar product with 99 % purity was measured using the device.

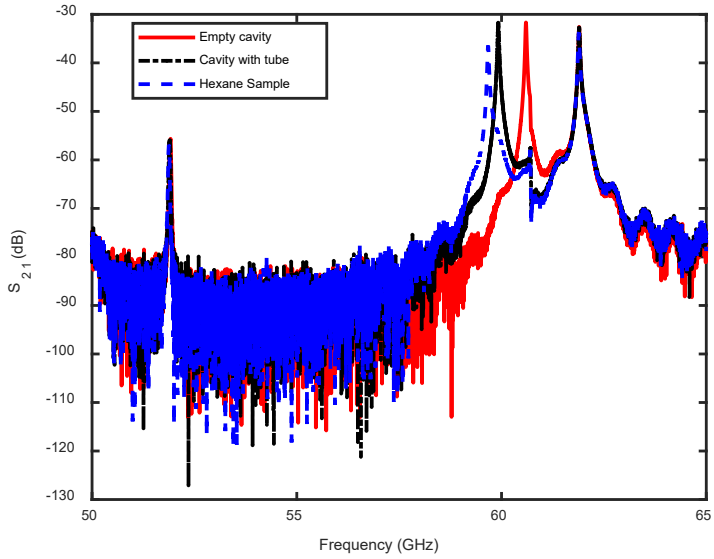

Figure 6.19 Measured S21 response of empty cavity, cavity with tube and sample

Table 6.3: Measured average results of 60 GHz resonator

Parameters	**Empty cavity**	**PTFE Tube**	**Hexane Sample**
Frequency (GHz)	60.58	59.88	59.71
***Q*-factor**	2157	2033	1875
Insertion loss (dB)	31.78	31.65	34.35

The sample was injected into the tube via a normal syringe with a needle of 0.3 mm O.D as shown in the measurement set-up in Figure 6.17. The measured S_{21} responses of the empty cavity, cavity with the tube and with the hexane sample are shown in Figure 6.19. The frequency shifts and changes in the *Q*-factor due to presence of material in the cavity can be clearly observed. The measurement was repeated seven times to determine the measurement repeatability and stability of the set-up. It is also interesting to see that, there is no shift at the resonant mode around 52 GHz and 62 GHz where the presence of the material has no effect due to the absence of electric field. This feature serves a means of

calibrating the device. The average results of the measured frequency, Q-factor and insertion loss are given in Table 6.3.

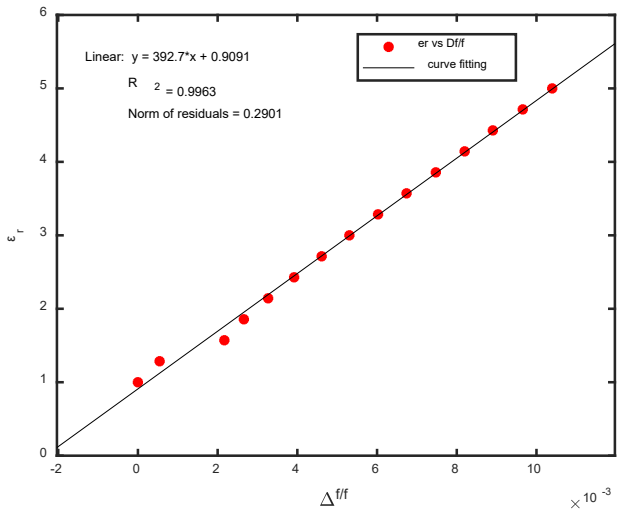

Figure 6.20 Relationship between change in resonance frequency and permittivity ε_r' and curve fitting

6.6 Evaluation of Dielectric Properties

The extraction of the dielectric properties of the measured material is based on an analytical model established from simulations using the design cavity. Similar approach described in Chapter 4 is considered. The parametric sweep of ε_r' from 1 – 5 at tan δ = 0 was carried out and the change in frequency due to dielectric constant is plotted as shown in Figure 6.20 and a linear relationship is observed from the results of the simulation. The equation in terms of ε_r' and $\Delta f/f$ is given as

$$\varepsilon_r' = 393\frac{\Delta f}{f} + 0.909 \tag{6.1}$$

The measured dielectric constant of n-hexane evaluated using (6.1) is ε_r = 2.025. This is about 10 % higher than the measured result of 1.89 presented earlier in Chapter 5. However, n-hexane has been reported to have complex permittivity value of 2.056 – j0.082

measured at 5.8 GHz using coaxial probe [135]. This agrees with the measured result obtained using the 60 GHz re-entrant cavity resonator with 1.5 % difference. The dielectric constant of hexane is the same over a wide frequency range, because of their low relaxation time. There is no frequency dispersion in the dielectric constant as shown by Debye characteristics curve plotted using the Debye parameters ($\varepsilon_s = 1.894$ $\varepsilon_\infty = 1.890$ and $\tau = 5.8$ *ps* [136]) calculated using equations (2.25) and (2.26) for real and imaginary part as shown in Figure 6.21 respectively.

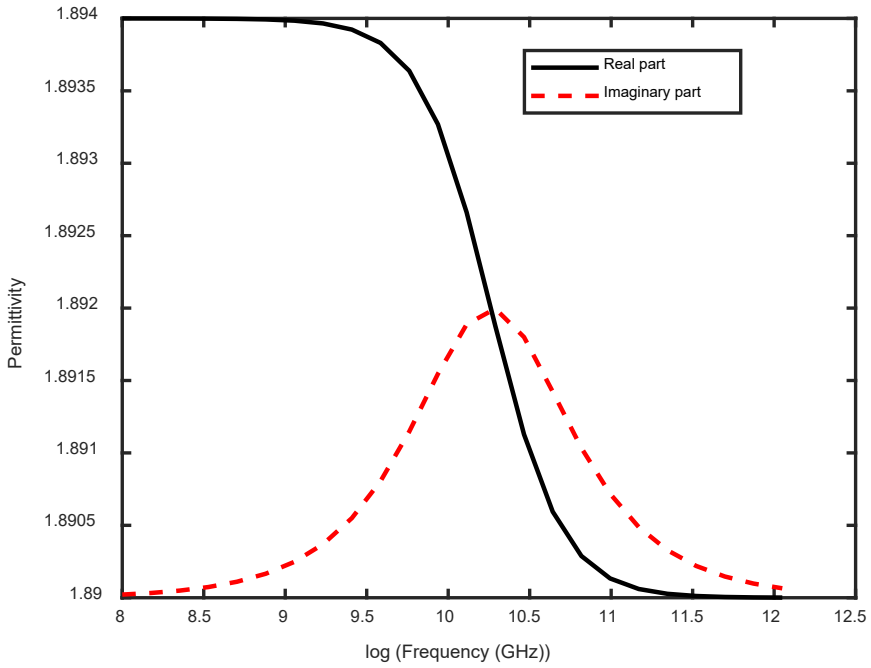

Figure 6.21 A Debye relaxation characteristic curve for Hexane

To further verify the results of the measurements, the sample was measured using the 2 GHz re-entrant cavity presented in Chapter 4 and the dielectric constant was found to be $\varepsilon_r = 1.91$. The difference in measured result can be attributed to measurement error associated with high frequency measurement and sensitivity of the device. For example, change in the outer diameter of the tube by 10 µm can result in frequency shift of 50 MHz which will in turn affect the ε_r value by about 3 %. Based on the results and associated

measurement errors presented the device can therefore be effectively used for dielectric measurement. The loss tangent measurement has not been considered in this part of the work. This is due the complicated nature of realising the mathematical model. The change in *Q*-factor due material loss as the dielectric constant varies is non-linear as observed in the case of the 2 GHz cavity sensor presented in Chapter 4. The possible reason is the introduction of additional curvature at the point where the cavity and the post join. This has further made the cavity structure more complex, and the change in dielectric constant therefore altered the field. This aspect is therefore recommended as part of future work.

6.7 Summary

High order mode 60 GHz re-entrant cavity resonator has been utilised for dielectric characterisation of low loss materials. The cavity was fabricated using SLA 3D printing. Analysis of the choice of electromagnetic mode and dielectric characterisation limit of the sensing device have been demonstrated based on simulations. The device was later validated by measurement of n-hexane and result of the dielectric constant was extracted from the measured S_{21} response. The result obtained has validated the device for dielectric metrology as well as the extraction method used within acceptable measurement uncertainty. The 3D printing capability of fabricating such a high frequency cavity resonator sensor for dielectric measurement presented is an effective and low-cost approach.

CHAPTER SEVEN: MEASUREMENT OF SOLID MATERIALS

This chapter is divided into two parts: Part A presents the measurement of dielectric property of substrate materials using a re-entrant cavity. Several substrate samples of 20 mm in diameter and varying thickness have been measured using the designed cavity resonator. A mathematical model based on simulation has been develop and utilise for the extraction of the dielectric property. In Part B, measurements of effective conductivity of flat samples made of aluminium, copper and stainless steel by CNC, 3D printed metals and metal coated polymer is presented. An analytical formula for the extraction of the effective conductivity has been derived in relation to energy loss in the volume of the cavity geometry. A method of resonant cavity characterisation of material based on microwave losses is utilised for the measurements. The approach offers a simplified analytical method and also supports the measurements of sample with arbitrary thickness. The cavity used for the liquid measurements in Chapter 4 was modified (re-designed) and fabricated using 3D printing for these measurements. The results obtained from both types of measurements have good agreement with values reported in literature within acceptable measurement uncertainty. The measurement uncertainties have also been analysed and captured in all the results of the measurements. The measurement approach presented in this chapter can be used for permittivity and conductivity measurements of various solids material for industrial application.

PART A: MEASUREMENTS OF SUBSTRATE MATERIALS

7.1 Overview of Solid Samples Dielectric Property Measurements

Measurement of material properties such as complex permittivity of substrate material is essential for many applications in microwave devices and circuits [137]. There are a number of methods reported in literature using different techniques for dielectric measurement. A detailed review can be found in [20]. The common and conventional one is the commercially available dielectric probe (open-ended coaxial line). The sample under test using this method must be valid at $|2\pi\varepsilon t/\lambda|<<1$, determined by the permittivity ε and thickness t of the sample, where λ is the wavelength. This has therefore limited the applicability of this approach [127]. The technique has also been classified as not accurate enough for low dielectric constant and low loss materials. A slotted coaxial resonator was reported in [138] for polystyrene sheet measurement at 1 GHz. This approach used two identical resonators placed in line in such a way that a slot is created between them. Sheet sample under measurement is placed into the slot between the two resonators and measured accordingly. Drawback of this method is the unwanted extension of the electric and magnetic field into the sample outside the resonator. This results in systematic errors that require corrections which can be complex. A split-cylindrical resonator [139] has also been used in a similar way, which also suffers from the same problem of electromagnetic field extending into the sample outside, when dimensions exceed the cavity diameter. Later, the authors provided a rigorous correction method in [140] to account for the field extending effect. However, the correction requires complex iteration. A full wave analysis was provided for split-cylindrical cavity in [141] when a rigorous and a well-defined model expression for evaluating the permittivity has been derived. However, the extraction

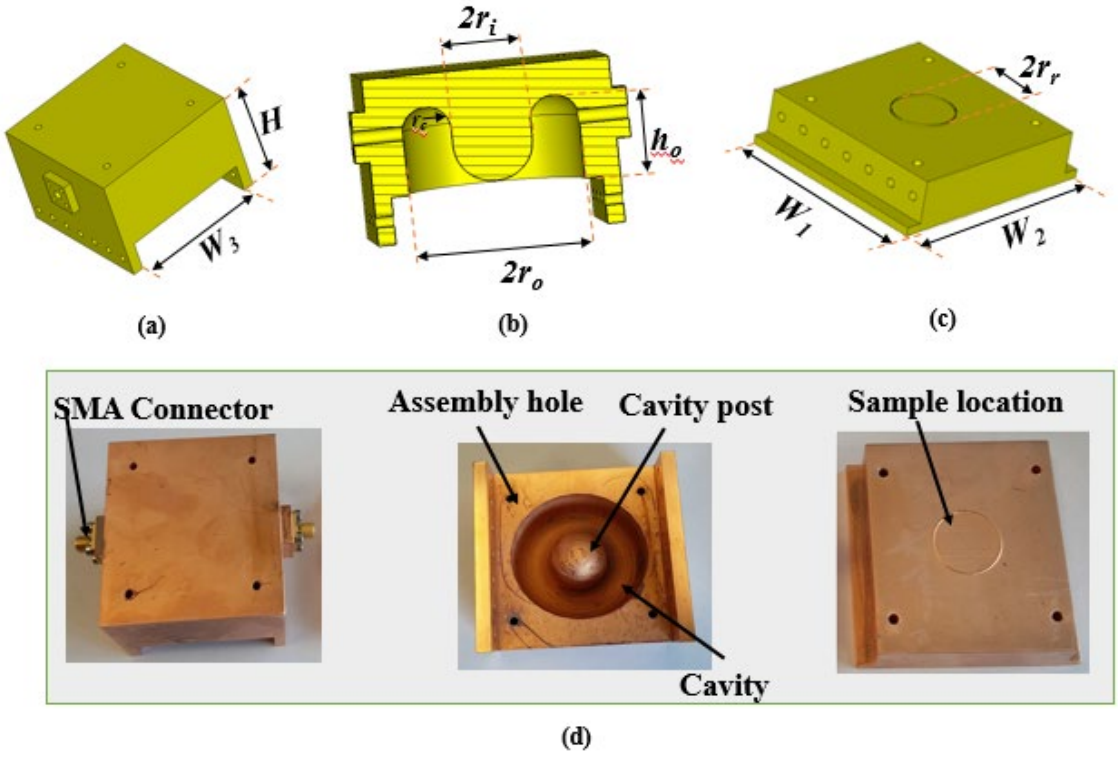

Figure 7.1 Re-entrant cavity resonator: (a) cavity top part; (b) cross-sectional view; (c) cavity base; (d) photograph of the cavity resonator prototype

process is very complicated due to the resonant modes considered in the work. Unlike the split cavity, closed resonant cavity encloses the electromagnetic field. Therefore, the boundary problem is relatively simple and extraction method is relatively easy to come by. Cavity based techniques have been considered to be more accurate. Sample preparation has been identified as one of the difficulties associated with using enclosed cavities. A re-entrant resonant cavity-based method that has the advantage of confined E-field for higher sensitivity is proposed for measurement of dielectric property of solid material at 2 GHz in this work. The re-entrant cavity used previously for liquids characterisation in Chapter 4 was modified and used for this purpose as will be described in Section 7.2.

7.2 Cavity Design and Fabrication

The cavity was designed to operate at a centre frequency of 2 GHz. It has a radius of r_o = 25 mm and a height of h = 26.785 mm. The semi-spherical head of the post has a radius of r_i = 11.25 mm and the capacitive gap between the cavity and post is 2 mm. The modification is done by removing the sample insertion hole and introduced a ring at the base of the cavity for samples to be placed as shown in Figure 7.1 (c). The ring has a radius of r_r = 10.25 mm with height and thickness of 0.4 mm. Additional rounded corners were introduced where the cavity wall and the post join with radius of r_c = 6.75 similar to the 60 GHz cavity in Chapter 6 as shown in Figure 7.1 (b). CST Microwave Studio is used for the design and simulations [142].

The device is fabricated using Stereolithography (SLA) 3D printing and is coated with 25 μm thick copper. The round corners introduced have further facilitated plating as sharp corner can be missed out during plating. A flat base made of stainless steel is used to secure the cavity base to avoid movement of the samples during assembling of the cavity and measurement. A photograph of the prototype cavity is shown in Figure 7.1 (d).

7.3 Measurements

An initial measurement of the empty cavity was carried out to compare the simulated and measured *S*-parameter response S_{21}, shown in Figure 7.2. The simulated resonance frequency and unloaded *Q*-factor of the cavity are 2.0 GHz and 6235 respectively, with an insertion loss of 27.62 dB, while the measured resonance frequency is 1.998 GHz and unloaded *Q*-factor is 4815 with an insertion loss of 31.95 dB. The results of resonance

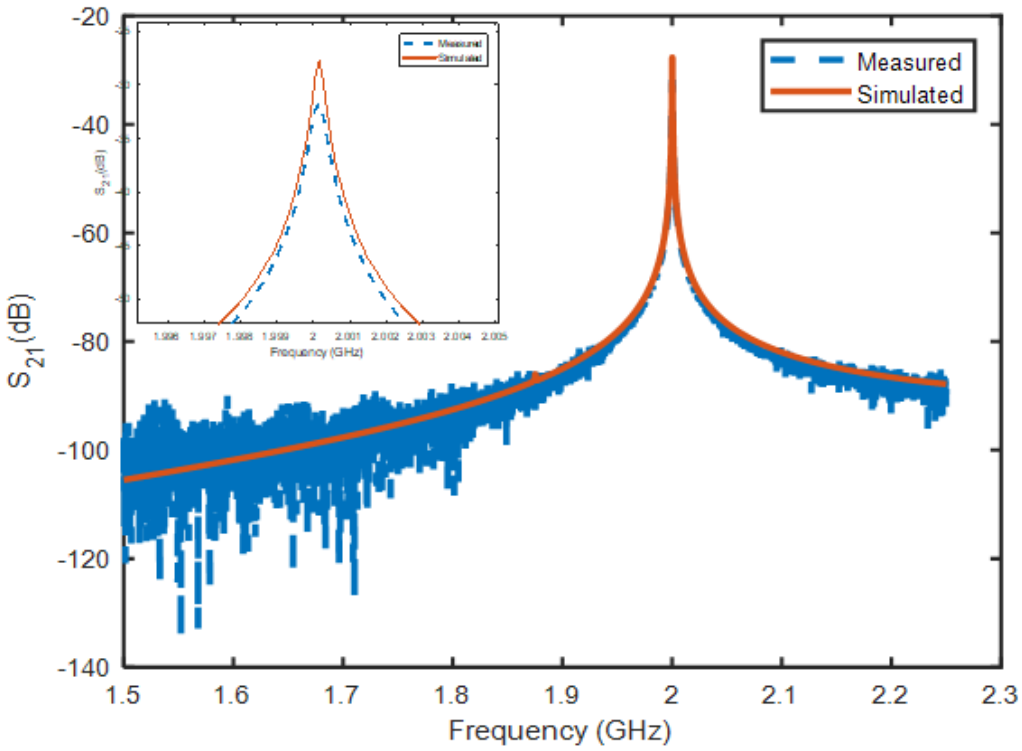

Figure 7.2 Measured and simulated S_{21} response of the empty cavity

frequency agree very well, except for the drop in *Q*-factor. A reduction of about 20 % in *Q*-factor can be attributed to quality of the plating and surface roughness. The average measured surface roughness of this device using Alicona microscope has an average Sa value within the range of 0.35 – 0.85 µm at various points. A simulation analysis carried out in CST shows a surfaces roughness of 0.5 µm would change the effective conductivity of the copper from 5.8×10^7 S/m to 4.78×10^7 S/m at 2 GHz. This can lead to about 10 % drop in the quality factor. This goes higher as the surface roughness increases.

To validate the use of the cavity resonator for the measurement of dielectric properties, various substrates were measured. This includes: Rohacell HF 51 foam, Aluminium oxide (Al_2O_3) crystal, Ferro A6M ceramic and several Rogers substrate materials. All samples are made to 20 mm diameter with different thicknesses. The

RT/Duroid samples were machined, and the copper coating was removed using ferric chloride 40 % solution prior to the measurement. First, the samples thickness and diameter

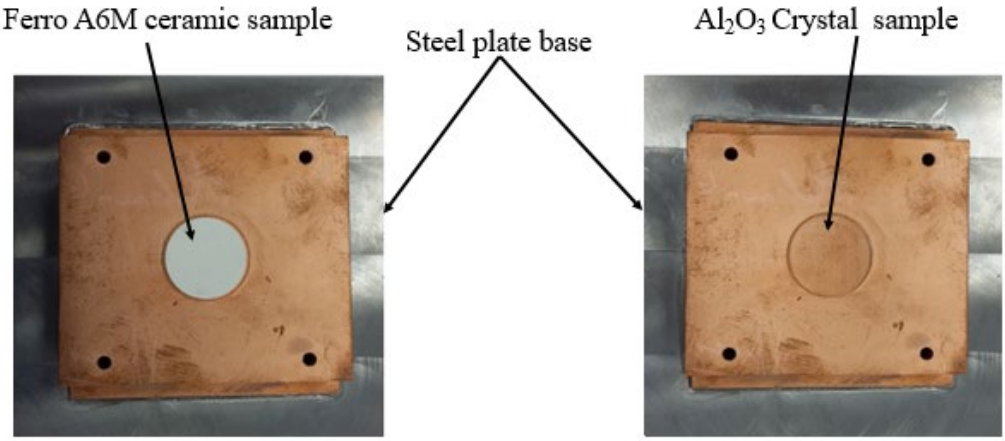

Figure 7.3. Sample placed on the cavity base: (a) with Ferro A6M ceramic sample; (b) with Al_2O_3 crystal sample

were measured using a digital micro-meter screw gauge. This measurement is done several times and at various points over the area of the disk. The average reading is used in the extraction of dielectric property. The sample was then placed on the base of the cavity within the ring as shown in Figure 7.3. The resonance frequency and *Q*-factor before and after the sample placement were recorded. The S_{21} responses of all the samples are shown in Figure 7.4. The samples were measured several times. Each time the cavity is disassembled, the sample is remounted before taking new measurement. Subsequently, the sample is also flipped and measured again. This is to observe changes, if any, as a result of either non-uniformity of the sample or any defects on the sides of the sample. For instance, the Al_2O_3 crystal has an anisotropic dielectric property, which means its dielectric property is not the same in all directions. Its dielectric constant is usually given for its c-axis (also referred to as parallel axis) and a-axis (referred to as perpendicular) respectively [143]. These are the two principal axes in its crystal structure.

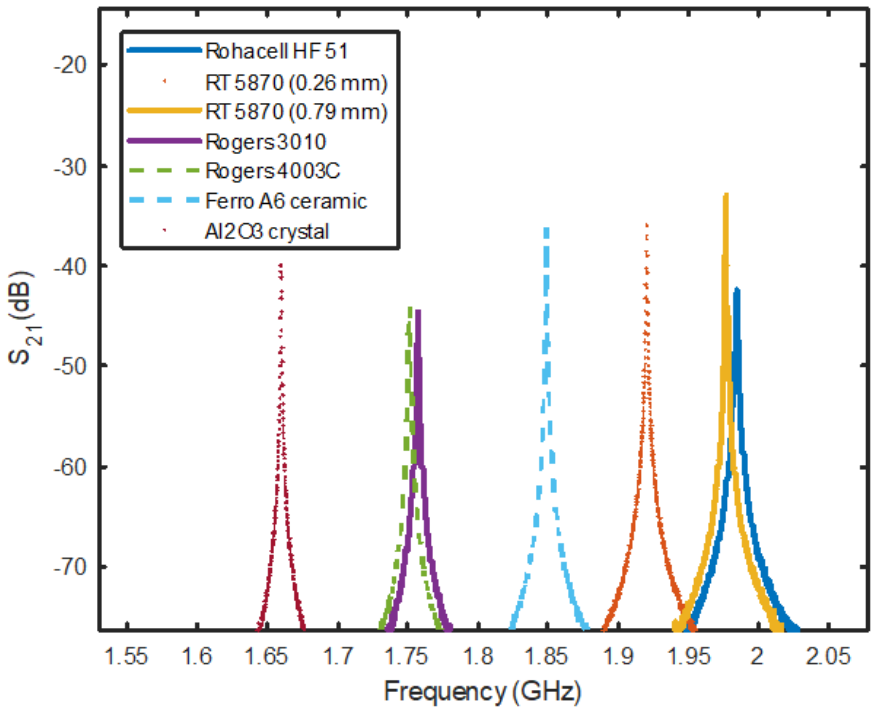

Figure 7.4 Measured S21 responses of the cavity and samples

The Al_2O_3 crystal used is grown along the direction parallel to c-axis (this is also its thickness direction). At the position of the sample in this cavity resonator, most of the E-field is expected to be along the thickness direction (from the post to the base) although there are also field components along the horizontal direction.

7.4 Dielectric Property Extraction of the Materials

7.4.1 Extraction Model

To extract the dielectric properties of the measured samples, an approach derived used in Chapter 4 is considered. A mathematical model is developed for evaluating the permittivity

based on simulation and the principle of cavity perturbation theory. This model was established using curve fitting on a simulated relationship between the dielectric constant

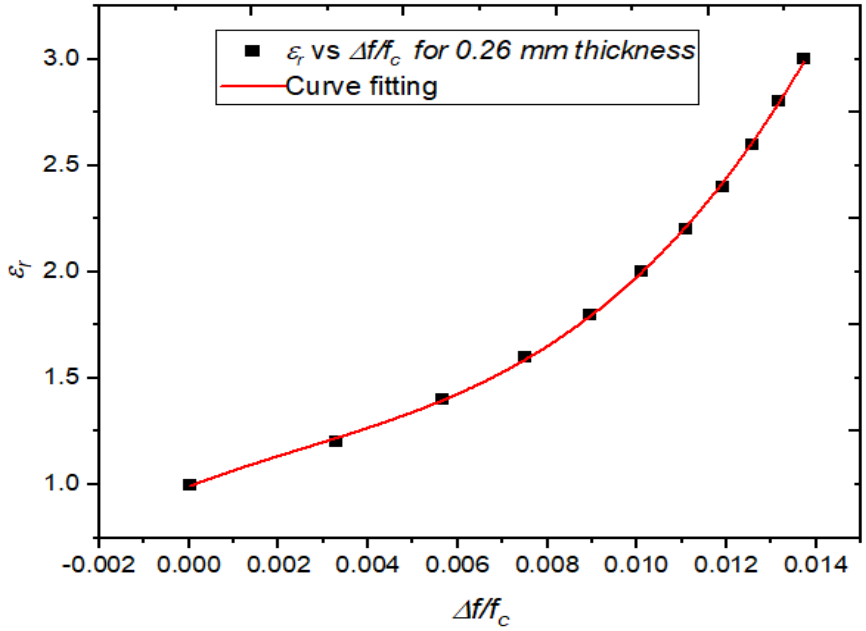

Figure 7.5 Relationship between the change in resonance frequency and the permittivity ε_r and curve fitting

ε_r values and ($\Delta f/f_c$) while keeping the loss tangent, tanδ, zero. Δf is the change in frequency with and without the sample and f_c is the resonance frequency of the empty cavity. However, a single mathematical model for the extraction of dielectric constant cannot be realised as the thickness of the sample varies. For this, polynomial curve fittings based on various thickness while keeping the diameter of 20 mm constant were utilised for the extraction. The relation from the curve fitting is provided by

$$\varepsilon_r = p1\left(\frac{\Delta f}{f_c}\right) + p2\left(\frac{\Delta f}{f_c}\right)^2 + p3\left(\frac{\Delta f}{f_c}\right)^3 + p4 \qquad (7.1)$$

The plot and curve fitting for the sample with a thickness of 0.26 mm is shown in Figure 7.5. The values of the coefficient $p1$ - $p4$ varies depending on the sample thickness as given in Table 7.1. The R-squared value of the curve fitting is 0.999 in all cases

indicating good fit of the equations. The extraction of the loss tangent is not considered in this work due to complex nature and a number of variables involved. More so, the change in *Q*-factor due to loss tangent is not linear in this case thereby making it more complicated than the liquid measurement model in Chapter 4.

Table 7.1: Coefficient of curve fitting for various thickness

Thickness (mm)	***p1***	***p2***	***p3***	***p4***
0.26	7.83×10^5	-6.03×10^4	80.45	1.00
0.80	1.65×10^5	-339.32	23.282	0.99
1.27	8.20×10^4	-2.88×10^5	3.40×10^4	-1.34×10^3
1.50	6.95×10^5	-3.36×10^5	5.43×10^4	-2.94×10^3

7.4.2 Uncertainty Analysis

The results of the measured solid material can be affected by several factors as described below. The level of uncertainty is determined in each case using simulations and/or measurements. Measures were adopted to mitigate most of these factors.

1) Measurement repeatability and cavity assembly

The measurements repeatability, for $n = 5$ where n is the number of repeated measurements, is determined for both cavity assemblies using the empty cavity and sample measurements using Al_2O_3 crystal as a reference sample. The results obtained show good measurement repeatability of the device and the stability of the measurement setup. The standard deviation (S.D.) and standard error (S.E.) of the measured frequency are found to be 4.76×10^{-4} and 2.38×10^{-4} for the cavity assembly while 2.61×10^{-4} and 1.30×10^{-5} for the

sample measurements, respectively. All samples are measured 5 times and the average reading is used in evaluating the dielectric property. We have used a large number of sweep points (6401) over a bandwidth which is about five times the 3 dB bandwidth. An IF bandwidth of 500 Hz reduces effect of noise in the response. This has greatly reduced the influence of measurement error resulting from the measurement of the frequency, the 3 dB bandwidth and the amplitude of the transmission coefficient.

2) Effect of air gap and changes in sample dimension

These factors were examined based on simulation in CST. Parametric study was performed by introducing varying air gaps, changes in sample thickness and diameter, again using aluminium oxide as a reference material. The nominal dielectric constant of ε_r = 9.9 and tan δ = 0.0001 (99.5% alumina) taken from the CST library is used for these simulations. A change of ± 2 % in thickness can lead to about 15 - 25 % decrease or increase in extracted dielectric property, respectively. As the dielectric constant of the material increases, the error becomes higher. A similar percent change in diameter has much less effect of only about 1.5 % change in the extracted dielectric constant value. An air gap of 50 μm would reduce the extracted ε_r by about 5% and this error increases with increasing air gap. To minimise the effect from these factors, samples dimensions are measured as stated earlier and the average is used. The samples are ensured to be smooth and flat. So is the base of the cavity, to minimise any air gap. However, it is difficult to ascertain the presence of small air gap between the sample and the cavity base.

3) Displacement of sample

The displacement in sample position is examined using simulation by shifting the sample within the circumference of the ring. Due to the presence of the ring, the shift is limited to

only a maximum of 0.25 mm within the circumference as shown in Figure 7.6. A shift of 0.15 mm and 0.25 mm results in a change in resonance frequency, which in turn affects the extracted dielectric constant by 0.18 % and 0.70 % respectively as demonstrated in Figure 7.7. This signifies a negligible effect, due to the presence of the ring.

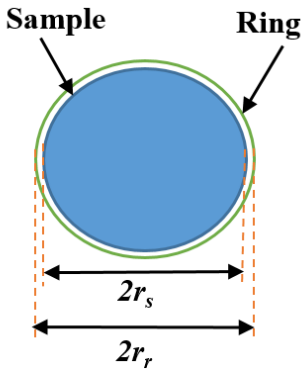

Figure 7.6 Sample position within the ring, the diameter of the ring $2r_r$ = 20.50 mm and the sample diameter $2r_s$ = 20.00 mm (i.e 0.25 mm spacing)

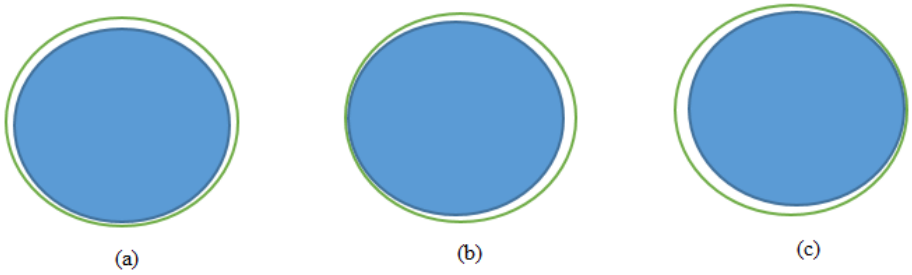

Figure 7.7 Illustration of sample shifting from the centre position within the ring: (a) a shift of 0.15 mm (b) a shift of 0.20 mm (c) a shift of 0.25 mm

The uncertainties resulting from the above-mentioned factors were determined separately in relation to changes in frequency for dielectric constants. The combined uncertainty and the expanded uncertainty assuming a normal probability distribution using a coverage factor value k = 2 (a confidence level of approximately 95 %) are 1.6×10^{-3} and 3.2×10^{-3} respectively. This is used to determine the result tolerance.

7.4.3 Permittivity

The change in measured frequency due to material is utilised for extraction of the permittivity values of MUT using the mathematical models. The results of the dielectric constant of the measured samples are presented in Table 7.2. The table also includes the average thickness of the MUT. To further verify the results, an industrial dielectric kit (16451B impedance measurement) is used to measure the samples at lower frequency within the limit of 10 MHz. Two methods of measurement were adopted, contact and non-contact method. The standard calibration and measurement guideline reported in the manual [144] have been followed. The appropriate electrode determined by the sample diameter was used to measure the capacitance in each case as shown by the measurement set-up in Figure 7.8. The analytical formulas used for the computation of the dielectric property using the measured capacitance are given by [144].

For the contact method:

$$\varepsilon_r = \frac{t_a \times C_p}{A \times \varepsilon_o} \tag{7.2}$$

$$A = \pi \left(\frac{d}{2}\right)^2 \tag{7.3}$$

where C_p is equivalent parallel capacitance [F], t_a average thickness of test material [m], A is the area of the guarded electrode [m^2], d is diameter of the guarded electrode [m] and ε_o is the constant of 8.854×10^{-12} [F/m]. The dielectric constant using the non-contact method is related by

$$\varepsilon_r = \frac{1}{1 - \left(1 - \frac{C_{s1}}{C_{s2}}\right) \times \frac{t_g}{t_a}} \tag{7.4}$$

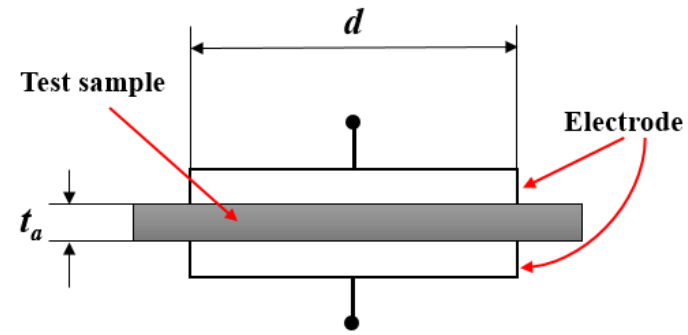

(a)

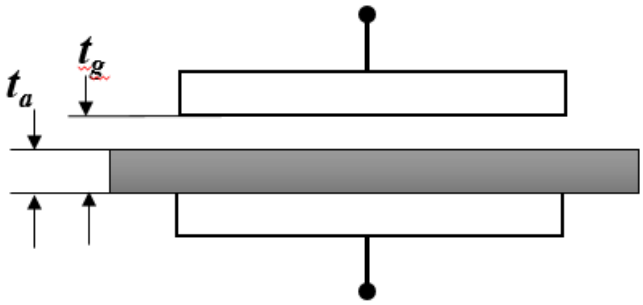

(b)

Figure 7.8 Illustration of measurements: (a) contact method (b) non-contact method

where C_{s1} and C_{s2} is series capacitance without and with material [F], t_g is the gap between guarded electrode and unguarded electrode.

The results of the two methods and that of the re-entrant cavity together with literature values (and data sheet for the substrates) [145] are captured in Table 7.2. The results agree well and validates the measurement method of the re-entrant cavity resonator. From the comparison, result of the thin RT/Duroid 5870 sample using the dielectric kit is lower compared to the same sample with a larger thickness. This influence of the sample thickness on dielectric property associated with measurements using a probe kit (open-end resonator) has been overcome by the re-entrant cavity technique. This is justified by the

almost identical results obtained for the two samples in consideration. Dielectric constant of a material is composed of four contributions such as electronic, ionic, dipolar or the space-charge polarisations depending on the type of material [146]. These factors can contribute and affect the results of the dielectric constant. However, the dielectric constant of the measured substrates materials is stable and constant within the tolerance limit specified over a broadband frequency range of 1-10 GHz as reported in the data sheet of RT/Duroid 5870 and 5880 laminates as captured in Table 7.2. The comparison here has validated the ability of cavity resonator to measured samples of varying thickness which has been the challenge associated with open resonator and dielectric kit measurement techniques.

7.5 Summary on Solid Measurements

The technique presented in this part of the chapter uses 3D printed re-entrant cavity resonator resonating at 2 GHz for dielectric measurement of substrate materials. Various samples measured have validated the measurement method. The samples were also measured using industrial dielectric kit to verify the accuracy of the measurements. The results obtained with the cavity resonator using the mathematical model developed agree well with the reported values. Sample thickness has been one of the challenges associated to the measurement of solid sample using conventional methods such as dielectric probe. The cavity resonator in principles has the advantage of measuring samples irrespective of their thickness in relation to dielectric constant value effectively.

Table 7.2: Comparison of the permittivity results of the measured samples using cavity resonator, dielectric kit and from literature

Sample	**Average Thickness (mm)**	**16451B Dielectric Kit**		**ε_r, Re-entrant cavity ~2 GHz**	**ε_r, Literature**
		ε_r, Non-contact	**ε_r, Contact**		
Rohacell foam HF 51	1.49	1.08	-	1.060 ± 0.003	1.057 @ 2.5 GHz
RT 5870	0.26	2.30	2.29	2.39 ± 0.01	2.33 ± 0.02 @ 1 MHz - 10 GHz
RT 5870	0.79	2.42	2.41	2.40 ± 0.01	2.33 ± 0.02 @ 1 MHz - 10 GHz
Rogers 3010	1.27	8.26	9.65	9.66 ± 0.03	10.2 ± 0.3@ 10 GHz
Rogers 4003C	1.50	3.75	3.86	3.81 ± 0.01	3.55 @ 8 GHz
Ferro A6 Ceramic	0.96	5.83	5.99	5.66 ± 0.02	5.7 @ 10 GHz
Al_2O_3 Crystal	1.49	11.11	10.92	11.65 ± 0.04	11.58 @ 3 GHz

PART B: EFFECTIVE CONDUCTIVITY MEASUREMENT OF 3D-PRINTED MATERIALS

7.6 Overview on Additive Manufacturing and Conductivity Measurements

Additive Manufacturing (AM) has been utilised in fabrication of microwave devices such as cavity-based resonator sensors, filters and antennas [147]. The technology has been used in producing structures of complex nature in separate parts or in a monolithic form giving them advantage over other fabrication methods [148]. For example, 3D printed polymer sensor made using Stereolithographic apparatus (SLA) process and coated with copper as presented in previous chapters of this work. Other examples include a 3D printed metallic filter fabricated by micro laser sintering (MLS) [149] and 3D printed horn antennas [150]. The performance of these 3D printed microwave devices greatly depends on the losses associated with the metallic surface or metallic coating. Accurate evaluation of the effective conductivity or surface resistance of the conductors at microwave frequencies are highly important for the modelling of these devices and predicting their performance. In principle, the loss characteristics of these structures can be computed theoretically based on analytical models with assumptions about the dc bulk conductivity and an ideal smooth wall [151]. However, in practice, the situation result is often inaccurate as this assumption cannot account for the effect of metallic surface quality (surface roughness, morphology, and composition) that may produce excess losses. For this, microwave measurement techniques for the characterisation of effective conductivity of materials have been studied and reported in [152] [153]. Two major techniques were adopted: Non-resonant method (such as the transmission line based) and resonant method. Both techniques have been

explained in detail in [152]. The resonant method is considered to provide results that are more accurate and precise due to the high *Q*-factor of the resonators [154]. The resonant method technique has the advantage that the losses within the cavity at the desired resonance frequency are sensitive to the changes in the conductivity of the material. This is in contrast to the transmission line techniques, where the conductor losses are often small, and resolving the conductivity becomes difficult. However, the transmission line method supports a broad range of frequencies while the resonant method is limited to discrete frequencies [133].

In [155], measurement of dc conductivity of highly conductive polyaniline films has been reported using three different methods at different frequencies. These include: resonant, surface impedance and transmission line techniques. In the resonant cavity technique, the sample was placed in the centre of the cavity where magnetic field is maximum to measure the changes due to material insertion and used the *Q*-factor to evaluate the conductivity of the materials. Results from all the methods were compared with value reported in the literature. The resonant techniques offer the highest accuracy with uncertainty mainly determined by sample placements [155]. Conductivity measurements of doped semiconductors materials have also been demonstrated [156]. The authors finding shows super-linear power law of frequency dependency of the conductivity. Similarly, a linear temperature dependence of copper resistivity has been reported using a novel toroid split-ring resonator [157].

A recent work has reported an estimation of surface resistance of materials for microwave applications based on Fabry-Perot open resonator over the range of 20 - 40 GHz [158]. The high *Q*-factor of the resonator allows measurements up to a conductivity with a magnitude of 10^4 S/m. The measured results using the approach presented by the

author agree with the expected values of MUT with about 30% difference. On the other hand, due to the effect of vibrations and spectral variation of the coupling level associated with this technique and the measurement set-up, materials with low conductivity can be greatly affected. This will lead to large errors. In [159] an investigation into aluminium-silicon-magnesium alloy for microwave devices by conductivity measurement is reported. Simple rectangular waveguide cavity structures were used. The study focuses on the large-scale geometry variation of the materials rather than the surface roughness. The measured average conductivity of the cavities from two manufacturers shows about 70 % difference from nominal conductivity of the aluminium alloy. The measured value was used in the simulation and result agrees well with the measurement. This has therefore validated the results of the measured conductivity of the materials under investigation [159].

More recently a study for an alternative test fixture for evaluating and distinguishing various materials through their electric resistance has been detailed in [160]. In this work, a new measurement approach is described using a re-entrant cavity resonator. The end wall replacements method similar to [161] is adopted. A simplified analytical formula is developed based on the energy stored in the cavity and simulations. This is different from [161] which used a more complex expression of the ohmic Q-factor associated with the mode of interest and the cavity geometry.

7.7 Resonator Design and Fabrication for Conductivity Measurement

The re-entrant cavity resonator used for solid measurements is utilised with a change in dimensions of the height, h = 25.45 mm. The ring introduced in the based for sample placement has also been removed making the base flat as shown in Figure 7.9. The device

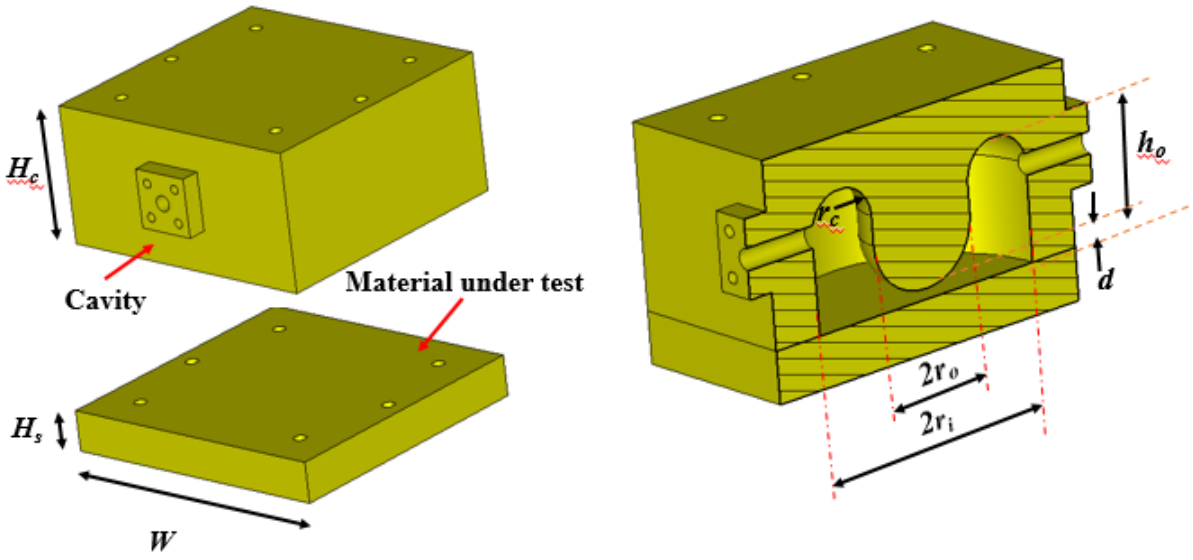

Figure 7.9 Re-entrant cavity resonator (a) 3D model of cavity and MUT) *Hc* = 35.45 mm, *Hs* = 10 mm, *W*= 70 mm (b) inner view and assembled cavity

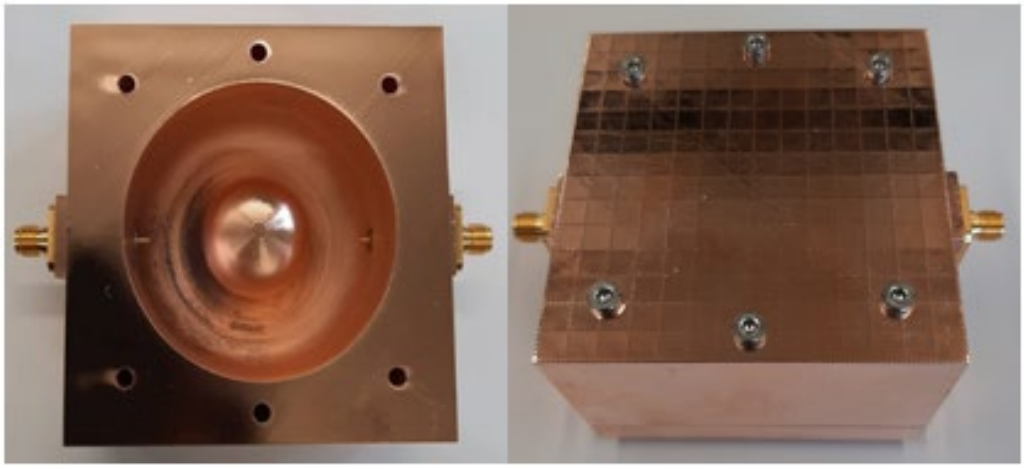

(a) (b)

Figure 7.10 Photograph of the 3D printed prototype (a) inner view of cavity without base (b) assembled cavity

was fabricated by Stereo-lithography (SLA) 3D printing using polymer and was coated with 25μm copper thickness as shown in the photo of the prototype in Figure 7.10. The cavity is housed in a rectangular frame and is split into two parts, the top part being the main cavity and the bottom part serve as the base as shown earlier in Figure 7.9 (a). The base is considered as MUT in this case. The cavity can be assembled via the six holes using 3 mm × 50 mm nuts and bolts as shown Figure 7.10 (b), or alternatively using a clamp for time-effective measurement.

7.8 Measurement Method and Samples

In material measurement using resonant techniques, the material properties are determined from the change in the frequency and the *Q*-factor due to material insertion at the desired resonant mode. In this measurement, as the conductivity is the only measurand, only the knowledge of the *Q*-factor is required. The method adopted is simple, and it has an advantage of not requiring samples to be cut into a precise thickness. The base (i.e MUT) can be replaced easily. The cavity is assembled and connected to PNA network analyser (Agilent Technology E8382C) for the measurements as shown in the measurement set-up in Figure 7.11. The network analyser is calibrated using 85052D kit. To minimize the measurement error in the high-*Q* resonance, a large number of sweep points (6401), over a bandwidth about five times the 3dB bandwidth was used. An intermediate frequency (IF) is set to 1 kHz. The measured 3D printed cavity copper coated polymer and simulated S-parameters response of the designed cavity with copper conductivity of 5.8×10^7 S/m both cavity and base is given in Figure 7.12. The measured resonance frequency *fr*, loaded *Q*-factor Q_l and insertion loss *IL* are 2.073 GHz, 5045 and 31.35 dB while the simulation results are 2.072 GHz, 6145 and 27.75 dB using the nominal conductivity of copper,

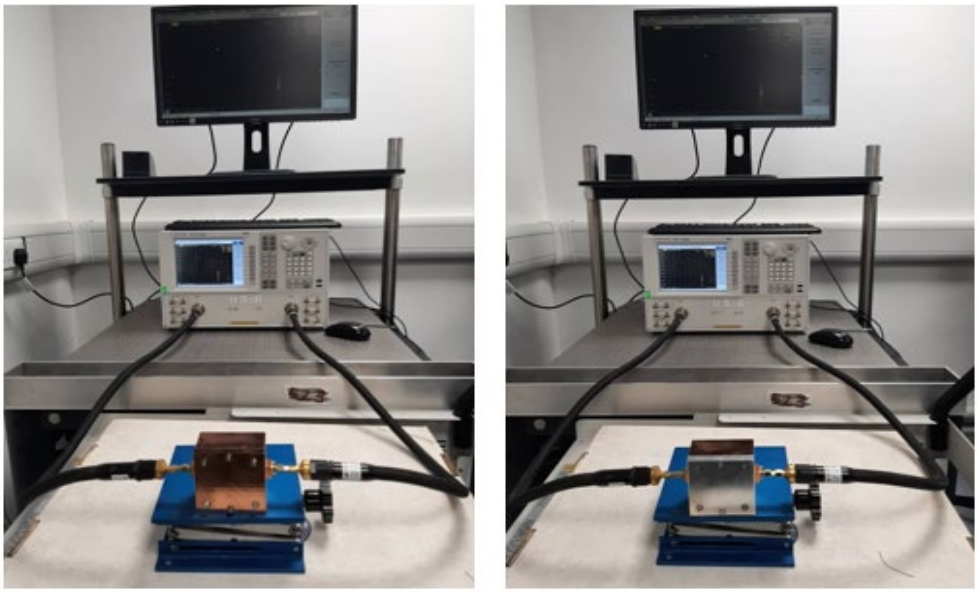

Figure 7.11 Photograph of the measurement setup of the resonator connected to PNA network analyser showing two different set of samples measurement at 2 GHz (a) Copper (reference) sample (b) Aluminium sample.

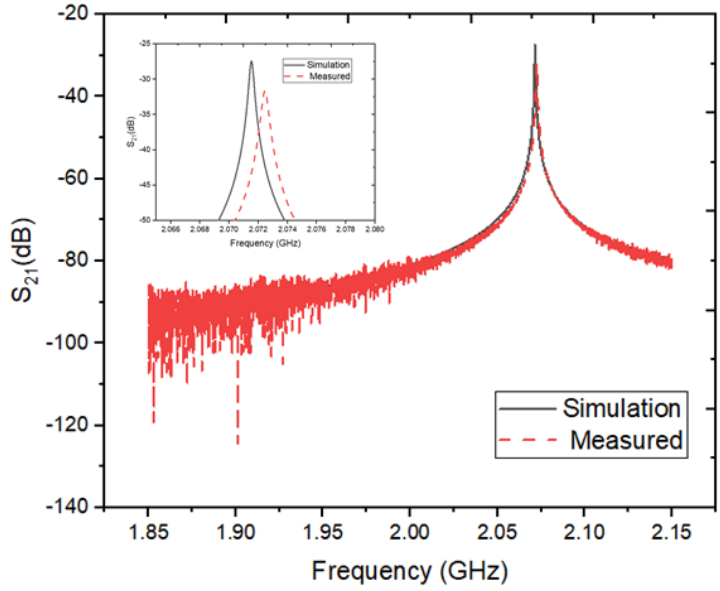

Figure 7.12 S_{21} response of the measured 3D cavity copper coated polymer and simulated cavity with copper conductivity

5.8×10^7 S/m. The results show very good agreements, with a small frequency shift. There is a relatively large *Q*-factor drop of about 15%. This can be largely attributed to the surface roughness associated with additive manufacturing, which degrades the electrical conductivity of the device. In addition, the quality of the copper plating can also be a factor. This is further explained in Section 7.9.

To validate the measurements technique, six flat samples made of aluminium, copper and stainless steel were measured. Three of the samples are made using 3D printing: one of which is made from Accura+ polymer and then coated with 25 μm copper, while the other two are metal 3D printed using aluminium alloy A20X (composed of 90.29 wt % Al and 4.07 wt % Cu) [162]. The two metals 3D printed samples are built from different orientation of 0° (i.e vertical orientation) and 90° (i.e horizontal orientation) as demonstrated in Figure 7.13 using SLM500HL machine from SLM solutions GmbH. The processing parameters used in the production are: 350 W laser power, at constant laser scanning speed of 1650 mm/s0.13 mm hatch spacing; and the contour power is 200 W with a scan speed of 800 mm/s. Both samples were polished using Sharmic vibration polishing with 3 mm ceramic particles. It was observed that the 3D metal printed aluminium sample built vertically is not as flat as the horizontal one. There is a little curvature in the sample. This will eventually alter the cavity volume and can affect the results of measurements. The remaining three samples are machined using Computer Numerical Control (CNC) from copper, aluminium and stainless steel. Photographs of all the samples are given in Figure 7.14. The direction of the surface current flow on the sample is indicated by the white arrows. Measurements of samples are taken several times to minimise random error. The average of the readings is used for the extraction of the effective conductivity. The transmission coefficient S_{21} of the measured samples is given in Figure 7.15. The measured

loaded Q-factor Q_l and the magnitude of the S_{21} are used in computing the unloaded Q-factor using the relation in (2.18). The results are given in Table 7.3. There is a standard deviation of 6.74×10^{-4} and standard error of 3.01×10^{-4} from 3 dB bandwidth readings and the amplitude of S_{21}. This signifies good repeatability of the measurements.

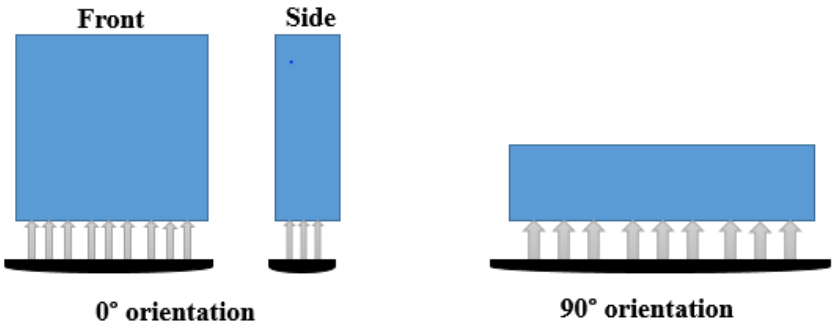

Figure 7.13 Illustration of vertical (0º) and horizontal orientation (90º) of 3D printing position

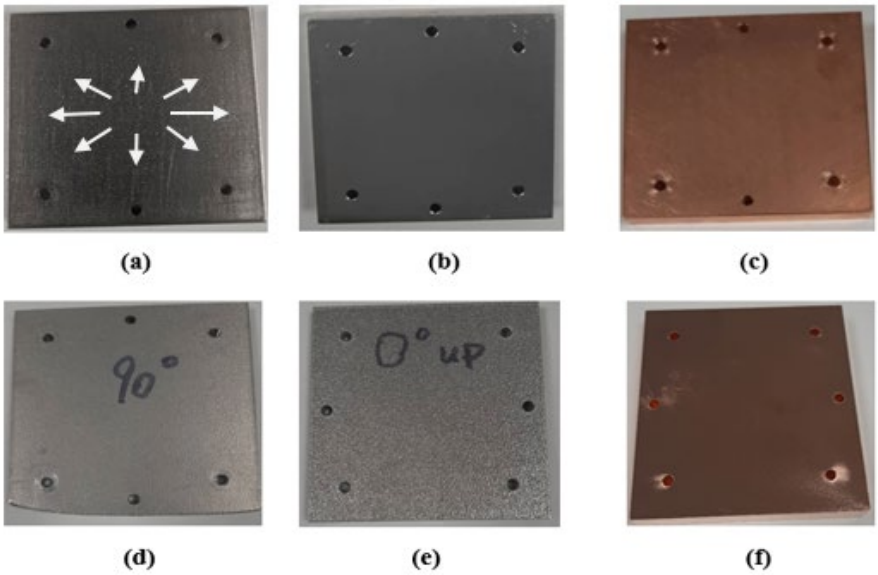

Figure 7.14 Photographs of the six samples: CNC machined: (a) stainless steel (b) aluminium (c) copper; 3D printed: (d) aluminium alloy horizontally built (e) aluminium alloy vertically built (f) polymer + copper plating

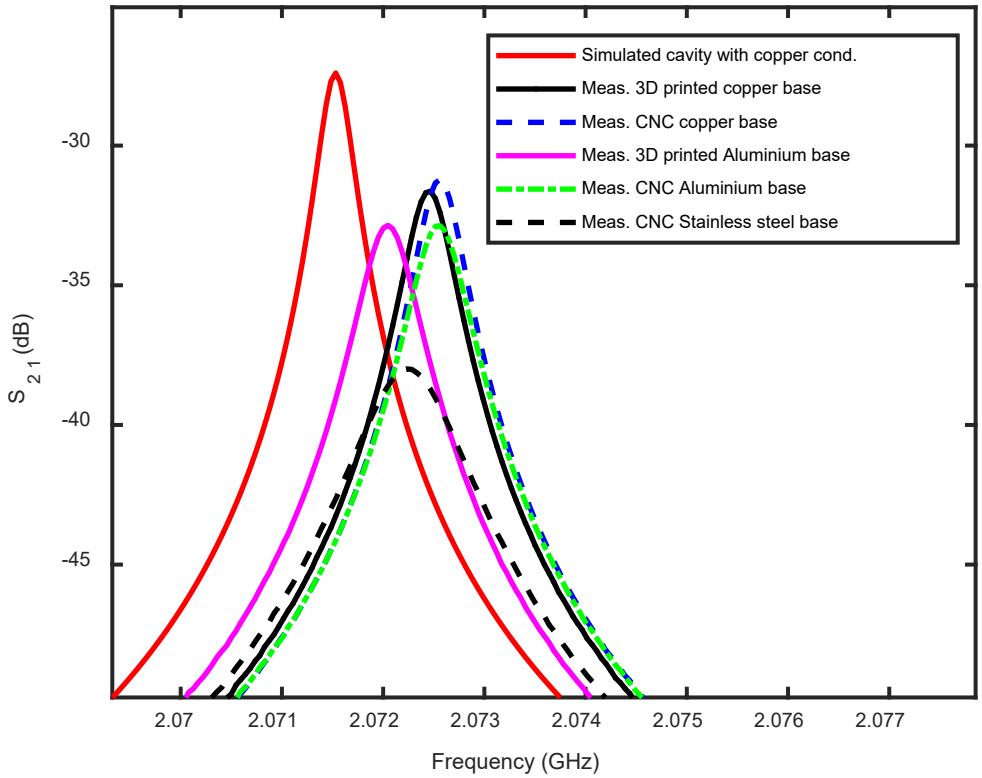

Figure 7. 15 S21 response of measured conductor materials

Table 7.3: Measured loaded *Q*, Insertion loss *IL* and evaluated unloaded *Q* using (2.18)

Samples	Q_l	***IL* (dB)**	***Qu***
3D printed polymer with copper coating	5045	33.65	5152 ± 25
CNC Copper	4936	34.01	5049 ± 15
3D printed Aluminium, built horizontally (90°)	4007	35.59	4075 ± 20
3D printed Aluminium, built vertically (0°)	3381	32.83	3459 ± 25
CNC Aluminium	4095	35.45	4165 ± 15
CNC Stainless steel	2426	40.15	2451 ± 20

7.9 Surface Roughness

Additive manufacturing process tends to introduce surface features that results in or relates to microwave loss and the electrical conductivity is degraded. The knowledge of surface roughness is therefore significant in this work. This is especially so when the surface texture is in orthogonal direction to the current flow. This is also because the current flow concentrates at the surface within a few skin depths [152]. The skin depth δ is defined by [163]

$$\delta = \sqrt{\frac{1}{f\sigma\mu\pi}} \tag{7.5}$$

where f is the frequency, σ is conductivity, μ is permeability of the conductor.

It is noted that the surface roughness in 3D printed metal parts can be comparable with or even larger than δ. This results in increasing surface resistance and significant impact on the power loss as described [160]. The 3D-printed polymer device by SLA tends to have smoother surface. The coating helps to reduce the surface roughness further giving it advantage over AM metals. To analyse the effect of surface roughness on the effective conductivity of MUT, the surface roughness of each sample was measured using Alicona microscope at three different locations. That is, the central point and two other places away from the centre. The measurement set-up is shown in Figure 7.14. The measurement area for each location is 1 mm × 1 mm and the images of the surfaces of 3D printed copper and aluminium alloy samples are shown in Figure 7.15. The average height of the selected area, S_a values of the three measured points are given in Table 7.4. From the results we can see that metal AM plates have higher surface roughness than the 3D printed polymer and the CNC plates. The S_a value of the polished vertically oriented built aluminium sample is higher than that of the polished horizontally printed sample by about 30%.

Table 7.4: Measured Sa value of surface roughness

Cavity and samples	Sa (µm) values at the three measured points
Main cavity (3D printed polymer with copper coating)	0.53, 0.54, 0.58
Base (3D printed polymer with copper coating)	0.34, 0.35. 0.38
Base (CNC Copper)	0.24, 0.245, 0.27
Base (3D printed Aluminium, 90°)	1.12, 1.18 1.23
Base (3D printed Aluminium, 0°)	1.44, 1.57, 1.65
Base (CNC Aluminium)	0.59, 0.60, 0.62
Base (CNC Stainless steel)	0.50, 0.55, 0.58

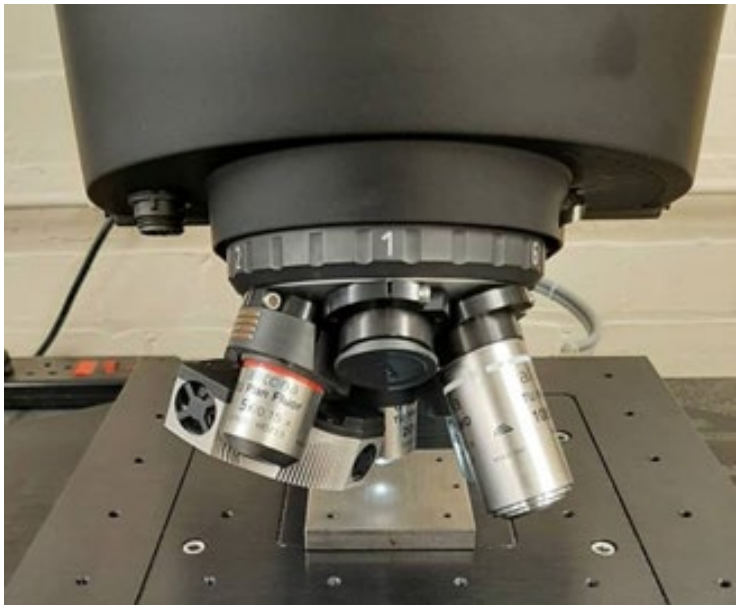

Figure 7.16 Measurement set up of surface roughness using Alicona microscope

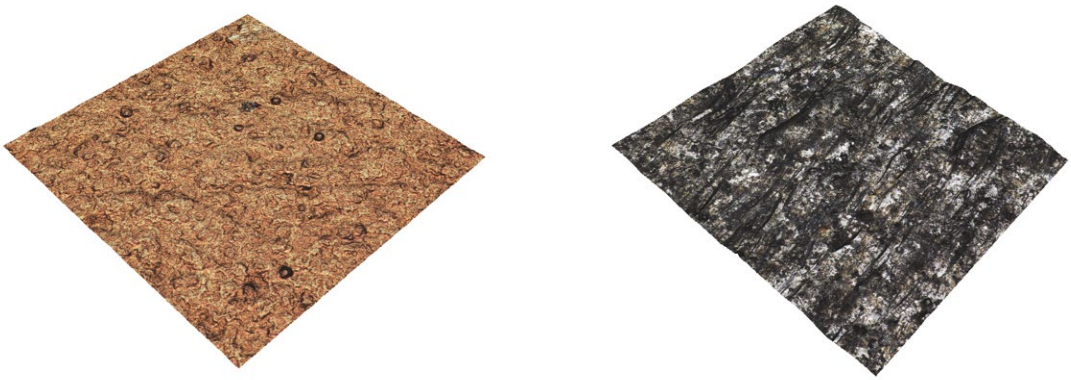

(a) (b)

Figure 7.17 Image of the surface roughness using Alicona: (a) 3D printed polymer copper base (b) 3D printed Aluminium alloy base

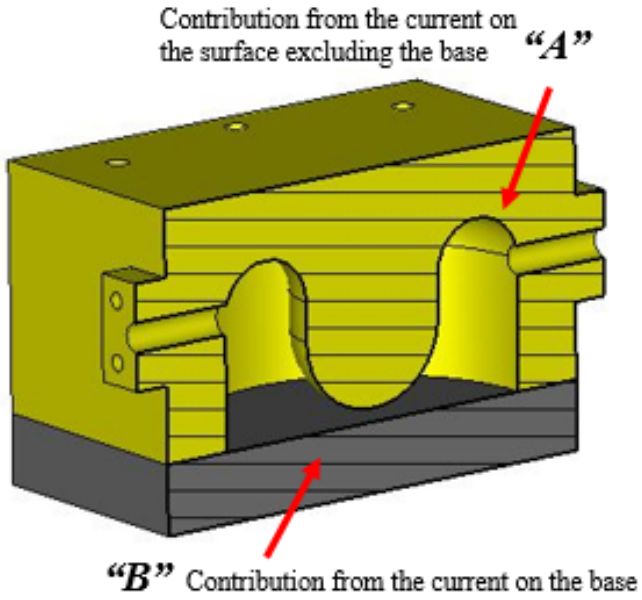

Figure 7.18 Illustration of contribution of current from the surface and base of the cavity: coefficient denotation

7.10 Extraction Method for Effective Conductivity

The unloaded Q is proportional to the ratio of the resonant wavelength and skin depth in any cavity structure [164]. The knowledge of Q_u can be used to evaluate the effective conductivity. This is so, for cavity with high symmetry and analytically solvable fields. However, this is not the case for the cavity used in this work. To evaluate the effective conductivity of the MUT, an approach used in [158] was adopted. A simple analytical formula can be derived based on the knowledge of the energy stored in the volume and base of the cavity. Considering the illustration shown in Figure 7.18, the contribution from the current on the main cavity is denoted by coefficient A, while that of the base is denoted by coefficient B. Two cases are considered: First, the main cavity and the base are of the same material (copper in this case and will also serve as the reference material). The second case is when main cavity is made of copper material and the base (MUT) is of other materials under test. Based on the first case the measured unloaded Q-factor of the cavity resonator, denoted by Q_0 is related to the conductivity of the copper, σ_{CU}, given by

$$\frac{1}{Q_0} = \frac{A}{\sqrt{\sigma_{CU}}} + \frac{B}{\sqrt{\sigma_{CU}}} \tag{7.6}$$

In the second case, when the base of the cavity is replaced by the MUT. The relationship changes to

$$\frac{1}{Q_1} = \frac{A}{\sqrt{\sigma_{CU}}} + \frac{B}{\sqrt{\sigma_{MUT}}} \tag{7.7}$$

where Q_1 is the measured unloaded Q-factor of the cavity resonator with MUT and σ_{MUT} is the effective conductivity of the MUT. Combining (3) and (4), the measured effective conductivity of the MUT can be evaluated using the following expressions

Table 7.5: Simulation model used to extract the coefficient *A* and *B*

Material	**Conductivity (S/m)**	**Unloaded *Q*-factor**	**Coefficient**
Copper base	4.76×10^7	5863	$A = 0.901$
Aluminium base	3.56×10^7	5658	$B = 0.275$

$$\sigma_{CU} = [Q_0(A+B)]^2 \tag{7.8}$$

$$\sigma_{MUT} = \frac{\sigma_{CU}\, B^2}{\left\{\left[\frac{Q_0}{Q_1}(A+B)\right] - A\right\}^2} \tag{7.9}$$

Since we can measure Q_0 and Q_1, we need to know the coefficient *A* and *B* in order to use (7.8) and (7.9). For this, the coefficients were determined based on simulation in CST in hypothetical experiments with given conductivity values. Two simulation models were used: one considering copper material for both the main cavity and the base, and the other considering copper material for the main cavity with an aluminium base. The nominal conductivity of these two materials taken from CST library was used in the simulation. However, following the measurements of the surface roughness of main cavity as presented earlier we have introduced surface roughness of 0.5 μm to the main part of the cavity and assume a zero roughness for the MUT as we are only concerned with the effective conductivity of the MUT. This effectively changes the conductivity of the copper material from 5.8×10^7 S/m to 4.76×10^7 S/m at the resonant mode based on calculation from CST. Using the results of the simulations and simultaneously solving (7.6) and (7.7) gives the coefficient *A* and *B* as in Table 7.5. It is important to note that the coefficients

Table 7.6: Measured effective conductivity

Samples	Measured effective conductivity σ_{MUT} (× 10^6 S/m)	Extracted bulk conductivity using measured roughness (× 10^6 S/m)	Bulk nominal Conductivity (× 10^6 S/m)
3D printed polymer with copper coating	36.7 ± 0.09	39.3	58
CNC Copper	31.0 ± 0.08	31.9	58
3D printed Aluminium, (90°)	8.09 ± 0.20	9.76	29
3D printed Aluminium, (0°)	4.67 ± 0.12	5.64	29
CNC Aluminium	9.05 ± 0.23	9.51	35
CNC Stainless steel	1.12 ± 0.03	1.13	1.45

are not sensitive to the materials, using different nominal conductivity in generating the coefficients would give similar outcome. The uncertainty propagation of the S-parameter (S_{21}) and the measurements repeatability of cavity are used in determining the uncertainty of the measured *Q*-factor at 95% confidence level [114]. The uncertainty of *Q*-factor and that of the coefficients *A* and *B* are used to evaluate expanded uncertainty and to arrive at 95% confidence level of the measured effective conductivity.

7.11 Results Discussion

The measured unloaded *Q*-factor (Table 7.3) and the coefficients *A* and *B* (Table 7.5) are utilised for computing the effective conductivity of the measured materials using (7.8) and (7.9). The results are given in Table 7.6 along with measurement uncertainty and extracted bulk conductivity taking to account the measured roughness using analytical formula in

Table 7.7: Comparison with other techniques

Type	Freq. GHz	Meas. *Q*-factor	Fabrication method	Features and limitations	Ref
Cylindrical Cavity	8.79	4045	CNC	3% accuracy on copper and brass; Analytical formula	[157]
Fabry-perot open resonator	20 -40	80,000	CNC	$10^4 \sim 10^7$ S/m demonstrated; bulky structure; a large number of resonances	[154]
Parallel plate resonator	5.3	1120	CNC	Compact resonator with relatively low *Q*	[156]
Re-entrant cavity	2.07	5045	3D printed coated polymer	Compact resonator with high *Q*; new manufacture technique	This work

[165]. The results show that the copper coating on the 3D printed polymer and the bulk copper by CNC machining have similar conductivity values. Between the 3D printed Aluminium alloy built in vertical and horizontal orientations, as expected, the one built vertically has lower conductivity compared to that of horizontally built one. This is consistent with the higher surface roughness recorded in the former and also in conformity with the findings in excess roughness exhibit by laser melting process [160]. For stainless steel, good agreement between the measured effective conductivity and nominal conductivity of bulk stainless steel is obtained as given in the Table 7.6. The effect of surface roughness is less for lower conductive materials such as the stainless steel compared to high conductive material such as copper. As for the measured effective conductivity of CNC Aluminium and that of the horizontally printed sample, they have similar values. This suggests good surface conductivity of the horizontally printed aluminium-copper alloy. This also indicates how aluminium alloy A20X can be promising for utilisation in fabricating microwave devices where polishing can be applied. Generally,

the results obtained are at the level of comparison with the nominal conductivity of the materials measured and reported values using other methods such as that of 3D metal printed aluminium alloy 8.65×10^6 S/m [159]. This has therefore validated the proposed measurement method and the evaluation formula derived and used in this work. The technique presented here offer a relatively easy and simplified measurement techniques enabled by high-Q and low-cost effective conductivity measurement method compared to other method as given in Table 7.7.

7.12 Summary on Conductivity Measurements

The measurement technique presented from Section 7.6 to 7.11 uses re-entrant cavity resonator for the estimation of effective conductivity of different metals under different manufacture condition or techniques. An analytical formula for evaluating the effective conductivity based on simulations of the designed cavity and knowledge of energy stored in the cavity has been derived. The results of the measured samples show the capability of the measurement technique in distinguishing materials due to varying electrical resistances using the analytical expression. The sensitivity of the measurement setup to changes due to printing orientation in additive manufacturing is evident from the results of the comparison measurements. This validates the usability of the measurement technique, simple and low-cost, within acceptable systematic and random errors associated with the measurements of conductive materials for microwave applications.

CHAPTER EIGHT: CONCLUSION AND FUTURE WORK

8.1 Conclusion

The work presented in this thesis is focused on the design and fabrication of cavity resonator sensors for dielectric metrology at microwave and millimetre wave frequencies. The cavities were fabricated using 3D printing technology and have been fully explored for their measurement capabilities for various liquid and solid materials. New cavity structures, characterisation techniques and evaluation methods have been presented. Analytical extraction-models established using simulation data for the evaluation of dielectric properties of liquid and solid materials have been derived. Similarly, new model for estimating the effective conductivity of several alloys produced using different techniques have been developed, utilised and verified.

Literatures relating to cavity resonators used for the measurements of materials dielectric properties using microwave sensing techniques have been reviewed and compared to the state of the art in dielectric metrology in Chapter 3. Various design approach and applications have been studied, and this has informed the choice of the cavity structure, type of fabrication and method of extraction adopted and used in this work.

Re-entrant cavity resonator was chosen, and this is due to their highly concentrated electric field at the gap region where sensing takes place. A modified 2 GHz re-entrant cavity resonator, with further enhanced electric field and optimised Q-factor was presented in Chapter 4. The cavity has shown good sensitivity for characterising common solvents of varying purity, and measurement of dielectric properties of complex fluids (such as crude oil and their derivative). The cavity sensor also works for concentration measurements of both binary and ternary solution as demonstrated in Section 4.10; this has therefore made the cavity resonator sensor designed suitable for various applications such

as petroleum, medical and pharmaceutical as well as food and agriculture. The results of the measurements are in very good agreement with literature results reported using different approach.

In Chapter 5, a novel approach to dielectric measurements using coaxial microwave cavity resonator, enabled by a simplified analytical formula, has been designed and fabricated. Measurements of various common solvent and crude oils was demonstrated have validated the measurement concept over a broad bandwidth from 2 GHz up to 8 GHz for four (4) different resonance. The absences of frequency dispersion effect in the tested materials between 2 GHz and 8 GHz has been observed in some of the materials as expected. This is because the samples have low Debye relaxation time. Cavity cleaning to perform repeated measurements remains the challenge of this approach. This is also depending on the type of MUT. For this, some future recommendations were given in Section 8.2.

The use of higher order mode in cavity resonators enables dielectric measurements at higher frequencies. This is because the cavity size decreases with the increase in frequency and therefore it becomes difficult to realise high frequency cavities for measurement based on perturbation theory. A 60 GHz higher order mode re-entrant cavity sensor has been designed and used for measurements of liquids materials in Chapter 6. The results show the potential use of this sensor in dielectric metrology especially for very low volume of liquids at millimetre-wave frequencies. This piece also has demonstrated that 3D printing can be a cost-effective manufacturing approach for cavity resonator sensors at these frequencies.

The use of substrate materials and additive manufacturing (AM) technology have been on the rise for applications such as sensors, communications devices, and other

microwave passive components in general. The need to precisely know the properties of substrate materials and the electrical conductivity of metals and alloys in AM is highly important. Chapter 7 has demonstrated and validated a novel measurement approach of dielectric constant and effective electric conductivity of various solid samples using a modified high-Q re-entrant cavity resonator. An analytical expression has been derived for the extraction of these properties in both cases enabled by simulations. Results from substrates of varying thickness and properties show the applicability of the devices for dielectric measurement of both thin and thick samples. Similarly, the simplicity of the measurement and extraction methods as well as the effectiveness of the measurement cavity in evaluating the effective conductivity of the materials (fabricated using different technology) have been shown in this work. The effect of surface roughness on measured conductivity has also been identified and discussed to validate the measurement results.

Throughout the thesis, 3D printing has been used to fabricate the cavity resonators. This rapid prototyping method has reduced the manufacturing and development time. It also provides more design flexibility in terms of making smooth edges and round corners without increasing the complexity in fabrication. For instant, complex device such as the coaxial resonators presented in Chapter 5. Therefore, 3D printing has demonstrated its capability in fabricating the cavity devices at both low microwave frequency (~ 2 GHz) and high millimetre-wave frequency (60 GHz) in a cost-effective way.

In General dielectric metrology using cavity resonator for liquids and solids materials using high-Q and sensitive cavity resonator sensors has been demonstrated and validated. This is by using simplified, reliable, and cost-effective measurement techniques in this work.

8.2 Future work

For the re-entrant cavity used for liquid measurements, large size tube was used due to the viscosity of some of the materials under consideration. To use the device for measurements of small volume of materials, the size of the placement hole can be reduced and smaller tube of 1 mm or less can utilised. It could also be useful to deploy flexible capillaries in order to perform measurements in a continuous flow form.

In the case of the cavity used for substrates measurement the gap between the cavity post and the base of the cavity was only 2 mm allowing for measurement of samples less than or equal 1.5 mm. To further increase the measurement capability to allow for thick substrate sample greater than 1.5 mm, the gap between the post and the base can be increased at the expense of reducing the electric field concentration. In addition, the extraction of the loss tangent has not been considered in this work due to the complex nature of the variables involved and non-linearity of the relationship between the loss tangent and Q-factor as the dielectric constant changes. Further work may be done by changing the design considering a trade-off between the Q-factor and realisation of the analytical formula. Alternatively, numerical algorithm can be used, however, this will increase the complexity of the parameter extraction.

To improve the accuracy of the measurement and reduce the effect of the environmental factor such temperature, the experimental measurement may be conducted in a control environment or by adding a sensor to monitor the temperature in real time and calibrate its effect.

The concept used in the coaxial cavity resonator was to fill the entire cavity with the fluids under measurement. Depending on the type of materials measured the cavity can become contaminated and therefore may require cleaning. This cleaning may result in

degradation of the copper coating applied to the polymer printed device. To overcome this, a thin film coating (e.g. hydrophobic coating for water-based liquids) of low dielectric loss material can be layered inside the cavity. However, it remains a risk for this type of cavity sensor if a variety of liquids are to be used.

The use of motorised control pressure pumps for measurement using 50 μm to 100 μm ID tubes for the 60 GHz cavity resonators is recommended for potentially utilisation in measurement of biological cells. As the size of tube becomes smaller injecting the fluids becomes difficult, and the use of pump can be deployed to overcome this challenge. Similarly, the loss tangent extraction can also be looked into by modifying the cavity while maintaining the high-Q and sensitivity of the device.

References

[1] B. Camli, E. Kusakci, B. Lafci, S. Salman, H. Toruna and A. Yalcinkaya, "A Microwave Ring Resonator Based Glucose Sensor," *Procedia Eng.,* vol. 168, pp. 465-468, 2016.

[2] A. M. Mohammed and Y. Wang, "Four-way Waveguide Power Dividers with Integrated Filtering Function," in *Eur. Microw. Conf.*, Paris, France, 2015.

[3] M. Skolnik, "Role of Radar in Microwaves," *IEEE Trans. Microw. Theory Techn. ,* vol. 50, no. 3, pp. 625-632, 2002.

[4] H. Sobol and K. Tomiyasu, "Milestones of Microwaves," *IEEE Trans. Microw. Theory Techn.,* vol. 50, no. 3, pp. 594-611, 2002.

[5] S. Wylie, A. Shaw and A. I. Al-Shamma'a, "Real-Time Measurements of Oil, Gas and Water Contents Using an EM Wave Sensor for Oil-Marine-Environment Industries," in *Eur. Microw. Conf.*, Manchester, UK, 2006.

[6] N. Meyne, G. Fuge, A.-P. Zeng and A. F. Jacob, "Resonant Microwave Sensors for Picoliter Liquid Characterization and Nondestructive Detection of Single Biological Cells," *IEEE J Electromag, RF Microw Med. Bio.,* vol. 1, no. 2, pp. 98-104, 2017.

[7] W. Guoa, X. Zhu, Y. Liu and H. Zhuang, "Sugar and water contents of honey with dielectric property sensing," *J. of Food Eng. ,* vol. 97, no. 2, pp. 275-281, 2010.

[8] S. Kulkarni and M. S. Joshi, "Design and Analysis of Shielded Vertically Stacked Ring Resonator as Complex Permittivity Sensor for Petroleum Oilsked," *IEEE Trans. Microw Theory Techn.,* vol. 63, no. 8, pp. 2411 - 2417, 2015.

[9] J. R. Baker-Jarvis, M. D. Janezic, B. F. Riddle, R. T. Johnk, C. L. Holloway, R. G. Geyer and C. A. Grosvenor, "Measuring the Permittivity and Permeability of Lossy Materials: Solids, Liquids, Metals, and negative-Index Materials," Technical Note (NIST TN), Boulder, US, 2015.

[10] E. F. May, L. Pitre, B. J. Mehl, M. R. Moldover and J. W. Schmidt, "Quasi-Spherical Cavity Resonators For Metrology Based On The Relative Dielectric Permittivity Of Gases," *Rev. Scient. Instrum.,* vol. 75, no. 10, pp. 3306 - 3317, 2004.

[11] S. El-Rayes, Y. Wang, M. J. Lancaster and X. Shang, "Enhancing The Selectivity Of Frequency Selective Surfaces For Terahertz Sensing Applications," in *Millimeter Waves and THz Technol Workshop (UCMMT)*, Cardiff, 2015.

[12] T. Chen, S. Li and H. Sun, "Metamaterials Application in Sensing," *Sensors,* vol. 12, no. 3, pp. 2742 - 2765, 2012.

[13] S. Moscato, M. Pasian, M. Bozzi, L. Perregrini, R. Bahr and T. Le, "Exploiting 3D Printed Substrate For Microfluidic Siw Sensor," in *Eur. Microw. Conf. (EuMC)*, Paris, 2015.

[14] P. Vélez, L. Su, K. Grenier, J. Mata-Contreras, D. Dubuc and F. Martín, "Microwave Microfluidic Sensor Based on a Microstrip Splitter/Combiner Configuration and Split Ring Resonators (SRRs) for Dielectric Characterization of Liquids," *IEEE Sensors J.,* vol. 17, no. 20, pp. 6589 - 6598, 2017.

[15] G. Bailly, A. Harrabi, J. Rossignol, M. Michel, D. Stuerga and P. Pierre, "Microstrip Spiral Resonator For Microwave-Based Gas Sensing," *Chem. Biolog. Sensors,* vol. 1, no. 4, pp. 1- 4, 2017.

[16] S. Moscato, N. Delmonte, L. Silvestri, M. Pasian, M. Bozzi and L. Perregrini, "Compact Substrate Integrated Waveguide (Siw) Components On Paper Substrate," in *Eur. Microw. Conf. (EuMC)*, Paris, 2015.

[17] K. Y. You, "Introductory Chapter: RF/Microwave Applications," in *Emerging Microwave Technologies in Industrial, Agricultural, Medical and Food Processing*, london , https://www.intechopen.com/chapters/58958 doi: 10.5772/intechopen.73574, 2018.

[18] M. Golio and J. Golio, RF and Microwave Circuits, Measurements, and Modeling (The Electrical Engineering Handbook), Arizona, USA: CRC Taylor& Francis Group, 2007.

[19] S. M. Boybay and O. M. Ramahi, "Material Characterisation Using Complementary Split-Ring Resonators," *IEEE Trans. Instrum. Meas.,* vol. 61, no. 11, pp. 3039 - 3046, 2012.

[20] A. P. Gregory and R. N. Clarke, "A Review of RF and Microwave Techniques For Dielectric Measurements on Polar Liquids," vol. 13, no. 4, pp. 727 - 743, 2006.

[21] K. C. Yaw, "Measurement of Material Dielectric Properties, Application Note," Rohde & Schwarz, Singapore, 2012.

[22] A. L. de Paula, M. C. Rezende and J. J. Barroso, "Modified Nicolson-Ross-Weir (NRW) method to retrieve the constitutive parameters of low-loss materials," in *SBMO/IEEE MTT-S Int. Microw. and Optoelectr Conf.*, Natal, Brazil, 2011.

[23] F. Costa, M. Borgese, M. Degiorgi and A. Monorchio, "Electromagnetic Characterisation of Materials by Using Transmission/Reflection (T/R) Devices," *Electronics 2017, 6(4), 95,* vol. 6, no. 4, pp. 1-27, 2017.

[24] Keysight Technology , "Basics of Measuring the Dielectric Properties of Material," Keysight Technology , USA, 2019.

[25] D. K. Ghodgaonkar, V. V. Varadan and V. K. Varadan, "A free-space method for measurement of dielectric constants and loss tangents at microwave frequencies,," *IEEE Trans Instrum Meas,* vol. 37, no. 3, pp. 789-793, 1989.

[26] B. Kapilevich and B. Litvak, "Optimized Microwave Sensor for Online Concentration Measurements of Binary Liquid Mixtures," *IEEE Sensors J,* vol. 11, no. 10, pp. 2611 - 2616, 2011.

[27] A. L. Gioia, E. Porter, I. Merunka, A. Shahzad, S. Salahuddin and M. Jones, “Open-Ended Coaxial Probe Technique for Dielectric Measurement of Biological Tissues: Challenges and Common Practices,” *MDPI Diagnostics ,* vol. 8, no. 40, pp. 1-38, 2018.

[28] M. A. H. Ansari and A. K. Jha, “Design andApplication of the CSRR-Based Planar Sensor for Noninvasive Measurement of Complex Permittivity,” *IEEE Sensors J,* vol. 15, no. 12, pp. 7181-7189, 2015.

[29] L. F. Cheng, C. K. Ong, C. P. Neo, V. V. Varandan and V. K. Varadan, Microwave Electronics: Measurement and Materials Characterisation, USA: John Wiley & Sons Ltd, 2004, pp. 251 -270.

[30] M. Abdolrazzaghi, M. Daneshmand and A. K. Iyer, “Strongly Enhanced Sensitivity in Planar Microwave Sensors Based on Metamaterial Coupling,” *IEEE Trans. Microw Theory Techn.,* vol. 66, no. 4, pp. 1843 - 1855, 2018.

[31] K. Saeed, R. D. Pollard and I. C. Hunter, “Substrate IntegratedWaveguide Cavity Resonators for Complex Permittivity Characterization of Materials,” *IEEE Trans. Microw. Theory Techn.,* vol. 56, no. 10, pp. 2340 - 2347, 2008.

[32] B.-H. Kim, Y.-J. Lee, H.-J. Lee, Y. Hong, J.-G. Yook, M. H. Chung, W. Cho and H. H. Choi, “A gas sensor using double split-ring resonator coated with conducting polymer at microwave frequncies,” in *Sensors* , Valencia, Spain, 2014.

[33] N. Sharafadinzadeh, M. Abdolrazzaghi and M. Daneshmand, “Highly Sensitive Microwave Split Ring Resonator Sensor Using Gap Extension for Glucose Sensing,” in *IEEE MTT-S Int. Microw. Workshop Series Adv. Mat. Proc.*, Pavia, Italy, 2017.

[34] G. Galindo-Romera, F. J. Herraiz-Martínez, M. Gil, J. J. Martínez-Martínez and D. Segovia-Vargas, “Submersible Printed Split-Ring Resonator-Based Sensor for Thin-Film Detection and Permittivity Characterization,” *IEEE Sensors J.,* vol. 16, no. 10, pp. 3587 - 3596, 2016.

[35] C.-M. Hsu, K.-Z. Chen, C.-S. Lee and C.-L. Yang, “Improved Approach Using Multiple Planar Complementary Split-Ring Resonators For Accurate Measurement Of Permittivity,” in *IEEE MTT-S Int. Wireless Symp. (IWS)*, Shanghai, China, 2016.

[36] M. H. Zarifi and M. Daneshmand, “Non-Contact Liquid Sensing Using High Resolution Microwave Microstrip Resonator,” in *IEEE MTT-S Int. Microw. Symp. (IMS)*, Phoenix, USA, 2015.

[37] A. A. M. Bahar, Z. Zakaria, S. R. Ab Rashid, A. A. M. Isa, A. R. Alahnomi and Y. Dasni, “Microfluidic Planar Resonator Sensor With Highly Precise Measurement For Microwave Applications,” in *Anten. Propag. (EUCAP) 11th Euro. Conf.*, Paris, 2017.

[38] D. J. Rowe, S. Al-Malki, A. A. Abduljabar, A. Porch and D. A. A. C. J. Barrow, "Improved Split-Ring Resonator For Microfluidic Sensing," *IEEE Trans. Microw. Theory Techn.,* vol. 62, no. 3, pp. 689 - 699, 2014.

[39] C. Rosenberg, N. Hermiz and R. Cook, "Cavity resonator measurements of the complex permittivity of low-loss liquids," *IEE Proceed. Microw Opt. Antenn.,* vol. 129, no. 2, pp. 71 - 76, 1982.

[40] C. K. Kling, K. W. Whites and G. L. J, "Accurate Specimen Placement For Dielectric Measurements in a TM0n0 Cylindrical Cavity," in *Antennas Propag (APSURSI), IEEE Int. Symp.*, Fajardo, Puerto Rico, 2016.

[41] S.-h. Chato, "Measurement Of Microwave Conductivity and Dielectric Consatant by the Cavity Pertubation Method and thier Errors," *IEEE Trans. Microw. Theory Techn.,* vol. 33, no. 6, pp. 519 - 526, 1985.

[42] R. A. Waldron, "Perturbation Theory of Resonant Cavities," *Proceed. IEE - Monographs,* vol. 107, no. 12, pp. 272 - 274, 1960.

[43] H. Kawabata, H. Tanpo and Y. Kobayashi, "A Rigorous Analysis of A TM0101 Mode Cylindrical Cavity For Measure Accuracy Complex Permittivity," in *Eur. Microw. Conf.*, Munich, 2003.

[44] T. Shimizu, S. Kojima and Y. Kogami, "Accurate Evaluation Technique of Complex Permittivity for Low-Permittivity Dielectric Films Using a Cavity Resonator Method in 60-GHz Band," *IEEE Trans. Microw. Theory Techn.,* vol. 63, no. 1, pp. 279- 286, 2015.

[45] G. Gennarelli, S. Romeo, M. R. Scarfì and F. Soldovieri, "A Microwave Resonant Sensor for Concentration Measurements of Liquid Solutions," *IEEE Sensors J.,* vol. 13, no. 5, pp. 1857 - 1864, 2013.

[46] P. A. Rizzi, "Microwave Resonators and Filter," in *Microwave Engineering Passive Devices*, New Jessy, Prentice-Hall International, Inc, 1230, pp. 411-418.

[47] D. M. Pozar, Microwave Engineering, 4th, Ed., United State of America: John Wiley and Sons, Inc, 2012.

[48] C. Lee, S. Lee and S. Chuang, "Plot of Modal Field Distribution in Rectangular and Circular Waveguides," *IEEE Trans. Microw. Theory Techn.,* vol. 33, no. 3, pp. 271-274, 1985.

[49] C. Zhu, Y. Zhuang, Chen, Yizheng and J. Huang, "A Hollow Coaxial Cable Fabry-Perot Resonator For Liquid Dielectric Constant Measurement," *Rev. Sci. Instrum.,* vol. 89, pp. 1-5, 2018.

[50] M. J. Lancaster, "Superconductive cavity resonators," in *Passive Microwave Device Applictaions Of High Temperature Supercoductors*, Cambridge, Cambridge University Press, 1997, pp. 67-125.

[51] K. Zhang and D. Li, "Metallic Waveguides and Resonant Cavities," in *Electromagnetic Theory for Microwaves and Optoelectronics*, Berlin, Heidelberg, Springer, 2008, pp. 235-316.

[52] K. Z. Dejie Li, "Metallic waveguide and resonant cavities," in *Electromagnetic Theory for Microwaves and Optoelectronics*, New York, Springer Berlin Heidelberg, 1998, pp. 235-3.

[53] J.-M. Floch, L. Y. Fan, D. M. Aubourg, N. Cros, Q. Carvalho, J. Shan, E. Bourhill and G. Humbert, "Rigorous analysis of highly tunable cylindrical Transverse Magnetic mode reentrant cavities," *Rev. Scient. Instrum.,* vol. 84, pp. 1-7, 2013.

[54] W. Xi, W. Tinga, W. Voss and B. Tian, "New Results for Coaxial Re-Entrant Cavity with Partially Dielectric Filled Gap," *IEEE Trans. Microw. Theory Techn.,* vol. 40, no. 4, pp. 747 - 753, 1992.

[55] K. Fujisawa, "General Treatment of Klystron Resonant Cavities," *IRE Trans. Microw. Theory Techn.,* pp. 344 - 58, 1958.

[56] J. Papapolymerou, J.-C. Cheng, J. East and L. Katehi, "A micromachined high-Q X-band resonator," *IEEE Microw Guided Wave Lett,* vol. 7, no. 6, pp. 168 - 170, 1997.

[57] M. T. Sebastian, " Measurement Of Microwave Dielectric Properties And Factors Affecting Them," in *Dielectric Materials for Wireless Communication*, Elsevier Science, 2010, pp. 11-45.

[58] M. Mehdizadeh, "The Impact of Field on Materials at RF/Microwave Frequencies," in *Microwave/RF Applicators and Probes for Material Heating, Sensing, and Plasma Generation*, Oxford, UK, William Andrew, 2009, pp. 35-36.

[59] R. Arora and W. Mosch, "Liquid Dielectrics, their Classification, Properties, and Breakdown Strength," in *High Voltage and Electrical Insulation Engineering*, Dresden, John Wiley & Son Inc, 2011, pp. 275-317.

[60] R. Z. M. Ulloa, G. H. Santiago and V. L. V. Rueda, "The Interaction of Microwaves with Materials of Different Properties," in *Electromagnetic Fields and Waves*, Rijeka, Croatia, Intech, 2019, pp. 93 - 117.

[61] D. Stuerga, "Microwave–Material Interactions and Dielectric Properties, Key Ingredients for Mastery of Chemical Microwave Processes," in *Microwaves in Organic Synthesis*, Weinheim, WILEY-VCH Verlag GmbH & Co, 2006, pp. 1-57.

[62] R. Kochetov, "Thermal and Electrical Properties of Nanocomposites, Including Material Properties," Saint-Petersburg State Electrotechnical University 'LETI', Russia, 2012.

[63] M. Gupta and W. W. L. Eugene, "Microwaves – Theory," in *Microwaves and Metals*, Singapore, John Wiley & Sons (Asia) Pte Ltd, 2007, pp. 35-40.

[64] S. O. Nelson and S. Trabelsi, “Factors Influencing the Dielectric Properties of Agricultural and Food Products,” *J. Microw. Power Electromag. Energy,* vol. 46, no. 2, pp. 93-107, 2012.

[65] M. Y. Onimisi and J. T. Ikyumbur, “Comparative Analysis of Dielectric Constant and Loss Factor of Pure Butan-1-ol and Ethanol,” *American J. Cond. Matter Phys,* vol. 5, no. 3, pp. 69-75, 2015.

[66] S. M. Hanham, C. Watts, W. J. L. Otter and N. Klein, “Dielectric Measurements Of Nanoliter Liquids With A Photonic Crystal Resonator At Terahertz Frequencies,” *Appl. Phys. Lett.,* vol. 107, no. 3, pp. 032903-5, 2015.

[67] A. P. Gregory and R. N. Clarke, “Tables of The Complex Permittivity of Dielectric Reference Liquids at Frequencies up to 5 Ghz,” National Physical Laboratory, London, 2012.

[68] A. K. Jha and M. J. Akhtar, “A Generalized Rectangular Cavity Approach for Determination of Complex Permittivity of Materials,” *IEEE Trans. Instrum. Meas.,* vol. 63, no. 11, pp. 2632 - 2640, 2014.

[69] G. Birnbaum and J. Franeau, “Measuremetn of the Dilectric Constant and Loss of Sloids and Liquids by a Cavity Pertubation Method,” *J. Appl. Sci.,* vol. 20, pp. 817-818, 1949.

[70] J. Sheen and C.-M. Weng, “Modification of cavity pertubation Techniques for Permittivity Measurements of Laminated Samples,” *IEEE Trans. Dielec. Electr. Insul.,* vol. 23, no. 1, pp. 532 - 536, 2016.

[71] C. H. Collie, J. B. Hasted and D. M. Ritson, “The Cavity Resonator Method of Measuring the Dielectric Constants of Polar Liquids in the Centimetre Band,” *Proceed. Physical Soc.,* vol. 60, no. 1, pp. 71 - 82, 1948.

[72] E. Bourdel, D. Pasquet, P. Denorme and A. Roussel, “Measurement Of The Moisture Content With A Cylindrical Resonating Cavity In TM010 Mode,” *IEEE Trans. Instrum. Meas.,* vol. 49, no. 5, pp. 1023 - 1028, 2000.

[73] H. Kawabata, T. Kobayashi, Y. Kobayashi and Z. Ma, “Measurement Accuracy of a TM0m0 Mode Cavity Method To Measure Complex Permittivity of Rod Samples,” in *2006 Asia-Pac. Microw. Conf.*, Yokohama, Japan, 2006.

[74] U. Faz, U. Siart and T. F. Eibert, “A cylindrical cavity resonator for material measurements with coupled resonant modes for sensing and position offset compensation of the dielectric specimen,” in *German Microw. Conf.*, Nuremberg, Germany, 2015.

[75] Sherko Zinal and Georg Boeck, “Complex Permittivity Measurements Using TE11p Modes in Circular Cylindrical Cavities,” *IEEE Trans. Microw. Theory Techn.,* vol. 53, no. 6, pp. 1870-1874, 2005.

[76] H. Fu, X. Xiao and J. Li, "Study On Material Relative Permittivity Using TE011 Cylindrical Microwave Cavity," in *Electromag. Applicat. Student Innov. Compet. (iWEM)*, Nanjing, 2016.

[77] C. Sangdao, "Feasibility Study of Dielectric Measurement Using a Concentric Cylindrical Cavity," in *7th Int. Electr. Eng. Cong. (iEECON)*, Hua Hin, Thailand, 2019.

[78] H. Guo, L. Yao and F. Huang, "A cylindrical cavity Sensor for Liquid Water Content Measurement," *Sens. Actuators A: Physic,* vol. 238, pp. 133 - 139, 2016.

[79] P. Sharma, L. Lao and G. Falcone, "A Microwave Cavity Resonator Sensor for Water-in-oil Measurements," *Sens. Actuators B: Chemical,* vol. 262, pp. 200- 210, 2018.

[80] A. H. Sklavounos and N. S. Barker, "Permittivity measurements of liquids at millimeter-wave frequencies using an overmoded cavity resonator," in *Int. Conf. Infrared, Millimeter THz Waves*, Houston, TX, USA, 2011.

[81] J. L. Jordan and G. E. Ponchak, "Rectangular waveguide resonator for gas permittivity measurement at X-band," in *IEEE Topical Conf. on Wireless Sens. Sens. Net. (WiSNet)*, Anaheim, CA, 2018.

[82] N. B. A. Y. M. S. Bin Abdul Karim and T. Kitazawa, "Scattering analysis of rectangular cavity with input and output waveguides and its application to material characterization," in *IEEE Asia Pac. Microw. Conf. (APMC)*, Kuala Lumpar, Malaysia, 2017.

[83] D. C. Karns, J. C. Weatherall, J. Greca, P. R. Smith, K. Yam, J. Barber and B. T. Smith, "Millimeter-Wave Resonant Cavity for Complex Permittivity Measurements of Materials," in *IEEE/MTT-S Int. Microw. Symp. - IMS*, Philadelphia, PA, USA, 2018.

[84] M. D. Belrhiti, S. Bri, A. Nakheli, M. Haddad and A. Mamouni, "Dielectric Constant Determination of Liquid Using Rectangular Waveguide Structure Combined with EM Simulation," *J. Mat. Environ. Sci.,* vol. 3, no. 3, pp. 575 - 584, 2012.

[85] Y. Ye, T. Liu, X. Zeng, J. He and C. Akyel, "Analysis and Optimization Design of High Order Mode Rectangular Cavities," in *Int. Symp. Microw., Anten. Propag. EMC Technol. Wireless Comm.*, Hangzhou, China, 2007.

[86] D. Dancila, B. Beuerle, U. Shah, A. Rydberg and J. Oberhammer, "Micromachined cavity resonator sensors for on chip material characterisation in the 220–330 GHz band," in *47th Eur. Microw. Conf. (EuMC)*, Nuremberg, Germany, 2017.

[87] A. Kik, "Complex Permittivity Measurement Using a Ridged Waveguide Cavity and the Perturbation Method," *IEEE Trans. Microw. Theory Techn.,* vol. 64, no. 11, pp. 3878 - 3886, 2016.

[88] C. Guo, X. Shang, M. J. Lancaster and J. Xu, “A 3-D Printed Lightweight X-Band Waveguide Filter Based on Spherical Resonators,” *IEEE Microw. Wireless Comp. Lett.,* vol. 25, no. 7, pp. 442-444, 2015.

[89] J. Le Floch, Y. Fan, G. Humbert, Q. Shan, D. Ferachou, R. Bara-Maillet, M. Aubourg, J. Hartnett, V. Madrangeas, D. Cros, J. Blondy, J. Krupka and M. Tobar, “Dielectric Material Characterization Techniques And Designs Of High-Q Resonators For Applications From Micro To Millimeter-Waves Frequencies Applicable At Room And Cryogenic Temperatures,” *Rev. Scient. Instrum.,* vol. 85, no. 3, pp. 031301 - 13, 2014.

[90] G. M. Rocco, N. Delmonte, D. Schreurs, S. Marconi and F. B. M. Auricchio, “3d-Printed Pumpkin-Shaped Cavity Resonator To Determine The Complex Permittivity Of Liquids,” *Microw. Opt. Technol. Lett.,* vol. 63, no. 4, pp. 1061 - 1066, 2020.

[91] F. Thompson, A. D. Haigh, B. M. Dillon and ,. A. P. Gibson, “Analysis And Design of a Re-Entrant Microwave Cavity For The Characterisation Of Single Wheat Grain Kernels,” *IEE Proc. Sci. Meas. Techn.,* vol. 150, no. 3, pp. 113-117, 2003.

[92] A. Murugkar, R. Panigrahi and K. J. Vinoy, “A novel approach for high Q microwave re-entrant cavity resonator at S-band,” in *Asia-Pac Microw. Conf. (APMC),*, New Delhi, 2016.

[93] H. Hamzah, A. Abduljabar, J. Lees and A. Porch, “Compact Microwave Microfluidic Sensor Using a Re-Entrant Cavity’,” *Sensors,* vol. 18, no. 3, pp. 1-12, 2018.

[94] S. Maruoka, Y. Nikawa, T. Izumikawa and S. Maji, “Oversized cylindrical cavity to measure complex permittivity in millimeter waves,” in *IEEE-Asia Pac Microw. Conf.*, Singapore, 2009.

[95] A. Webb, “Cavity- And Waveguide-Resonators In Electron Paramagnetic Resonance, Nuclear Magnetic Resonance, And Magnetic Resonance Imaging,” *Prog. Nucl. Magn. Res. Spectr.,* vol. 83, pp. 1-20, 2014.

[96] B. García-Baños, A. J. Canós, J. M. Catalá-Civera and P. J. Plaza-González, “Accurate Permittivity Measurements With A Coaxial Resonator Independently Of Coupling Level,” in *IEEE MTT-S Int. Microw. Symp. Dig. (MTT)*, Seattle, WA, USA, 2013.

[97] A. J. C. Marín, B. García-Baños, J. M. Catalá-Civera, F. L. Peñaranda-Foix and J. D. Gutierrez-Cano, “Improvement in the Accuracy of Dielectric Measurement of Open-Ended Coaxial Resonators by an Enhanced De-Embedding of the Coupling Network,” *IEEE Trans. Microw. Theory Techn.,* vol. 61, no. 12, pp. 4636 - 4645, 2013.

[98] L. H. Chua and D. M. Syahkal, “Accurate and Direct Characterization of High-Q Microwave Resonators Using One-Port Measurement,” *IEEE Trans. Microw. Theory Techn.,* vol. 51, no. 3, pp. 978 - 985, 2003.

[99] T. Sasaki, K. Takahagi, Y. Kogami and T. Shimizu, “Complex permittivity measurements of a PTFE substrate in W band by the cut-off circular waveguide method,” in *Asia-Pac. Microw. Conf. (APMC)*, Kyoto, 2018.

[100] T. Shimizu, H. Inada and Y. Kogami, “Complex permittivity measurement for a low loss dielectric rod using a novel 50 GHz band TM010 mode cavity,” in *89th ARFTG Microw. Meas. Conf.* , Honololu, HI, 2017.

[101] S. Balmus, B. Pascariu, F. Creanga, I. Dumitru and D. D. Sandu, “The Cavity Perturbation Method For The Measurement Of The Relative Dielectric Permittivity In The Microwave Range,” *J. Optoelectron. Advanc. Mat.,* vol. 8, no. 3, pp. 971 - 977, 2006.

[102] Z. Peng, J.-Y. Hwang and M. Andriese, “Maximum Sample Volume for Permittivity Measurements by Cavity Perturbation Technique,” *IEEE Trans. Instrum. Meas.,* vol. 63, no. 2, pp. 450 - 455, 2014.

[103] Y. Zhang, M. Adam, A. Hart, J. Wood and S. P. Rigby, “Impact of Oil Composition on Microwave Heating Behavior of Heavy Oils,” *Energy Fuel ,* vol. 32, no. 2, pp. 1592-1599, 2018.

[104] Z. Li, Z. Meng, A. Haigh, P. Wang and A. Gibson, “Characterisation of Water In Honey Using a Microwave Cylindrical Cavity Resonator Sensor,” *J. Food Eng.,* vol. 292, pp. 1 - 9, 2021.

[105] Z. Li, A. Haigh, P. Wang and A. Gibson, “Characterisation and Analysis of Alcohol In Baijiu With A Microwave Cavity Resonator,” *LWT-Food Sci. Technol.,* vol. 141, pp. 1 - 9, 2021.

[106] S. Kim, H. Melikyan, J. Kim, A. Babajanyan, J.-H. Lee, L. Enkhtur, B. Friedman and K. Lee, “Noninvasive In Vitro Measurement Of Pig-Blood D-Glucose By Using A Microwave Cavity Sensor,” *Diabetes Research Clin. Pract.,* vol. 96, no. 3, pp. 379- 384, 2012.

[107] A. Tameishi, T. Kamijo, K. A. Y. Suzuki, M. Taki and K. Sasaki, “Complex Permittivity Measurement Method of High Loss Materials Using Cylindrical Cavity Resonator in Millimeter-wave Band,” in *Int. Symp. Electromag. Compat.*, Tokyo, 2014.

[108] Computer Simulated Technology, “Microwave Studio,” 2018. [Online]. Available: http//www.cst.com/.

[109] B. T. McAllister, Y. Shen, G. R. Flower, S. R. Parker and M. E. . Tobar, “Higher Order Reentrant Post Modes in Cylindrical Cavities,” *J. Apply. Phys,* vol. 112, pp. 1-8, 2017.

[110] Z. Wei, J. Huang, J. Li, G. Xu, Z. Ju, X. Liu and X. Ni, "A High-Sensitivity Microfluidic Sensor Based on a Substrate Integrated Waveguide Re-Entrant Cavity for Complex Permittivity Measurement of Liquids," *Sensors,* vol. 18, no. 11, pp. 1-17, 2018.

[111] K. Fenske and D. Misra, "Dielectric Materials At Microwave Frequencies," *Appl. Microw. Wireless,* vol. 12, no. 10, pp. 92 - 100, 2000.

[112] L. F. Cheng, C. K. Ong, C. P. Neo, V. V. Varandan and V. K. Varadan, "Resonant-perturbation Methods," in *Microwave Electronics: Measurement and Materials Characterisation* , USA, John Wiley & Sons Ltd, 2004, pp. 251 -270.

[113] E. Kasuya, "On The Use Of R And R-Squared In Correlation And Regression," *Ecol. Res,* vol. 34, p. 235–236., 2019.

[114] S. Bell, "A Beginner's Guide to Uncertainty of Measurement," National Physics Laboratory , Middlesex, United Kingdom, 2001.

[115] M. Mohsen-Nia, H. Amiri and B. J. Jazi, "Dielectric Constants of Water, Methanol, Ethanol, Butanol and Acetone: Measurement and Computational Study," *J. Sol. Chem,* vol. 39, p. 701–708, 2010.

[116] J. M. Santos, A. Vetere, A. J. Wisniewski, M. N. Eberlin and W. Schrader, "Comparing Crude Oils with Different API Gravities on a Molecular Level Using Mass Spectrometric Analysis. Part 2: Resins and Asphaltenes," *Energies ,* vol. 11, no. 2767, pp. 1-14, 2018.

[117] ASTM International. ASTM D2007, Standard Test Method for Characteristic Groups in Rubber Extender and Processing Oils and Other Petroleum-Derived Oils by the Clay-Gel Absorption Chromatographic Method, West Conshohocken, PA: ASTM International, 2007.

[118] J. O. Alvarez, ,. D. Jacobi and G. Bernero, "Dielectric Characterization of Geochemical Properties of Crude Oils and Gas Condensate at 25ºC," in *Geosci. Rem Sens Symp (IGARSS)*, Fort Worth, 2018.

[119] L. Hu, H. A. Li, T. Babadagli and M. Ahmadloo, "Experimental investigation of combined electromagnetic heating and solvent-assisted gravity drainage for heavy oil recovery," *J. Pet Sci and Eng,* vol. 154, pp. 589-601, 2017.

[120] A. Punase and B. Hascakir, "Stability Determination of Asphaltenes through Dielectric Constant Measurements of Polar Oil Fractions," *Energy Fuels,* vol. 31, no. 1, pp. 65-72, 2017.

[121] M. Adam, "Private Communication," Aug. 2019.

[122] Z. Z. Abidin, F. N. Omar and D. R. A. Biak, "Dielectric Characterization of Ethanol and Sugar Aqueous Solutions for Potential Halal Authentication," *Int. J. Microw Optic. Technol,,* vol. 9, no. 1, pp. 39-43, 2014.

[123] R. Olmi, V. V. Meriakri, A. Ignesti, S. Priori and C. Riminesi, “Monitoring Alcoholic Fermentation By Microwave Dielectric Spectroscopy,” *J. Microw. Pow. Electromag. Energy ,* vol. 41, no. 3, pp. 38 - 50, 2007.

[124] U. Raveendranath, S. Bijukumar and K. Mathew, “Broadband coaxial cavity resonator for complex permittivity measurements of liquids,” *IEEE Trans. Instrum. Meas.,* vol. 49, no. 6, pp. 1305-1312, 2000.

[125] B. Filali, F. Boone, J. Rhazi and G. Ballivy, “Design and Calibration of a Large Open-Ended Coaxial Probe for the Measurement of the Dielectric Properties of Concrete,” *IEEE Trans. Microw. Theory Techn.,* vol. 56, no. 10, pp. 2322 - 2328, 2008.

[126] S. Kouji, “Broadband Measurement of Complex Permittivity for Liquids Using the Open-ended Cut-off Circular Waveguide Reflection Method,” in *Proceed. Prog. Electromag. Research Symp.* , Guangzhou, China, 2014.

[127] L. Nagy and Z. Szalay, “Coaxial Resonator and Measuring System for Dielectric Parameter Measurements,” in *Eur. Conf. Anten. Propag. (EUCAP)*, Prague, Czech Republic, 2012.

[128] Z. Szalay, I. Ther and L. Nagy, “Permittivity measurement using coaxial reso,” in *Int. Conf. Appl. Electromag. Comm. (ICECom)*, Dubrovnik, Croatia, 2013.

[129] Y.-M. Lee, J.-K. Kim and J. Hur, “Study On The Empirical Design Of Open-Ended Coaxial Cavity Resonator,” *Microw. Opt Technol Lett.,* vol. 56, no. 3, pp. 606-610, 2014.

[130] Y.-M. Lee, “The Design of the Rain Sensor using A Coaxial Cavity Resonator,” *Microw. Opt Technol. Lett.,* vol. 58, no. 1, pp. 128-133, 2016.

[131] K. Shibata and M. Kobayashi, “Measurement of complex permittivity for liquids using the coaxial line reflection method,” in *Asia-Pac. Symp. Electromag. Compat. (APEMC)*, Taipei, Taiwan, 2015.

[132] M. Hoft and S. Burger, “Q-factor Improvement of Combline Resonators,” in *German Microw. Conf*, Ulm, Germany, 2015.

[133] S. Hasan, M. Sundaram, Y. Kang and M. Howlade, “Measurement of Dielectric Properties of Materials using Transmis sion/Reflection Method with Material filled Transmission Line,” in *IEEE Proceed. Instrum. Meas. Technol. Conf.* , Ottawa, ON, Canada, 2005.

[134] X. Yang, X. Liu, S. Yu, L. Ga, J. Zhou and Y. Zeng, “Permittivity of Undoped Silicon in the Millimeter Wave Range,” *MDPI Electronics,* vol. 8, no. 8, pp. 1-12, 2019.

[135] L. Hu, H. A. Li and M. Ahmadloo, “Determination of the permittivity of n-hexane/oil sands mixtures over the frequency range of 200 MHz to 10 GHz,” *The Canadian J. Of Chem. Eng.,* vol. 96, pp. 2650 - 2660, 2018.

[136] Ali A. Abduljabar David J. Rowe, A. Porch and D. A. Barrow, “Novel Microwave Microfluidic Sensor Using a Microstrip Split-Ring Resonator,” *IEEE Trans. Microw. Theory Techn,* vol. 62, no. 3, pp. 679 - 688, 2014.

[137] D. C. Dube, M. T. Lanagan, J. H. Kim and S. J. Jang, “Dielectric Measurements on Substrate Materials at Microwave Frequencies using A Cavity Perturbation Technique,” *J. Appl. Phys. ,* vol. 63, no. 7, pp. 2466 - 2468, 1988.

[138] S. Matytsin, K. N. Rozanov and N. A. Simonov, “Permittivity Mesaurement Uisng Slotted Coaxial Resonator,” in *IEEE Instrum. Meas. Techn. Conf*, Brussels, Belgium, 1996.

[139] G. Kent, “Nondestructive Permittivity Measurement of Substrates,” *IEEE Trans. Instrum. Meas,* vol. 45, no. 1, pp. 102-106, 1996.

[140] G. Kent and S. M. Bell, “The Gap Correction for the Resonant-Mode Dielectrometer,” *IEEE Trans. Instrum. Meas,* vol. 45, no. 1, pp. 98-101, 1996.

[141] M. D. Janezic and J. Baker-Jarvis, “Full-Wave Analysis of a Split-Cylinder Resonator for Nondestructive Permittivity Measurements,” *IEEE Trans. Microw. Theory Tech.,* vol. 47, no. 10, pp. 2014-2020, 1999.

[142] Computer Simulated Technology, “Microwave Studio,” 2019. [Online]. Available: http//www.cst.com/.

[143] M. Ma, Y. Wang, M. Navarro-Cíac, F. Liua, F. Zhanga, Z. Liua, Y. Lid, S. M. Hanham and Z. Hao, “The Dielectric Properties of Some Ceramic Substrate Materials at Terahertz Frequencies,” *Eur. Ceram. Soc,* vol. 39, no. 14, pp. 4424-4428, 2019.

[144] Keysight, “16451B Dielectric Test Fixture,” 01 October 2000. [Online]. Available: http://literature.cdn.keysight.com/litweb/pdf/16451-90020.pdf. [Accessed 10 November 2020].

[145] Rogers Corporation, “RT/duroid Laminates,” 10 December 2017. [Online]. Available: https://rogerscorp.com/-/media/project/rogerscorp/documents/advanced-connectivity-solutions/english/data-sheets/rt-duroid-5870---5880-data-sheet.pdf. [Accessed 10 December 2020].

[146] S. Govinda and K. V. Rao, “Dielectric Properties of Single Crystal of Al2O3 and Al2O3 Doped with Chromium or Vanadium,” *Phys. Stat. Sol,* vol. 27, no. 2, pp. 639-644, 1975.

[147] A. Périgaud, S. Bila, O. Tantot, N. Delhote and S. Verdeyme, “3d Printing Of Microwave Passive Components By Different Additive Manufacturing Technologies,” in *IEEE MTT-S Int. Microw. Workshop Series Adv. Mat. Proc. RF, THz Applic. (IMWS-AMP)*, Chengdu, China, 2016.

[148] J. Strycharz and P. Piasecki, “3D Printed Circular And Rectangular Waveguide Mode Converters,” in *22nd Int. Microw. Radar Conf. (MIKON)*, Poznan, Poland, 2018.

[149] T. Skaik, M. Salek, Y. Wang, M. Lancaster, T. Starke and F. Boettcher, “180 GHz Waveguide Bandpass Filter Fabricated by 3D Printing Technology,” in *13th UK-Europe-China Workshop on mm-Waves THz Technol. (UCMMT)*, Tianjin, China, 2020.

[150] P. T. Timbie, J. Grad, D. Weide, B. Maffei and G. Pisano, “Stereolithographed Mm-Wave Corrugated Horn Antennas,” in *Int. Conf. Infrared Millimeter THz Waves*, Houston, TX, USA, 2011.

[151] A. Hernandez, E. Martin, J. Margineda and J. M. Zamarro, “Resonant cavities for measuring the surface resistance of metals at X-band frequencies,” *J. Phys. E: Scient. Instrum.,* vol. 19, no. 3, pp. 222 - 225, 1986.

[152] E. Maxwell, “Conductivity of Metallic Surfaces at Microwave Frequencies,” *J. Appl. Phys.,* vol. 18, no. 7, pp. 628 - 638, 1947.

[153] A. Nakayama, Y. Terashi, H. Uchimura and A. Fukuura, “Conductivity Measurements at the Interface Between the Sintered Conductor and Dielectric Substrate at Microwave Frequencies,” *IEEE Trans. Microw. Theory Techn.,* vol. 50, no. 7, pp. 1665 - 1674, 2002.

[154] J. Krupka, “Frequency domain complex permittivity measurements at microwave frequencies,” *Meas. Sci. Technol.,* vol. 17, no. 6, pp. R55--R70, 2006.

[155] H. Rmili, J.-L. Miane, T. E. Olinga and H. Zangar, “Microwave Conductivity Measurements of High Conductive Polyaniline Films,” *Eur. Phys. J Appl. Phys. ,* vol. 29, pp. 65-72, 2005.

[156] E. Ritza and M. Dressel, “Analysis of Broadband Microwave Conductivity and Permittivity Measurements of Semiconducting Materials,” *J. Appl. Phys,* vol. 103, pp. 1-8, 2008.

[157] J. S. Bobowski and A. P. Clements, “Permittivity and Conductivity Measured using a Novel Toroidal Split-Ring Resonator,” *IEEE Trans. Microw. Theory Techn.,* vol. 65, no. 6, pp. 2132 - 2138, 2017.

[158] J. Cuper, B. Salski, T. Karpisz, A. Pacewicz and P. Kopyt, “Conductivity measurement in mm-wave band with a Fabry-Perot open resonator,” in *IEEE/MTT-S Int. Microw. Symp. (IMS)*, Los Angeles, CA, USA, 2020.

[159] R. G. Edwards, C. M. Norton, J. E. Campbell and D. Schurig, “Effective Conductivity of Additive-Manufactured Metals for Microwave Feed Components,” *IEEE Access,* vol. 9, pp. 59979-59986, 2021.

[160] R. Gumbleton, J. A. Cuenca, S. Hefford, K. Nai and A. Porch, “Measurement Technique for Microwave Surface Resistance of Additive Manufactured Metals,” *IEEE Trans. on Microw. Theory Techn.,* vol. 69, no. 1, pp. 189 - 197, 2021.

[161] J. J. Barroso, P. J. Castro and J. P. L. Neto, “Electrical Conductivity Measurement Through the Loaded Q Factor of a Resonant Cavity,” *Inter. J. of Infra. Millimeter Waves,* vol. 24, p. 79–86, 2003.

[162] P. Bale, “Feeding Properties Of The Highly Grain Refined A20x Alloy,” Uni. of Birmingham, Birmingham, 2011.

[163] P. A. Rizzi, Microwave Engineering Passive Circuit, 2nd ed., New Jessy: Prentice Hall, 2002.

[164] H. S. Kim, “Electromagnetic Wave in Cavity Design,” in *Behaviour of Electromagnetic Waves in Different Media and Structures*, Crotia, InTech, 2011, pp. 80-83.

[165] E. Hammerstad and O. Jensen, “Accurate Models for Microstrip Computer-Aided Design,” in *IEEE MTT-S Int. Microw. Symp. Dig.*, Washington, DC, USA, 1980.